TECHNISCHE UNIVERSITÄT MÜNCHEN
Lehrstuhl für Analysis

Crystalline Order, Surface Energy Densities and Wulff Shapes: Emergence from Atomistic Models

Yuen Au Yeung

Vollständiger Abdruck der von der Fakultät für Mathematik der Technischen Universität München zur Erlangung des akademischen Grades eines

Doktors der Naturwissenschaften (Dr. rer. nat.)

genehmigten Dissertation.

Vorsitzender:		Univ.-Prof. Dr. Daniel Matthes
Prüfer der Dissertation:	1.	Univ.-Prof. Gero Friesecke, Ph. D.
	2.	Univ.-Prof. Dr. Georg Dolzmann Universität Regensburg
	3.	Prof. Irene Fonseca, Ph. D. Carnegie Mellon University, Pittsburgh, USA (schriftliche Beurteilung)

Die Dissertation wurde am 17.4.2013 bei der Technischen Universität München eingereicht und durch die Fakultät für Mathematik am 7.8.2013 angenommen.

Zusammenfassung

Wir analysieren Teilchensysteme mit kurzreichweitiger Paar–Wechselwirkung. Im Limes großer Teilchenzahl und kleiner Gesamtenergie leiten wir die Entstehung eines wohldefinierten makroskopischen Clusters konstanter Dichte und eines effektiven Oberflächenenergiefunktionals her; letzteres mithilfe von Gamma–Konvergenz. In physikalisch interessanten Fällen bestimmen wir das Oberflächenfunktional und die Gestalt des aus energieminimierenden Teilchenkonfigurationen entstehenden Clusters explizit.

Abstract

We investigate particle configurations interacting through a short–range pair–potential. In the limit of large particle number and at low total energy, we establish the emergence of a well–defined macroscopic cluster of constant density, and of an effective surface energy functional arising as a Gamma–limit. The surface functional and the cluster shape arising from minimising particle configurations are determined explicitly in examples of physical interest, including arbitrary 2D configurations and 3D subsets of the face–centred cubic lattice interacting via the Heitmann–Radin potential.

Acknowledgements

My most sincere thanks go to my supervisor, Gero Friesecke, for introducing me to this vivid research area. I have benefited a lot, scientifically and personally, from the enlightening discussions and from the countless support for participation in international summer schools, conferences and workshops during the past years. Thank you, Gero!

Further scientific thanks go to Bernd Schmidt for the rich discussions, when we worked on our joint paper, and to Dominik Jüstel for introducing me to symmetry groups.

In the past years, I have also enjoyed a lovely environment at the university, which made my work as pleasant as I wished. I am sure that my colleagues contributed a lot to it; to name a few, Carl–Friedrich Kreiner, Andreas Leiseifer, Dominik Jüstel and Michael Fauser, Frauke Bäcker, Florian Rupp and everybody else for our continuous small talks.

I would like to express my gratitude to all the support I received from the elite fast–track programme TopMath.

Last but not least, I am indebted to my parents Sheung and Mei Wan, my sister So Man and my partner Werner for all the continuous support and patience.

Thank you!

Yuen

Contents

1 Introduction **1**

2 Approaches to Crystallisation and Crystal Growth **13**

2.1 Model energies 13

2.1.1 Non–relativistic quantum mechanics 14

2.1.2 Classical models 15

2.2 Atomistic–to–continuum limits 17

2.3 Kinetic theory 19

2.4 Statistical mechanics 23

2.5 Numerics for Lennard–Jones clusters 26

3 Surface Energy Density **29**

3.1 Preliminaries 31

3.1.1 Basic notions 31

3.2 Surface energy density 32

3.2.1 Surface energy density as thermodynamic limit 32

3.2.2 Calculation of e 35

3.2.3 Fundamental domain and extension to sphere 39

3.3 Calculations for 2D triangular lattice 41
3.4 Calculations for 3D fcc and hcp crystals 42
3.4.1 Face–centered cubic crystals 42
3.4.2 Hexagonal close–packed crystals 46

4 Compactness and Formation of Clusters **53**
4.1 Two dimensions 56
4.1.1 Atomistic energy 58
4.1.2 Compactness and mass conservation 62
4.1.3 Proof of formation of clusters with constant density and finite perimeter 67
4.2 Three dimensions 73

5 Wulff Shapes through Atomistics **83**
5.1 Two dimensions: triangular lattice 87
5.1.1 Lower bound: lower semicontinuity 91
5.1.2 Upper bound: attainment of lower bound 94
5.1.3 Identification of Wulff set 97
5.2 Three dimensions: face–centred cubic lattice 98
5.2.1 Lower bound: lower semicontinuity 101
5.2.2 Upper bound: attainment of lower bound 123
5.2.3 Identification of Wulff shape 128

A Gamma–convergence **131**

B Functions of bounded variation **133**

List of publications **137**

Chapter 1

Introduction

Crystals have ever played a role in human history long before the scientific age. Diamonds, rubies and emeralds are valuable gems; these are macroscopic crystals, but the fascinating origin of their flat surfaces is hidden in atomistic scales, about 10^{-8} times smaller.

But what are crystals? Loosely speaking, a crystal is a huge amount of atoms or molecules that is ordered periodically and that has a macroscopic,i geometric shape.

Contribution of this thesis: —A bridge between two research communities. Vivid research has been done in this fascinating area and there are two major, but rather decisive, differences in how to tackle and model problems related to crystal growth. We relate these two approaches to atomistic and continuum practice. This thesis contributes to linking these two approaches for the problem of crystal shapes.

The *atomistic community* uses model energies which contain information about individual particles, like positions, momenta, mass, etc. It is generally believed that phenomena in nature occur, because these phenomena are minimisers of the atomistic

model energy. Mathematically, this accounts to a minimisation of the respective energy among all admissible minimisers.

Of course, this truly leads to a physically meaningful and mathematically rigorous justification. It could even lead to predictions that we have not observed yet; however, such atomistic models suffer from a big drawback: The state space of the model energy must be highly dimensional (depending on the particle number) to predict properties that could be observed. But this demand meets with the obstacles that the energy is non–convex and that the number of local minimisers grows fast with the particle number. This is why, atomistic energy minimisation seems not to be promising for establishing macroscopic properties of crystals. Remarkable results concerning characterisations of exact minimisers could be found in [GR79], [HR80], [Har74] and in [Rad81].

Limitations apply also to numerical simulations. Computational calculations can only be performed for "small" systems. Nevertheless, numerics can and do give us a hint for how very small crystals might behave.

The *continuum viewpoint* suppresses the atomistic scaling. Following Josiah W. Gibbs (see [Gib78]) a macroscopic equilibrium shape is modelled as solution to the following optimisation problem:

$$\min_{E\subset\mathbb{R}^N \text{ smooth}} \int_{\partial E} e(n)\,\mathrm{d}\mathcal{H}^{N-1} \quad \text{subject to} \quad \mathrm{vol}(E) = \text{const}, \tag{1.1}$$

where E is a smooth subset of $\mathbb{R}^N$, e is a surface energy density function and n is the outward unit normal to the boundary of E. This formulation of Gibbs is due to Herring (see [Her51]). Remarkably a complete mathematical theory for such optimisation problems exists, see [Tay75] in the language of geometric measure theory and [FM91] in the framework of boundary integrals for sets of finite perimeter. Also note that (1.1)

could be understood as an anisotropic isoperimetric problem, to which it reduces in the case $e = 1$. Exact minimisers to problem (1.1) can be determined explicitly by the well–known Wulff construction, once the surface energy density function e is known. However, the continuum approach neither supplies us with such a function, nor does it give us a rigorous justification for any specific choice of a surface energy density. In particular, on the one hand, the optimisation problem (1.1) sounds intuitively reasonable, but on the other hand, a rigorous derivation starting from atomistic energy minimisation is missing.

The *ultimate goal of this thesis* is to build a bridge between the atomistic and continuum viewpoints, to employ the strengths of the respective approaches and, finally, to rigorously determine a specific macroscopic model starting from atomistic energy consideration.

We give an energetic picture of the formation of solid–vapour interfaces and the growth of solids in case of zero temperature and an energy of pair–potential type with sufficiently short–range potential.

The mathematical analysis enters as soon as we associate to any particle configuration a probability measure μ_N, a so–called re–scaled empirical measure, which is why the analysis will be performed on the space of probability measures. In particular, the limit of large particle number is treated as the limit of the measures μ_N with respect to the weak$*$ and L^1 convergence.

The mathematical treatment in terms of probability measures unveils the formation of clusters as a compactness result for probability measures which are associated to low–energy configurations. This involves a careful study of the weak$*$ limit of μ_N. We will show that the weak$*$ limit of μ_N associated to low–energy configurations (in three dimensions subject to lattice states) will converge to a constant multiple of a charac-

teristic function over a set E. The set E is our macroscopic cluster and is rigorously derived from atomistic considerations.

Note that, not past this point, our configurations are allowed to lie in quite general lattices; in two dimensions even no lattice constraint is needed.

The exact identification of the cluster's shape will be done for configurations subject to triangular and subject to face–centred cubic lattice states. To do so, we will solve (1.1) explicitly for our specific settings. However, recall that the optimisation problem (1.1) is solely macroscopic and no atomistic information seem to be captured. So, a rigorous explanation why (1.1) is suitable for our needs is due, before we can proceed to solve (1.1).

In fact, we will prove that the considered functional in (1.1) arises naturally as the variational Gamma–limit of atomistic energy functionals which are defined on the space of probability measures. A merit of Gamma–convergence comes into operation: It implies that minimisers of the discrete energy functionals must also converge to minimisers of the macroscopic surface functional; hence, the "macroscopic" minimisation in (1.1) could be seen, from a mathematical point of view, as a rigorous consequence of Gamma–convergence.

This is the bridge that we want to build: It connects rigorously atomistic with continuum models and it does make macroscopic approaches appear as the natural outcomes of atomistic considerations.

Furthermore, we give a precise meaning to the surface energy density of a lattice in terms of a thermodynamic limit. In fact, we adhere to the view, that our interpretation of surface energy density is the suitable one for short–range energies which eventually amount to "bond counting". In addition, the surface energy densities for the two–dimensional triangular lattice and for the three–dimensional face–centred cubic as well

as for the hexagonal close–packed lattices are explicitly determined.

These mathematical derivations are to the best of our knowledge new; they hopefully unify the two completely different approaches of atomistic and continuum understanding. In particular, our belief why equilibrium shapes emerge is in full accordance to Gibbs.

After we have established the unifying treatments, we apply the available powerful methods for optimisation problems of type (1.1) to arbitrary configurations subject to lattice states (triangular in 2D and face–centred cubic in 3D) which interact via a soft potential. Our investigations show that the ensuing equilibrium shapes are given by a regular hexagon in two dimensions and by a regular truncated octahedron in three dimensions (see Figure 1.1 for a three–dimensional equilibrium shape).

The explicit determination of crystal equilibrium shapes as a consequence of atomistic energy minimisation is new to the best of our knowledge. Rigorous mathematical proofs and ansatz which really consider atomistic energies from the onset have not been presented so far. To summarise, research in the area of continuum models is very rich:

- ingredient for hybrid formulations in models with competing bulk and surface terms, e.g., to describe material void in a linearly elastic solid (see [FFLM11]), Mumford–Shah functional in image analysis (see [GCL89], [AT90]), Blake–Zisserman model (see [CLT97]), surfactants (see [FMS07]),
- approximations by diffuse interface models (see [GK10]),
- evolution problems such as motion by crystalline curvature (see [Tay91], [IS98]).

We do not develop a new theory in the continuum setting, but we justify existing models by atomistic energy investigations and we apply existing methods to predict specific equilibrium crystal shapes.

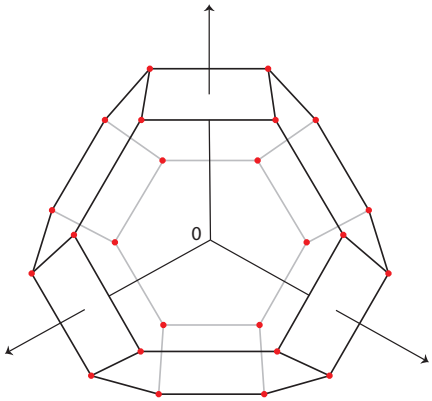

Figure 1.1: The Wulff shape for the face–centred cubic lattice is a regular truncated octahedron and minimises the Gibbs functional. For a proof and for explanations see Chapter 5.

While a significant amount in applied mathematics is currently emerging which connects atomistic and continuum models (see the brief discussion in Section 2.2), to the best of my knowledge the problem of crystal shapes has hitherto not been addressed mathematically.

Relevance of Results. The results should be of interest for experiments in crystal growth, where

- the temperature is low,
- interactions other than nearest–neighbour interactions are negligibly small,
- the crystal grows "perfectly", *i.e.*, the crystal is prevented from forming defects and vacancies, impurities,...,
- the relaxation time is sufficiently long, *i.e.*, one waits until a deposited atom attaches and until the $(N+1)$–particle configuration attains an equilibrium,

before another atom is released. Because of this, our model could be understood as a quasi–static limit.

Our results suggest that the emergence of clusters, the surface energy densities and the selection of the crystal shape are already mainly governed by the nearest–neighbour interactions.
Indeed, the interaction potential selects a lattice (or a union of lattices) into which particles assemble at an atomistic scale. In a second step, the surface energy density emerges automatically by the atomic arrangements into lattices, and it finally selects the equilibrium cluster shape.
In contrast, surface relaxation, smoothing of "corners" and "edges" in the Wulff shape, finer properties like the formation of staple sequences and its order might well require the consideration of higher–order forces.

Historical roots. The shape problem has an astonishingly long history which traces back to the early modern period when Robert Hooke, a fellow of the Royal Society, made his observations with a microscope public in his *Micrographia* [Hoo65] in 1665. The decisive observations concerning crystallisation were:

a. Gravels in urine. For any reason, gravel in urine attracted his interest which is why he investigated them. Gravels of size $\sim$ 0.2mm appeared, much to his surprise, not only as "plates", but had polygonal shapes (see Figure 1.2).

b. Cornish Diamonds. Hooke provided himself with small pellucid crystals from a rock hollow in Cornwall. And again his microscope magnified regular geometric crystals. His drawn observations (see Figure 1.3) are in all respects remarkable in as far as they reveal polyhedral shapes. Note in particular the right crystal which is a truncated octahedron and which is the predicted shape (see Figure 1.1) in this thesis. Hooke also

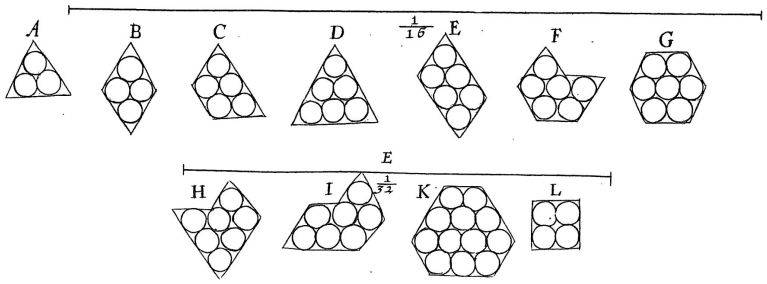

Figure 1.2: Drawings form page 82 in [Hoo65]. These are reconstructed drawings from his observations of gravels in urine. The diameter of a polygon is roughly 0.2mm; the indicated lengths $\frac{1}{16}$ and $\frac{1}{32}$ are w.r.t. imperial inch. Hooke explained the emergence of such polygons, by postulating the existence of circular *Globulars*. These globulars were supposed to arrange on an equilateral lattice and to fill the observed polygons.

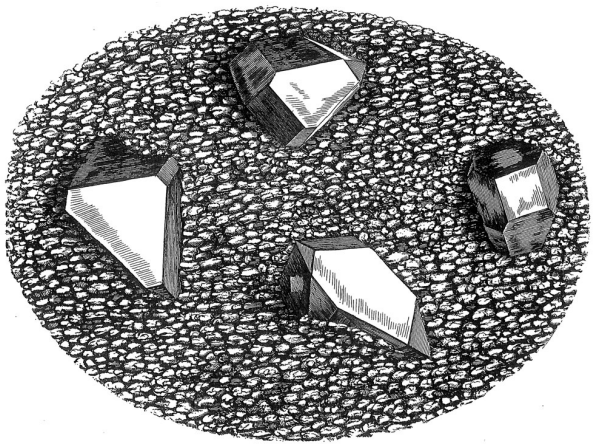

Figure 1.3: Drawings from page 82 in [Hoo65]. Hooke drew the geometric shapes which he observed when magnifying crystals from Cornwall. The crystals have in common that they are polyhedral and bounded by planes. The right drawing is very close to our prediction in Chapter 5, according to which minimisers of the Heitmann–Radin energy subject to fcc lattice states self–assemble into a truncated octahedron.

provided an explanation for the emergence of these crystals: He assumed that circular *Globulars* constituted the crystals and that these globulars were located on a triangular lattice (see Figure 1.2). Here is a short quotation from his observations:

> "... for that which makes an Enquiry pleasant, are, first a noble *Inventum* that promises to crown the successfull endeavour; and such must certainly the knowledge of the efficient and concurrent causes of all these curious Geometrical Figures be... and here we meet nothing less than the *Mathematicks* of nature, having every day a new Figure to contemplate, or a variation of the same in another body...
> Which do afford us a third thing, which will yet more sweeten the Enquiry, and that is, a multitude of information; we are not so much to grope in the dark, as in most other Enquiries, where the *Inventum* is great; for having such a multitude of instances to compare, and such easie ways of generating, or compounding and of destroying the form, as in the *Solution* and *Crystallization* of Salts, we cannot but learn plentifull information to proceed by." (1665, Robert Hooke in [Hoo65, p. 87])

Hooke's globular models could be understood as non–overlapping atoms of equal size. Moreover, his self–evident arrangement consisted in maximising the number of contact points. In fact, these non–overlapping globulars are modeled by our Heitmann–Radin energy introduced in Section 2.1.2.

Organisation of thesis. In Chapter 2 we begin by collecting some approaches to crystallisation and crystal growth. We do not claim that the survey is exhaustive; it rather provides selected major results to better put the results of this thesis into perspective.

In Chapter 3 the surface energy density is introduced as a thermodynamic limit for lattice configurations interacting through short–range potentials that eventually amounts to "bond counting", like the Heitmann–Radin potential does. It turns out, that the surface energy densities must only be calculated on a dense subset of a fundamental domain; the remaining values of the surface energy density are obtained by continuity

and by a unique periodic extension according to the point symmetry group of the lattice in question.
Further, the surface energy density is calculated explicitly for the two–dimensional triangular lattice, for the face–centred cubic lattice and for the hexagonal close–packed crystal.

Chapter 4 addresses the crystallisation problem for monatomic crystals. In two dimensions, at zero temperature and for pair–interaction energies with sufficiently short–range interactions, it is shown that low energy configurations converge to a well–defined crystalline cluster with local density $2/\sqrt{3}$ (*i.e.*, the density of atoms per unit volume of the triangular lattice). We mention that the hypotheses on the low energy configurations allow irregularities (cracks, vacancies, inclusions of phases with different lattice structure) as long as the occupied area is "small" enough (see Figure 4.1 for examples of such irregularities).
In three dimensions we present a compactness result for low energy *lattice* configurations. An additional assumption on the boundedness of diameters is needed for our Theorem. Our results apply, like in two dimensions, to systems at zero temperature whose energy is of pair–interaction form with a sufficiently short–range interaction range. On the one hand, our compactness theorem might appear restrictive, because configurations have to be lattice states (contrary to the two dimensional case), but on the other hand it admits a huge degree of freedom: it applies to all sequences of bounded low–energy configurations which lie in *any* (among the infinitely many) close–packed lattice.
The results from this chapter allow us to deduce that minimisers of the surface functionals, derived in Chapter 5, converge to minimisers of the limiting functional.

In Chapter 5 we present a variational formulation of the problem in the framework of

Gamma–convergence.

Chapter 5 determines rigorously the ensuing cluster of minimising configurations (subject to the triangular lattice in 2D or to the face–centred cubic lattice in 3D) which interact through a short–range potential. We remark that in two dimensions it is not necessary for the Heitmann–Radin sticky disc potential to constrain configurations to the triangular lattice.

First, the surface energy of an N–particle configuration is formulated in terms of the surface energy density, derived in Chapter 3, as a variational surface integral. By passing to the Gamma limit, we obtain a macroscopic, effective functional which describes the macroscopic surface energy. Finally, we appeal to an existence and uniqueness theorem which states that minimisers of the effective functional among all smooth subsets of $\mathbb{R}^N$ with constant mass are—up to a set of zero measure and up to translation and rotation—a multiple of the *Wulff set*.

Thanks to the compactness results in Chapter 4 and thanks to the established Gamma–convergence in Sections 5.1 and 5.2 we may deduce that ground states of the energy converge (in an appropriate sense) to a constant multiple of the Wulff set.

Chapter 2

Approaches to Crystallisation and Crystal Growth

This chapter is a review on the state–of–the–art in crystallisation and crystal growth. It discusses selected models, approaches and their viewpoints.

2.1 Model energies

It is generally believed, that a particle configuration is a (local, global) equilibrium if it minimises the model energy. In other words, an equilibrium configuration is an energetically favourable state.

A model energy is therefore an essential function that has to be fixed first, before any study on properties and behaviour can be performed.

Depending on the desired properties to be studied, there are plenty of different energy functions. A concise overview of energy functions and functionals could be found for instance in [TFar].

2.1.1 Non–relativistic quantum mechanics

We consider a molecule with M atoms at positions $X = (X_1, \dots, X_M) \in (\mathbb{R}^3)^M$ and charges $Z_i \in \mathbb{N}$, $i = 1, \dots, M$. Loosely speaking, the Born–Oppenheimer approximation says that the wavefunction for the molecule can be factorised into an electronic and a nuclear wavefunction; the nuclei are often treated classically.

Electron configurations are interpreted as *electronic wavefunctions*: Vectors of the form $x = (x_1, s_1, x_2, s_2, \dots, x_N, s_N) \in (\mathbb{R}^3 \times \mathbb{Z}_2)^N$ contain the positions and spins of N electrons in $\mathbb{R}^3$. The set of admissible electronic wavefunctions is defined as

$$\mathcal{A}_N := \left\{ \psi \in H^1((\mathbb{R}^3 \times \mathbb{Z}_2)^N; \mathbb{C}) \ : \ \|\psi\|_{L^2} = 1, \ \psi \text{ is antisymmetric} \right\}.$$

Here, H^1 denotes the Sobolev space which contains all square–integrable functions with square–integrable distributional derivative; H^1 is necessary to make the kinetic term in the energy (see below for definition) well–defined. By antisymmetric we mean

$$\psi(\dots, x_i, s_i, \dots, x_j, s_j, \dots) = -\psi(\dots, x_j, s_j, \dots, x_i, s_i, \dots) \text{ for all } i < j.$$

The energy functional is given by $E(X, \psi) = \int_{(\mathbb{R}^3 \times \mathbb{Z}_2)^N} \psi^* H \psi$, where H is the Hamiltonian

$$H = -\sum_{i=1}^{N} \sum_{k=1}^{M} \frac{Z_k}{|x_i - X_k|} - \frac{1}{2} \sum_{i=1}^{N} \nabla_{x_i}^2 + \sum_{1 \le i < j \le N} \frac{1}{|x_i - x_j|} + \sum_{1 \le k < \ell \le M} \frac{Z_k Z_\ell}{|X_k - X_\ell|}.$$

The first term models Coulomb attraction by the nuclei, the second models the kinetic energy of the electrons, the penultimate describes Coulomb repulsion and the last term takes the nuclei–nuclei interaction into account.

The ground state energy is obtained by solving the variational problem

$$\min_{\psi \in \mathcal{A}_N} E(X, \psi).$$

A big disadvantage of this model is that an explicit solution is out of reach. Furthermore, discretisations of the phase space $(\mathbb{R}^3 \times \mathbb{Z}_2)^N$ may require a high computational complexity that even grows exponentially, for there are $6N$ variables to discretise. This exponential complexity is often referred to the "curse of dimensions". Careful and smart approximations for computational simulations are therefore not avoidable, for instance Hartree–Fock theory or Density Functional Theory.

2.1.2 Classical models

A possibility to simplify the analysis and to overcome the "curse of dimensions" are classical models. The model energies will only consider parameters of the nuclei as variables, but no information on any electronic structure is needed for the models. Further, we restrict our presentation to the special case of zero temperature and monatomic configurations.

A. Energies of pair–potential type. A prime example for such simplifying models is an energy of pair–potential type

$$E(x_1, \ldots, x_N) := \sum_{1 \leq i < j \leq N} V(|x_i - x_j|), \tag{2.1}$$

where $x_i \in \mathbb{R}^d$, $i = 1, \ldots, N$, are the particle positions and where V is some suitably chosen pair–interaction potential. Here is a short, non–exhausive list of possible potentials:

Lennard–Jones (6,12) potentials. This potential could be used to describe noble gases and noble metals. Modifications are limited by two empirical parameters a, b:

$$V : (0, \infty) \to \mathbb{R},\ V(r) := ar^{-12} - br^{-6}.$$

Short–range potentials. Any pair–interaction potential V can be simplified by imposing a cutting radius, so that interactions beyond this range are neglected, *i.e.*, $V(r) = 0$ for r larger than the cutting radius.

Heitmann–Radin potential. This is a specific short–range potential introduced in [HR80] and one of the potentials used in this thesis. The overlapping of two atoms is forbidden ("hard–core") and the equilibrium distance between two neighbouring particles is one.

$$V : (0, \infty) \to \mathbb{R} \cup \{\infty\},\ V(r) := \begin{cases} +\infty, & r < 1 \\ -1, & r = 1 \\ 0, & r > 1. \end{cases} \tag{2.2}$$

Note that this potential does not allow any elasticity. In particular, any configuration is infinitely brittle. Heitmann and Radin proved that ground states of the Heitmann–Radin energy, *i.e.*, the energy has form (2.1) and the potential V is the Heitmann–Radin potential, are—up to translation and rotation—a subset of the triangular lattice. A similar result is shown for the "soft–disc" potential; see [Rad81].

B. Mass–spring models. Bonds between atoms are assumed to be springs and configurations arise as admissible deformations of a reference configuration $R_N := \{x_1, \ldots, x_N\} \subset \mathbb{Z}^d$. The interaction radius is limited by r_{cut} and the model energy for

an admissible deformation is

$$E(\{y(x_1),\dots,y(x_N)\}) := \sum_{x_i,x_j\in R_N\,:\,|x_i-x_j|\leq r_{cut}} K_{ij}(|y(x_i)-y(x_j)|-\ell_{ij})^2,$$

where K_{ij} is a spring constant and ℓ_{ij} is the equilibrium length between the ith and jth deformed particle.

2.2 Atomistic–to–continuum limits

An often pursued setting in the passage from atomistic to continuum is the *Lagrangian* viewpoint. A reference configuration $R_N \subset \mathbb{R}^d$, $|R_N| = N$, with N elements is fixed a priori and admissible particle configurations are interpreted as deformations $y : R_N \to \mathbb{R}^d$ of the reference state; hence, the energy E is defined as a function of deformations and, in particular, a ground state is defined as a minimiser of the energy among all deformations (possibly subject to some boundary conditions).
Note that there is the *Eulerian* viewpoint in contrast to the Lagrangian one. We adopt for our purposes the Eulerian viewpoint in Chapters 4 and 5. The Eulerian viewpoint is for example also used in [CF09] in the study of many–particle energies in the context of Coulomb systems and in [LM10]; the latter is a mesoscopic model to describe low–energy configurations that may exhibit crystal defects, and it optimally fits a Bravais lattice for a locally reference–free configuration.

Theil passes to the limit from a two–dimensional atomistic model for quite general pair–potentials that satisfy some growth and regularity assumptions. Although he minimises his energy over deformations of a reference configuration, his viewpoint is not the Lagrangian one; for the reference configuration is not fixed a priori. As the

particle number N gets large, it is shown in [The06] that

1. the energy densities per particle converge to the respective energy density per particle in the two–dimensional triangular lattice $\mathcal{L}^{2D}$,

2. crystallinity is inherited from and mediated by crystalline boundary conditions.

Let us denote by $R_N \subset \mathbb{R}^2$ a reference configuration with N particles. The energy in question is of pair–potential type and the temperature is zero by default, *i.e.*, as a function of deformations $y : R_N \to \mathbb{R}^2$,

$$E(\{y\}) := \frac{1}{2} \sum_{x,x' \in R_N \,:\, x \neq x'} V(|y(x) - y(x')|).$$

Theorem. *(Theorem 1.1 and Corollary 1.3 in [The06]) There exists a constant $\alpha_0 \in (0, \frac{1}{3})$ such that for any $\alpha \in (0, \alpha_0)$ and every potential $V : [0, \infty) \to [0, \infty]$ which has the properties*

(normalisation) $\lim_{r\to\infty} V(r) = 0$ *and* $\min_{r>0} \sum_{\xi \in \mathcal{L}^{2D} \setminus \{0\}} V(r|\xi|) = -6$,

(smoothness) V is in C^2 in $(1 - \alpha, \infty)$,

(growth) V behaves in the following way:

$$\begin{aligned} V(r) &\geq \frac{1}{\alpha} && \text{for } r \in [0, 1-\alpha], \\ V''(r) &\geq 1 && \text{for } r \in (1-\alpha, 1+\alpha), \\ V(r) &\geq -\alpha && \text{for } r \in [1+\alpha, \frac{4}{3}], \\ |V''(r)| &\leq \alpha r^{-7} && \text{for } r > \frac{4}{3}. \end{aligned}$$

Then the following holds:

1. (energy density per particle)

$$\lim_{N\to\infty} \min_{y:R_N\to\mathbb{R}^2} \frac{1}{N} \sum_{\{x,x'\}\subset R_N} V(|y(x)-y(x')|) = -3.$$

2. (Propagation of crystallinity)

Let $C \subset \mathcal{L}^{2D}$ be finite and define the energy

$$\tilde{E}(\{y\}) := \sum_{\{x,x'\}\subset C\,:\,\{x,x'\}\cap\mathcal{L}^{2D}\neq\emptyset} V(|y(x)-y(x')|).$$

Minimisers of $\tilde{E}$ subject to all deformations $y : \mathcal{L}^{2D} \to \mathbb{R}^2$ which satisfy the crystalline boundary condition $y(x) = x$ in $\mathcal{L}^{2D}\backslash C$ are also crystalline in C, i.e.,

$$\{y_{min}(x) \;:\; x \in \mathcal{L}^{2D}\} = \mathcal{L}^{2D}.$$

In [EL09] the above result was shown for the two–dimensional hexagonal lattice; the considered potential incorporates a pair–potential and a three–body potential of Stillinger–Weber type.

2.3 Kinetic theory

Another interesting question in crystal growth is "how" a new crystal facet evolves in time. This involves the study of the kinetics of the morphology. A suitable environment to investigate theoretically and experimentally crystal growth is to "grow" a new facet on a crystalline substrate. The new facet preferably inherits the properties from the substrate. Such a crystal growing procedure is called *epitaxy* and could, for instance,

be realised experimentally by a molecular beam epitaxy (MBE).

Even nearly a decade before the invention of MBE, Burton, Cabrera and Frank presented in [BCF51] the first mathematical model for epitaxial growth. Hitherto there have been several other promising approaches to model and simulate epitaxial growth (see [PV98], [JW99], [Caf06]).

The Burton–Cabrera–Frank model (BCF) is a hybrid step–flow model: On the one hand, the height of the respective terraces and islands are kept discrete; on the other hand, steps separating two successive terraces are coarse–grained and represented as smooth curves.

Crystal growth is assumed to result from the evolution of steps by attaching or detaching atoms, so–called *adatoms*, to and from steps. Further, deposition arises from a source with rate F. The governing equation for the adatom density ρ on a terrace is

$$\partial_t \rho = \nabla \cdot (D \nabla \rho) + F - \tau^{-1} \rho. \tag{2.3}$$

Here, D is the diffusion coefficient, that is not necessarily constant, F is the deposition flux rate and τ^{-1} is the desorption rate. The first term on the right hand models the diffusion of the adatoms and the second the deposition from a source, for example from an MBE. The above PDE could also be extended to consider nucleation effects, but it is not done here.

The fluxes of the adatoms in the direction of the step's normal are assumed to arise from Fick's first law for steady states and from convection effects:

$$f_+ = -D \nabla \rho_+ \cdot n - v \rho_+ \tag{2.4}$$

$$f_- = D \nabla \rho_- \cdot n + v \rho_-, \tag{2.5}$$

where n is the unit normal of the step that points from the upper to the lower terrace, v is the normal velocity of the step and f_+ (and f_-) is the flux from the upper (and lower resp.) terrace to the step.

Depending on the choice of boundary conditions at a step, the model PDE (2.3) will be called differently. Two common boundary conditions are:

a. *BCF model.*

The adatom density equals the equilibrium density ρ^* on the step, *i.e.*,

$$\rho_+ = \rho_- = \rho^* \tag{2.6}$$

b. *Attachment–Detachment regime.*

The net flux of the adatoms is caused by a deviation of ρ from the equilibrium density at a step; in particular, the net flux is proportional to the deviation, *i.e.*,

$$f_+ = k_+(\rho_+ - \rho^*) \tag{2.7}$$

$$f_- = k_-(\rho_- - \rho^*). \tag{2.8}$$

Here, k_+ and k_- model the kinetic attachment rates from the upper (and lower resp.) terrace to the step.

One might believe, as [BCF51] did, that it makes energetically no difference, whether an attached adatom at a step comes from the upper or from the lower terrace; hence, one could assume that $k_+ = k_-$. This assumption is, in general, incorrect due to the *Ehrlich–Schwoebel* barrier. Ehrlich and Hudda observed in [EH65] by a field ion microscopy that Tungsten atoms on the upper terrace might be reflected at steps. Schwoebel gave in [Sch66] a physical explanation for

this effect: An adatom on the upper terrace must first overcome an energetically unfavourable position with fewer neighbours, *i.e.*, it first has to overcome an energy barrier, before it can be attached to the step.

We finally note limited regimes which are often considered: By assuming mass conservation, the step velocity is proportional to the adatom fluxes,

$$v = f_+ + f_-.$$

At this stage, one can impose simplifying assumptions on the step velocity v. In fact, the differential equation for v incorporates terms $\frac{D}{k_\pm}$ (D diffusion coefficient, $k_\pm$ attachment and detachment rates) and the length ℓ of a terrace.
We speak of *attachment–detachment limited regime* (ADL regime) if we neglect the terrace length ℓ in the ODE for v, *i.e.*, if we assume $\frac{D}{k_\pm} \gg \ell$. This is justified, because the attachment $\frac{D}{k_\pm}$ dominates the diffusion on the terrace. On the other hand, we speak of *diffusion limited regime* (DL regime) if the diffusion governs the attachment, *i.e.*, $\frac{D}{k_\pm} \ll \ell$.
Epitaxial growth has been investigated enormously in the last decades, and attention was drawn for example at

- the derivation of macroscopic PDEs starting from a discrete BCF scheme (e.g. in [MK06]),

- numerical simulations using a level set method (e.g. in [CMO$^+$99]),

- a justification of the relationship between the growth rates of facet and the attachment energy (e.g. in [LB96]),

- a continuum model in the height to describe evaporation–condensation dynamics below the roughening temperature (e.g. in [Spo93]),

- investigation of other models, such as kinetic Monte Carlo with Arrhenius type hopping rates.

2.4 Statistical mechanics

Dobrushin, Kotecký and Shlosman adopted in [DKS92] the statistical mechanics point of view and analysed at low temperature a two–dimensional ferromagnetic Ising model. Excellent mathematical and physical introductions to statistical mechanics and Ising models are for instance [Gal99], [Pre09].

The Ising ferromagnet is modeled on a discrete torus T_N, *i.e.*, it is an $N \times N$ square with periodic boundary conditions, and the admissible spins at a lattice site are ± 1. Further, the Hamiltonian of any spin configuration $\sigma = \{\sigma_t \ : \ t \in T_N\} \in \{-1, 1\}^{T_N}$ is

$$H_h(\sigma) = -\frac{1}{2} \sum_{s,t \in T_N \colon |s-t|=1} J\sigma_s\sigma_t - h \sum_{t \in T_N} \sigma_t. \tag{2.9}$$

Here, $J > 0$ is a positive coupling constant and $h \in \mathbb{R}$ models the "strength" of an external magnetic field. The key statistical ensemble of interest in [DKS92] is the *small canonical one*. In other words, the

- Hamiltonian has no external magnetic field $h = 0$,

- probability distributions are given by densities of Boltzmann type $e^{-\beta H_0}$,

- temperature and total parity are fixed.

Let $\beta = \frac{1}{k_B T}$, where k_B is the Boltzmann constant and T is the temperature, and let R be a total parity that lies between $-\sharp T_N$ and $\sharp T_N$. Then any probability distribution of type

$$\hat{P}_{N,\beta,R}(\sigma) = \begin{cases} \frac{1}{\hat{Z}(N,\beta,R)} \cdot e^{-\beta H_0(\sigma)}, & \text{if } \sum \sigma_t = R \\ 0, & \text{otherwise} \end{cases} \tag{2.10}$$

is called *ferromagnetic Gibbs distribution in the canonical ensemble*. The *partition function* $\hat{Z}$ is a normalising factor and equals

$$\hat{Z}(N,\beta,R) = \sum_{\sigma,\, \sum \sigma_t = R} e^{-\beta H_0(\sigma)}.$$

Dobrushin, Kotecký and Shlosman make use of Peierls' contour argument in [Pei36] and associate unique contours to every spin configuration $\sigma = \{\sigma_t \ : \ t \in T_N\}$: any two neighbouring lattice sites $s, t \in T_N$ of different spins $\sigma_s \neq \sigma_t$ can be separated by a unit bond that is perpendicular to the line segment $\overline{st}$ and that intersects $\overline{st}$ in the midpoint. The collection of all separating bonds then constitutes the set of contours associated to σ.[1]

This construction yields a one–to–two correspondence between a set of contours and a spin configuration. The factor two appears, because the inverted spin configuration, *i.e.*, substituting every $\sigma_t, t \in T_N$, by $-\sigma_t$, has the same set of contours.

The key theorem [DKS92] is now stated.

[1]Note that the contour can be defined more elegantly in the spirit of dual lattices: Because the dual of the square lattice is $(\mathbb{Z}^2)^* = \mathbb{Z}^2 + \binom{1/2}{1/2}$, every unit bond in $(\mathbb{Z}^2)^*$ separates two lattice sites $s, t \in \mathbb{Z}^2$ that have distance $\frac{1}{2}$ from the bond. In the same vein, a unit length bond in $T_N^* = T_N + \binom{1/2}{1/2}$ is a separating bond, whenever there are lattice sites $s, t \in T_N$, $|s - t| = 1$, that are only distance $1/2$ away from the separating bond and that have opposite spins $\sigma_s \neq \sigma_t$.

Theorem. *(Theorem 1.9 in [DKS92]) For any $\rho_0 > \frac{1}{2}$ there exist a parameter β_0 and an open interval I for the mean spin value ρ such that for all $\beta > \beta_0$, for all $\rho \in I$ and for all $\rho_N = R_N/|T_N| \to \rho$ as $N \to \infty$ the probabilities of the sets A_N—to be specified later—tend to one,*

$$\lim_{N\to\infty} \hat{P}_{N,\beta,R_N}(A_N) = 1.$$

The set A_N consists of all configurations σ in $\{-1,1\}^{T_N}$ with total spin $\sum \sigma_t = R_N$ and satisfies, for some constants K and κ, the properties

1. *The family of contours of σ contains exactly one "large" contour Γ_0; all remaining contours are small in the sense that their diameters do not exceed $K \log N$.*

2. *The area $|int\,\Gamma_0|$ of the interior of Γ_0 satisfies the bound*

$$\Big| |int\,\Gamma_0| - \lambda_N N^2 \Big| \leq K N^{6/5} (\log N)^{\kappa},$$

   where λ_N is an explicit constant that depends only on β and ρ_N.

3. *There exists a translation vector x_0 such that the Hausdorff distance d between the shifted "large" contour and the re–scaled Wulff curve $N\gamma_{\lambda_N}$ satisfies*

$$d(x_0 + \Gamma_0, N\gamma_{\lambda_N}) \leq K N^{3/4} (\log N)^{3/2}.$$

   The Wulff curve γ_{λ_N} is obtained by minimising the Curie–Gibbs–Wulff type functional

$$\gamma \mapsto \int_\gamma e_\beta(n) \mathrm{d}\mathcal{H}^1,$$

   among all self–avoiding rectifiable curves subject to the volume constraint $|int\,\gamma| \geq \lambda_N$. Here, e_β is a surface energy density function and emerges from a well–defined

thermodynamic limit.

4. *The length of the contour* Γ_0 *can be estimated by*

$$|\Gamma_0| \leq 2N.$$

5. *The configurations in* A_N *attain the value* -1 *at all lattice sites* $t \in int\Gamma_0$ *whose distance from* Γ_0 *is* $\frac{1}{2}$.

2.5 Numerics for Lennard–Jones clusters

A variety of algorithms has been developed to determine numerically Lennard–Jones (micro-)clusters. These are small monatomic clusters with N atoms for which the total energy is modelled as

$$E(x_1, \ldots, x_N) = \sum_{i \neq j} V(|x_i - x_j|),$$

where V is a Lennard–Jones type potential $V(r) = ar^{-12} - br^{-6}$. Naive algorithms fail to determine a global minimiser for this energy, for it is non–convex and for one expects that the number of local minimisers grows exponentially with N (see for instance [Sti99]).

Global optimisation algorithms could be characterised into two main categories: biased and non–biased methods. A careful review of such methods could be found in [Lea97].

Many approaches work by performing several times the following two steps and by taking the best match among the computed configurations.

Step 1. For fixed particle number, generate a set of initial configurations with preferably low energy.

Step 2. Relax the initial configurations by some numerical algorithm.

Depending on the choice, whether a configuration is (partially) prescribed on some specific positions, like for example a lattice, or whether they are drawn at random, we speak of biased and non–biased methods. We present two promising models, but emphasise that there are a couple of other approaches, such as the minima–hopping and the random tunelling methods or the particle swarm optimisation, that are worth to be studied.

A. Northby's method. In [Nor87] Northby performed the above programme in the biased setting for particle numbers between 13 and 147. His bias is to restrict initial configurations on two specific lattices, namely on the IC and the FC lattices (see [Mac62] and [Nor87] for details), which he considers as "good candidates". The set of initial configurations is found through interchanging an occupied particle with a vacancy and to compare the energies not w.r.t the chosen Lennard–Jones potential, but rather w.r.t. a potential which enhances neighbour–counting.
Only now, the initial configurations are relaxed under some gradient search method w.r.t. the Lennard–Jones potential.

However, some of his simulated global minimisers turned to be false and were corrected in the course of years (see [Lea97] for references of the corrections). For "larger" N Leary found in [Lea97] another counter–example, which is for our purposes very interesting and in agreement with our rigorous result in Chapter 5: For $N = 2142$ he constructed configurations by filling up sites in truncated octahedra with varying cut ratio. His trial configuration was energetically lower than any best performed simulation using Northby's algorithm.

Another method, introduced in [SCC04], is the dynamic lattice search method. It con-

sists again in randomly occupying lattice sites on a specific lattice and in interchanging randomly more than one particle from the "inner" shells with vacancies. Here, the number of interchanged atoms remains constant in every iteration. In [WH12] a modified dynamic lattice search method was used to determine small stable aluminum clusters $Al_{510-800}$ which are again of truncated octahedral shape.

B. Leary's method. Leary gets rid of the bias in [Lea00] by drawing an initial configuration randomly and independently from a Gaussian. Subsequent candidates are then obtained by repeated random perturbation of the initial configuration (again drawn from a Gaussian, but with different parameters) and by relaxing the perturbed states.

His method succeeded in recovering a plenty of putative global minimisers listed in the Cambridge Cluster Database.

Chapter 3

Surface Energy Density

Surface energy densities w.r.t. an ambient lattice are discussed in this chapter. Their concept and interpretation as thermodynamic limits are new. The explicit evaluation of the surface energy densities reduces to calculating a quantity which MacKenzie et al. ([MMN62], [MN62]) determined. Our calculation differs from MacKenzie et al. in the following aspects: (1) it derives rigorously the surface energy density as a unique thermodynamic limit, (2) the resulting surface energy density function is not restricted to specific normals, but is well–defined on the whole sphere, (3) the extension to the whole sphere is explained in terms of fundamental domains of groups, and (4) it omits redundant steps.

Interactions are modeled by the Heitmann-Radin energy (2.1), (2.2). Albeit the explicit values of the surface energy densities is essential to our main concern later on, namely the prediction of the corresponding Wulff shape, we believe that there is a major insight in this chapter that is worth recording:

1. The surface energy density should be calculated in the reciprocal lattice, but represented in Cartesian coordinates.

2. The surface energy density, as a function of the Miller indices, is piecewise 1–homogenous.

We begin by stating the main results in this chapter:

Proposition 3.1. *(Surface Energy Densities for 2D triangular lattices, [AFS12]) The surface energy density for a two–dimensional triangular lattice is given by the* $\frac{\pi}{3}$*–periodic extension of*

$$e^{2D}(v_1, v_2) = 2\left(\frac{v_1}{\sqrt{3}} + v_2\right),$$

where $(v_1, v_2) = (\cos\varphi, \sin\varphi)^T$ *and* $\varphi \in [0, \pi/3]$.

Proposition 3.2. *(Surface Energy Densities for fcc and hcp) The surface energy densities of a face-centered cubic and a hexagonal close–packed lattice are the periodically extended functions*

$$e^{fcc}(n_1, n_2, n_3) = 2n_2 + 4n_3$$

$$e^{hcp}(n_1, n_2, n_3) = \begin{cases} 2\sqrt{2}n_1 + 2\sqrt{6}n_2 + 4\sqrt{3}n_3, & \textit{in region I} \\ 2\sqrt{2}n_1 + \frac{8}{3}\sqrt{6}n_2 + \frac{8}{3}\sqrt{3}n_3, & \textit{in region II} \\ 3\sqrt{2}n_1 + \frac{7}{3}\sqrt{6}n_2 + \frac{8}{3}\sqrt{3}n_3, & \textit{in region III} \\ 3\sqrt{2}n_1 + 3\sqrt{6}n_2 + \frac{4}{3}\sqrt{3}n_3, & \textit{in region IV} \\ 2\sqrt{2}n_1 + \frac{10}{3}\sqrt{6}n_2, & \textit{in region V} \\ 4\sqrt{2}n_1 + \frac{8}{3}\sqrt{6}n_2, & \textit{in region VI.} \end{cases}$$

The above functions are defined on suitably chosen fundamental domains of the respective point groups acting on S^2 *and the regions I–VI will be specified later.*

3.1 Preliminaries

3.1.1 Basic notions

To set the stage for our discussion, we briefly review well–known notions from crystallography. All terms will be introduced in three space dimension, but apply analogously to two dimensions.

Any three linearly independent vectors e_1, e_2 and e_3, called *lattice base vectors*, span a *Bravais lattice* $\mathcal{L}$ through

$$\mathcal{L} = e_1\mathbb{Z} \oplus e_2\mathbb{Z} \oplus e_3\mathbb{Z} = \{ae_1 + be_2 + ce_3 \,:\, a, b, c \in \mathbb{Z}\}.$$

To every lattice base there corresponds a *reciprocal* lattice base $\{b_1, b_2, b_3\}$,

$$b_1 = \frac{e_2 \times e_3}{e_1 \cdot (e_2 \times e_3)},\ b_2 = \frac{e_3 \times e_1}{e_2 \cdot (e_3 \times e_1)},\ b_3 = \frac{e_1 \times e_2}{e_3 \cdot (e_1 \times e_2)},$$

that for itself spans another Bravais lattice $\mathcal{R}$, the so–called *reciprocal lattice*,

$$\mathcal{R} = b_1\mathbb{Z} \oplus b_2\mathbb{Z} \oplus b_3\mathbb{Z} = \{hb_1 + kb_2 + \ell b_3 \,:\, h, k, \ell \in \mathbb{Z}\}.$$

The reciprocal basis can also be found through the identity

$$(b_1 b_2 b_3) = ((e_1 e_2 e_3)^T)^{-1}.$$

In fact, this identity has the advantage that it is also well–defined in other dimensions than three, and can be used in two dimensions.

Lattice vectors $x \in \mathcal{L}$ can be expressed as a linear combination of e_1, e_2, e_3, say $x =$

$ae_1 + be_2 + ce_3$. In that case, we will simply write

$$x = [abc].$$

We further make use of the convention to denote negative integers with a bar, for instance we write $\overline{1}$ for the integer -1. From time to time we will also write $[a, b, c]$, when we believe that this increases legibility.

In the same vein, a rational normal vector n can now be represented in the basis b_1, b_2, b_3, say for example $n = hb_1 + kb_2 + \ell b_3$. These numbers h, k, ℓ are called *Miller indices* of n if h, k, ℓ are integers with greatest common factor 1. In that case we write

$$n = (hk\ell),$$

where we again make use of the convention to equip a negative integer with a bar while omitting its sign, *i.e.*, $\overline{h}$ is the integer $-|h|$.

3.2 Surface energy density

3.2.1 Surface energy density as thermodynamic limit

We need to define carefully what is meant by the surface energy density e. Our model potential energy for a particle configuration $\mathcal{S}_N = \{x_1^{(N)}, \ldots, x_N^{(N)}\} \subset \mathcal{L}$ is defined as

$$E_N(\{x_1^{(N)}, \ldots, x_N^{(N)}\}) := \sum_{i \neq j} V(|x_i^{(N)} - x_j^{(N)}|), \tag{3.1}$$

where V is the Heitmann–Radin potential (2.2). We introduce the associated surface energy similar to Gibbs (see page 386 in [Gib78]), namely as the excess between the energy in (3.1) and the energy that the same particle configuration attains in an infinitely large crystal, *i.e.*, as

$$SE_N(\{x_1^{(N)}, \dots, x_N^{(N)}\}) := E_N(\{x_1^{(N)}, \dots, x_N^{(N)}\}) + E_b \cdot N, \tag{3.2}$$

The quantity E_b denotes the bulk energy per particle

$$E_b := \left| \min_N \min_{\mathcal{S}_N} \sum_{x \in \mathcal{S}_N} V(|x|) \right|, \tag{3.3}$$

where the second minimisation is taken over every N–particles configuration in $\mathbb{R}^3$ ($\mathbb{R}^2$ resp.) with mutual particle distance larger equal one. The number E_b equals 6 in two dimensions and is 12 in three dimensions.

In fact, the determination of E_b is well–known as the kissing number problem and goes back to the end of the 17th century. David Gregory argued that there can be 13 non–overlapping balls of unit volume that touch a given unit ball, whereas Isaac Newton believed 12 was the proper answer. Although this question possesses a striking clarity and simplicity, the proof in three dimensions took almost three hundred years (see for instance [CS99], [SvdW53], [Lee56] and for a newer proof see [Mae01]).

We assume that atoms crystallise into a given Bravais lattice $\mathcal{L}$ with unit lattice constant.

To introduce the surface energy density along a cutting hyperplane H^n with normal $n \in S^2$, we define the cut crystal $\mathcal{L}^n$ and its boundary $\partial\mathcal{L}^n$ by

$$H^n := \{x \in \mathbb{R}^3 \, : \, \langle x, n \rangle = 0\}, \tag{3.4}$$

$$\mathcal{L}^n := \{x \in \mathcal{L} \ : \ \langle x, n\rangle \leq 0\}, \tag{3.5}$$

$$\partial\mathcal{L}^n := \{x \in \mathcal{L}^n \ : \ \sharp\{x' \in \mathcal{L}^n \ : \ |x - x'| = 1\} < E_b\}, \tag{3.6}$$

where E_b is the number of first neighbours, in other words $E_b = \sharp\{x \in \mathcal{L} \ : \ |x| = 1\}$. Now the bracketed quantity in the following expression

$$\frac{1}{\text{area}(B_R \cap H^n)} \cdot \Bigg(\sum_{\substack{x \in \partial\mathcal{L}^n \cap B_R, \\ y \in \mathcal{L}^n \cap B_R}} V(|x - y|) + E_b \cdot \sharp(\partial\mathcal{L}^n \cap B_R) \Bigg) \tag{3.7}$$

compares the summed–up energy excesses between the boundary atoms in $\partial\mathcal{L}^n \cap B_R$ with the energy that would arise if the atoms were bulk atoms; thus, it can be interpreted as a surface energy along the cutting plane H^n. Motivated by this viewpoint, we now define the surface energy density as follows:

Definition 3.3. (Surface energy density)
Let $\mathcal{L}$ be a Bravais lattice with lattice constant 1, $n \in S^2$, $H^n, \mathcal{L}^n$ and $\partial\mathcal{L}^n$ be defined as in (3.4), (3.5) and (3.6).
Then the *surface energy density* is defined as the function $e : S^2 \to \mathbb{R}$,

$$e(n) := \lim_{R\to\infty} \frac{1}{\text{area}(B_R \cap H^n)} \cdot \Bigg(\sum_{\substack{x \in \partial\mathcal{L}^n \cap B_R, \\ y \in \mathcal{L}^n \cap B_R}} V(|x - y|) + E_b \cdot \sharp(\partial\mathcal{L}^n \cap B_R) \Bigg). \tag{3.8}$$

Our definition of e can be thought of as a thermodynamic limit of the quantity (3.7), because the number of involved particles grows as B_R approaches $\mathbb{R}^3$. A more accurate way, to state this, is to say that (B_R) is a cofinal sequence for $\mathbb{R}^3$. Note that the function e is only dependent on the crystal lattice $\mathcal{L}$, which is prescribed.
We introduce a bond graph on $\mathcal{L}$: This is the graph with vertices in $\mathcal{L}$. Two vertices connect an edge if and only if their mutual distance equals 1. Then the bracketed

quantity in the definition of e,

$$\sum_{\substack{x\in\partial\mathcal{L}^n\cap B_R,\\ y\in\mathcal{L}^n\cap B_R}} V(|x-y|) + E_b \cdot \sharp(\partial\mathcal{L}^n \cap B_R),$$

can be interpreted graphically: It counts the number of edges which intersect $B_R \cap H^n$. Thus it is desirable to find an expression which evaluates explicitly the number of such edges crossing the area $B_R \cap H^n$; we call such edges *broken bonds*.

3.2.2 Calculation of e

We make the convention to only consider bonds/edges which have at least one vertex lying in the half–plane $\{x \in \mathbb{R}^3 \ : \ \langle x, n\rangle < 0\}$.

A necessary condition for a bond u to be broken is that the angle between the projection of u onto the chosen normal n of the hyperplane is smaller than $\frac{\pi}{2}$. In other words, we require that $\langle u, n\rangle$ is positive (see Figure 3.1 for an illustration).

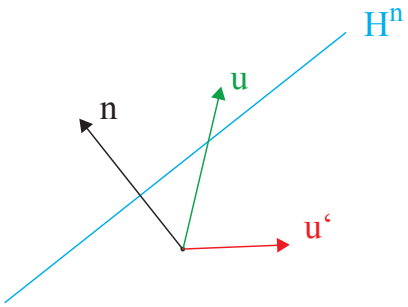

Figure 3.1: The green bond u is a broken bond, because the angle between u and n is obviously smaller than $\pi/2$, whereas u' is not broken, because the angle is strictly larger than $\pi/2$.

Motivated by this observation, we define the set of all broken bonds as

$$B(n) := \{u : u \in B, \langle n, u\rangle > 0\},$$

where B is the set of admissible broken bonds. For the purposes of this thesis,

$$B := \{u \in \mathcal{L} \ : \ |u| = 1\}$$

is the set of all first–neighbours in the lattice $\mathcal{L}$. This set B could be easily modified to only comprise second–neighbours: the condition $|u| = 1$ needs only be substituted by $|u| = c$, where c is the second–neighbour distance.

Remember that the necessary condition for u to be broken is $\langle u, n\rangle > 0$. In other words, a bond u (–irrespective to which particle it is attached–) can only be broken if its projective part along n is positive. Therefore, particles x for which the bond u is broken must lie between the planes

$$\{x \in \mathbb{R}^3 \ : \ \langle x, n\rangle = 0\}, \qquad \{x \in \mathbb{R}^3 \ : \ \langle x, n\rangle = \langle u, n\rangle\}.$$

These two planes are parallel and have mutual distance $\frac{1}{|n|}\langle u, n\rangle$. Note that this distance is also the volume of a cylinder with rectangular bases in these planes and unit base area (see Figure 3.2). Now divide the cylinder volume by the volume V of a primitive unit cell, to get the number of particles x in the cylinder for which the bond u is broken:

$$\sharp\,\text{cylinder particles with broken}\,u := \begin{cases} \frac{\langle u,n\rangle}{V|n|}, & \text{if } \langle u, n\rangle \geq 0, \\ 0, & \text{else.} \end{cases} \tag{3.9}$$

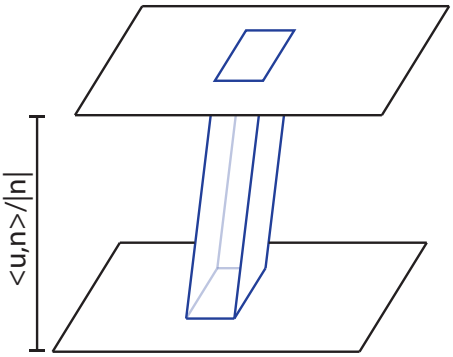

Figure 3.2: Two parallel planes at a distance $\frac{1}{|n|}\langle u, n\rangle$. The bases of the blue cylinder have unit area and the volume of the cylinder itself is the interplanar distance $\frac{1}{|n|}\langle u, n\rangle$.

A summation over all admissible broken bonds yields the total number of broken bonds for all particles in the cylinder, *i.e.*,

$$\sharp\,\text{broken bonds in cylinder} = \sum_{u\in B(n)} \frac{\langle u, n\rangle}{V|n|} = \tilde{e}(n). \tag{3.10}$$

The function $\tilde{e}$ can be expressed by introducing yet another auxiliary function ρ:

$$\rho : S^2 \to \mathbb{R}^3, \qquad \rho(n) := \sum_{u\in B(n)} u. \tag{3.11}$$

This function could be understood as the "averaged direction" of the broken bonds for the normal n. Note that ρ is a step function on S^2, because ρ is constant on the following open neighbourhood of n:

$$U(n) := \{n' \in S^2 \ : \ B(n') = B(n)\} = \bigcap_{u\in B(n)} \{n' \in S^2 \ : \ \langle u, n'\rangle > 0\}.$$

By construction, every normal n' in $U(n)$ has broken bond set $B(n)$. From the facts that $B(n)$ is an element of the power set of B and the finiteness of 2^B we infer that there must exist finitely many $n_1, \ldots, n_m$ such that

$$\rho = \sum_{i=1}^{m} a_i \chi_{\overline{U(n_i)}}, \tag{3.12}$$

where $a_i = \sum_{u \in B(n_i)} u$ and $\bigcup \overline{U(n_i)} = S^2$; hence, equation (3.10) can be re–written as

$$\tilde{e}(n) = \frac{1}{V|n|} \langle \rho(n), n \rangle . \tag{3.13}$$

To put it simple, by (3.9) the function $\tilde{e}$ counts the number of cylinder particles for which the averaged–direction–bond (–no account is taken for the length–) $\rho(n)$ is broken.

Now, the set $B_R \cap H^n$ can be partitioned by the rectangular cylinder bases up to an area of order R. Therefore, the area of $B_R \cap H^n$ times $\tilde{e}(n)$ equals up to an error of order $O(R)$ the number of broken bonds which intersect $B_R \cap H^n$. In other words,

$$\sum_{\substack{x \in \partial\mathcal{L}^n \cap B_R, \\ y \in \mathcal{L}^n \cap B_R}} V(|x-y|) - E_b \cdot \sharp(\partial\mathcal{L}^n \cap B_R) = \text{area}(B_R \cap H^n)\tilde{e}(n) + O(R),$$

establishing finally,

$$e(n) = \lim_{R \to \infty} \frac{\text{area}(B_R \cap H^n) \cdot \tilde{e}(n) + O(R)}{\text{area}(B_R \cap H^n)} = \tilde{e}(n).$$

Our thermodynamic surface energy density e can therefore be calculated by $\tilde{e}$ and we identify $\tilde{e}$ with e.

Indeed, the calculation of $\tilde{e}$, *i.e.*, the number of broken bonds per unit surface area, can be further simplified by using the point symmetry group of the lattice, for one could extend $\tilde{e}$ to the sphere S^2, once it is determined on a fundamental domain. A further simplification is to investigate only rational normals in a fundamental domain, then to extend the function by continuity to the fundamental domain and finally to S^2 by periodic extension according to the point group.

3.2.3 Fundamental domain and extension to sphere

Much of our calculation could be reduced by considering the *point group* and a *fundamental domain* of the lattice. The point group G of a Bravais lattice $\mathcal{L}$ is defined as the finite subgroup of $O(3)$ (or $O(2)$ in two dimensions):

$$G := \{R \in O(3) \ : \ R\mathcal{L} = \mathcal{L} \text{ and } \exists x \in \mathcal{L} : \ Rx = x \ \}.$$

In other words, G contains all orthogonal matrices that leave at least one point in the lattice fixed and that keep the lattice invariant. We will neither classify point groups, nor will we introduce the customary *Schönflies* and *orbifold* notations to denote point groups, because this would go beyond the scope of this thesis.
The quotient group S^2/G could be written as the union of orbits

$$S^2/G = \bigcup_{n \in S^2} orb_G(n),$$

where the orbit of n is Gn, and a fundamental domain of G acting on the sphere S^2 is a family of representatives of the quotient group S^2/G.
So, how does this concept help us? Calculations of the surface energy density must

only be performed on a fundamental domain, because the function e is constant on every orbit of G; the value in an orbit is the calculated value of the representative in the chosen fundamental domain.

Our programme to determine the surface energy density can be summarised as follows.

Step–by–step calculation of surface energy density

1. Choose a connected fundamental domain of the point group acting on S^2.

2. Fix the set of admissible bonds B as the set of all first–neighbours.

3. Determine the set of broken bonds $B(n)$ at all rational normals n in the chosen fundamental domain.

4. Calculate $e(n) = \dfrac{1}{V|n|} \langle \rho(n), n \rangle$.

5. Extend $\tilde{e}$ continuously to the fundamental domain and then to S^2.

The representation of e in the third step and equation (3.12) immediately show that e is piecewise 1–homogenous on the sets $U(n_i)$, $i = 1, \ldots, m$.
Indeed, note that $\langle u, n \rangle$ is an integer for all $u \in \mathcal{L}$. This follows from the fact that each of the reciprocal lattice base vectors b_i is orthogonal to two lattice base vectors and parallel to the remaining lattice base vector. From $u = [abc]$, $n = (hk\ell)$ and $\langle e_i, b_j \rangle = \delta_{ij}$ we infer

$$\begin{aligned} \langle u, n \rangle &= \langle ae_1 + be_2 + ce_3, hb_1 + kb_2 + \ell b_3 \rangle \\ &= ah \langle e_1, b_1 \rangle + bk \langle e_2, b_2 \rangle + c\ell \langle e_3, b_3 \rangle \\ &= ah + bk + c\ell \in \mathbb{Z}. \end{aligned} \tag{3.14}$$

3.3 Calculations for 2D triangular lattice

The two–dimensional triangular lattice $\mathcal{L}^{2D}$ is spanned by the base vectors

$$e_1 := \begin{pmatrix} -1/2 \\ \sqrt{3}/2 \end{pmatrix}, \qquad e_2 := \begin{pmatrix} 1 \\ 0 \end{pmatrix}$$

and the set of admissible broken bonds is

$$B = \{[10],\, [01],\, [11],\, [\overline{1}0],\, [0\overline{1}],\, [\overline{11}]\}.$$

Due to the symmetry of the lattice, the calculation of e may be restricted to normals $n = (n_1 n_2)^T$ that are rational, *i.e.*, for which there exist Miller indices $h, k \geq 0$ such that $n = (hk)$ in the reciprocal lattice. For such normals n the set of broken bonds $B(n)$ is given by the first three bonds above; the remaining three bonds are not broken for sign reasons. In formula,

$$B(n) = \{[10],\, [01],\, [11]\}.$$

The averaged–direction function ρ simplifies to

$$\rho(n) = \sum_{u \in B(n)} u = [22] = 2\begin{pmatrix} 1 \\ 0 \end{pmatrix} + 2\begin{pmatrix} -1/2 \\ \sqrt{3}/2 \end{pmatrix} = \begin{pmatrix} 1 \\ \sqrt{3} \end{pmatrix}$$

yielding the explicit value for the surface energy density e:

$$e(n_1, n_2) = \frac{1}{V|n|} \langle \rho(n), n \rangle = \frac{1}{V|n|}(n_1 + \sqrt{3} n_2) \tag{3.15}$$

$$= \frac{2}{|n|} \left(\frac{n_1}{\sqrt{3}} + n_2 \right), \tag{3.16}$$

where we have used that $V = \frac{\sqrt{3}}{2}$ is the volume of a Voronoi cell in $\mathcal{L}^{2D}$. With a slight abuse of notation, e can be represented in polar coordinates by setting $n = \binom{n_1}{n_2} = \binom{\cos\varphi}{\sin\varphi}$, $\varphi \in \left[0, \frac{\pi}{3}\right]$:

$$e(\varphi) = 2\left(\frac{\cos\varphi}{\sqrt{3}} + \sin\varphi\right).$$

Note that this is exactly the surface energy density function in Theorem 5.1 in [AFS12] and this completes the proof of Proposition 3.1.

3.4 Calculations for 3D fcc and hcp crystals

3.4.1 Face–centered cubic crystals

The face–centred cubic lattice is defined as $\mathcal{L}^{fcc} := e_1\mathbb{Z} + e_2\mathbb{Z} + e_3\mathbb{Z}$, where

$$e_1 := \frac{1}{\sqrt{2}}\begin{pmatrix}0\\1\\1\end{pmatrix}, e_2 := \frac{1}{\sqrt{2}}\begin{pmatrix}1\\0\\1\end{pmatrix}, e_3 := \frac{1}{\sqrt{2}}\begin{pmatrix}1\\1\\0\end{pmatrix}.$$

The reciprocal base vectors are,

$$b_1 := \frac{\sqrt{2}}{2}\begin{pmatrix}-1\\1\\1\end{pmatrix}, b_2 := \frac{\sqrt{2}}{2}\begin{pmatrix}1\\-1\\1\end{pmatrix}, b_3 := \frac{\sqrt{2}}{2}\begin{pmatrix}1\\1\\-1\end{pmatrix}.$$

Fundamental domain. We explicitly determine the point group of the face–centred cubic lattice, because they play a crucial role in the subsequent chapters. It suffices to consider the 1–neighbourhood cell of any point in the lattice $\mathcal{L}^{fcc}$, e.g. of the origin, that is to say, we consider all $x \in \mathcal{L}^{fcc}$ with $|x| = 1$.

The point group consists of exactly all rotations with rotation axis passing through the origin such that it keeps the 1–neighbourhood invariant. The 24 rotations that keep the mid–point fixed and that keep the cell invariant are listed below (Figure 3.3 shows a typical 1–neighbourhood cell with three rotation axis.)

quantity	rotation axis
3	4–fold axis passing through the midpoints of two opposite squares, allowed angles of rotation: $\frac{\pi}{2}, \pi$ and $\frac{3}{2}\pi$
4	3–fold axis passing through the midpoints of two opposite triangles, allowed angles of rotation: $\frac{2}{3}\pi, \frac{4}{3}\pi$
6	2–fold axis passing through two opposite vertices on the mid–plane, allowed angle of rotation: π
1	1–fold axis (identity) allowed angle of rotation: 0

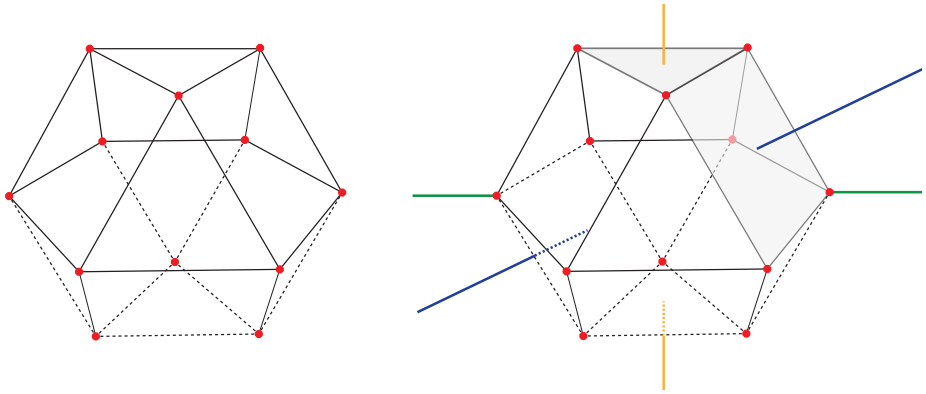

Figure 3.3: Left: 1–neighbourhood cell at $x \in \mathcal{L}^{fcc}$ w.r.t. the face–centred cubic lattice is a cuboctahedron centred at x. The dashed lines display the "lower" half of the 1–neighbourhood cell. The red circles represent the first neighbours of x, *i.e.*, all $y \in \mathcal{L}^{fcc}$ such that $|x - y| = 1$, and the edges represent the bonds among the neighbours of x. Right: The blue line shows a 4–fold, the orange line shows a 3–fold and the green line shows a 2–fold rotation axis.

This point group is called the octahedral point group O_h (in Schönflies notation) or simply $*432$ (in orbifold notation) and a fundamental domain is for example a spherical triangle with angles $\frac{\pi}{4}, \frac{\pi}{3}, \frac{\pi}{2}$. We therefore restrict to normals n of the form

$$n = hb_1 + kb_2 + \ell b_3, \qquad h \geq k \geq \ell \geq 0,$$

Step 1. (Admissible broken bonds)

The set of admissible broken bonds is

$$[1,0,0],\ [0,1,0],\ [\overline{1},0,0],\ [0,\overline{1},0],\ [1,\overline{1},0],\ [\overline{1},1,0], \tag{3.17}$$

$$[0,0,1],\ [0,\overline{1},1],\ [\overline{1},0,1],\ [0,0,\overline{1}],\ [0,1,\overline{1}],\ [1,0,\overline{1}]. \tag{3.18}$$

By equation (3.9) we only need to take those bonds into consideration for which its inner product with $n = (hk\ell)$ is positive for $h \geq k \geq \ell \geq 0$, so

$$B(n) \subseteq \{[1,0,0],\ [0,1,0],\ [1,\overline{1},0],\ [\overline{1},1,0], [0,0,1], \tag{3.19}$$

$$[0,\overline{1},1],\ [\overline{1},0,1],\ [0,1,\overline{1}],\ [1,0,\overline{1}]\} \tag{3.20}$$

Step 2. (Calculation of broken bonds)

Since the bonds $[1,0,0]$, $[0,1,0]$, $[0,0,1]$ always have positive inner product with (hkl) whenever $h, k, \ell \geq 0$, these three bonds are always broken.

Furthermore, the bonds $[1,\overline{1},0]$, $[0,1,\overline{1}]$ and $[1,0,\overline{1}]$ are always broken, because of $h \geq k \geq \ell \geq 0$. The remaining six bonds in $B(n)$ are never broken. For example $[\overline{1},1,0]$ is not broken, since this implies $k \geq h \geq 0$. Therefore the set of broken bonds $B(n)$ for

any $n = (hk\ell)$, $h \geq k \geq \ell \geq 0$, is given by

$$B(n) = \left\{ [1,0,0],\ [0,1,0],\ [0,0,1],\ [1,\overline{1},0],\ [0,1,\overline{1}],\ [1,0,\overline{1}] \right\}.$$

So, the resulting density e^{fcc} for a unit normal $n = (n_1 n_2 n_3)^T$ in Cartesian coordinates is:

$$e^{fcc}(n) = \frac{1}{\Omega|n|} \sum_{u \in B(n)} \langle u, n \rangle = \frac{1}{\Omega|n|} \left\langle n, \sum_{u \in B} u \right\rangle = \frac{1}{\Omega|n|} \left\langle n, [31\overline{1}] \right\rangle \tag{3.21}$$

$$= \frac{1}{\Omega|n|} \langle n, 3e_1 + e_2 - e_3 \rangle = \frac{1}{\Omega|n|} (\sqrt{2} n_2 + 2\sqrt{2} n_3) \tag{3.22}$$

$$= 2n_2 + 4n_3, \tag{3.23}$$

where we have made use of the fact that the volume of a primitive unit cell is $\frac{\sqrt{2}}{2}$. Let us record the values of e at a 2–fold, 3–fold and a 4–fold axis in the chosen fundamental domain; in particular, e attains these values at all rotation axis by reasons of extension.

axis	reciprocal coordinate	Cartesian coordinate	value of e
2–fold	$(2,1,1)$	$\frac{\sqrt{2}}{2}(0,1,1)^T$	$3\sqrt{2} \approx 4.243$
3–fold	$(1,1,1)$	$\frac{\sqrt{3}}{3}(1,1,1)^T$	$2\sqrt{3} \approx 3.461$
4–fold	$(1,1,0)$	$(0,0,1)^T$	4

3.4.2 Hexagonal close–packed crystals

A hexagonal close–packed crystal can be thought of as the union of two identical Bravais lattices spanned by

$$e_1 := \begin{pmatrix} -\frac{1}{2} \\ \frac{\sqrt{3}}{2} \\ 0 \end{pmatrix}, \; e_2 := \begin{pmatrix} 1 \\ 0 \\ 0 \end{pmatrix}, \; e_3 := \begin{pmatrix} 0 \\ 0 \\ \frac{2}{3}\sqrt{6} \end{pmatrix},$$

that is to say,

$$\mathcal{L}^{hcp} := \delta s + e_1\mathbb{Z} + e_2\mathbb{Z} + e_3\mathbb{Z}, \qquad \delta \in \{0, 1\},$$

where $s = \frac{1}{6}[243]$ denotes the shift vector. Remember that [243] is the representation w.r.t. e_1, e_2, e_3 and means $2e_1 + 4e_2 + 3e_3$.

The point group of hcp is D3h (in Schönflies notation) or $*223$ and consists of the following six rotations that keep the origin fixed:

quantity	rotation axis
0	4–fold axis passing through the midpoints of two opposite squares,
1	3–fold axis perpendicular to the mid–plane,
	allowed angles of rotation: $\frac{2}{3}\pi, \frac{4}{3}\pi$
3	2–fold axis passing through two opposite vertices on the mid–plane,
	allowed angle of rotation: π
1	1–fold axis (identity)
	allowed angle of rotation: 0

A fundamental domain would be a spherical triangle with angles $\frac{\pi}{2}, \frac{\pi}{2}, \frac{\pi}{3}$ and is sketched in Figure 3.4.

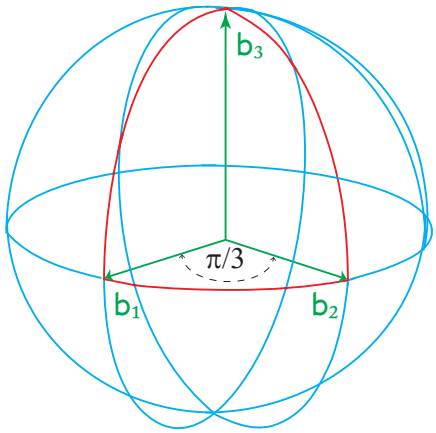

Figure 3.4: A fundamental domain of hcp is given by the red spherical triangle. The base vectors b_1, b_2 and b_3 are the reciprocal lattice base vectors corresponding to e_1, e_2, e_3. The vectors b_1, b_3 and b_2, b_3 are perpendicular to each other.

It therefore suffices to restrict our calculations to $h, k, \ell \geq 0$.

Step 1. (Admissible broken bonds)

The set of admissible broken bonds depends on whether δ is zero or one. We first list all lattice points that have, independent of δ, the distance 1 from a point given $x \in \mathcal{L}$. Bonds that are definitely not broken will be displayed in blue.

$$[100],\ [010],\ [110],\ [\bar{1}00],\ [0\bar{1}0],\ [\bar{1}10]. \tag{3.24}$$

In case $\delta = 0$, the above list is extended by the following bonds

$$\frac{1}{6}[243],\ \frac{1}{6}[2\bar{2}3],\ \frac{1}{6}[\bar{4}23],\ \frac{1}{6}[24\bar{3}],\ \frac{1}{6}[2\bar{2}\bar{3}],\ \frac{1}{6}[\bar{4}2\bar{3}], \tag{3.25}$$

and in the remaining case $\delta = 1$, the further bonds are

$$\frac{1}{6}[\overline{2}43],\ \frac{1}{6}[423],\ \frac{1}{6}[\overline{2}23],\ \frac{1}{6}[\overline{243}],\ \frac{1}{6}[42\overline{3}],\ \frac{1}{6}[\overline{2}2\overline{3}]. \tag{3.26}$$

We now list in detail the regions in which the above bonds are broken. To do this, we need to recall that a bond $[abc]$ is broken if $\langle n, [abc]\rangle > 0$. Therefore, the normals for which the bond $[abc]$ is broken is bounded by the hyperplane $\langle n, [abc]\rangle = 0$. As we restrict our calculations to a fundamental domain, the region in which a bond is broken is separated by a great circle, namely the intersection of the hyperplane with the fundamental domain. In the following we list for each admissible bond its corresponding region in the fundamental domain, in which it is broken.

bond	**region**	**bond**	**region**
$[100]$	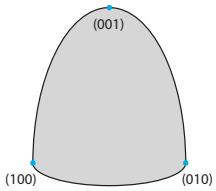	$\frac{1}{6}[24\overline{3}]$	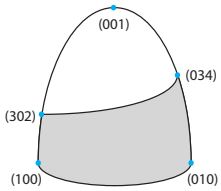
$[010]$	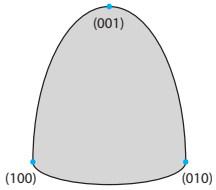	$\frac{1}{6}[2\overline{23}]$	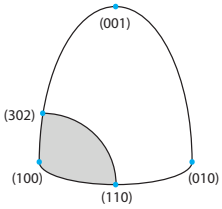

bond	region	bond	region
$[110]$	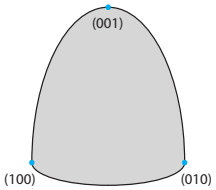	$\frac{1}{6}[\overline{2}43]$	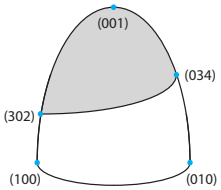
$\frac{1}{6}[243]$	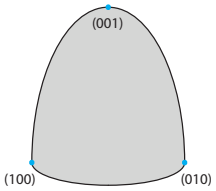	$\frac{1}{6}[423]$	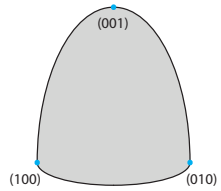
$\frac{1}{6}[2\overline{2}3]$	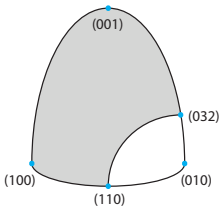	$\frac{1}{6}[\overline{2}23]$	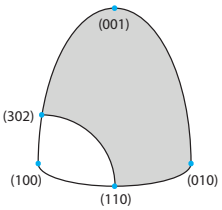
$\frac{1}{6}[\overline{4}23]$	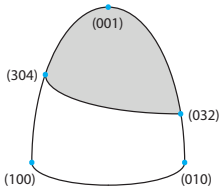	$\frac{1}{6}[42\overline{3}]$	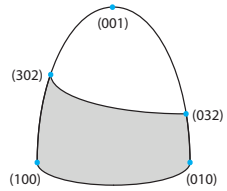
$\frac{1}{6}[\overline{2}2\overline{3}]$	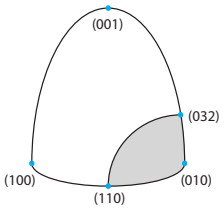		

One easily sees that the fundamental domain is divided into six regions:

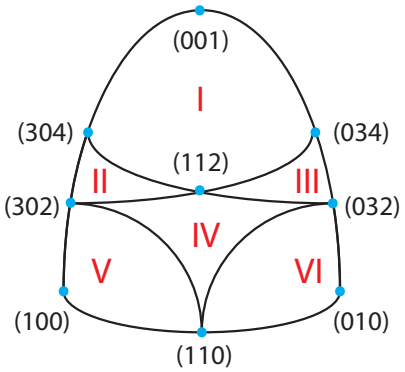

Figure 3.5: Regions I–VI in which the sum of broken bonds remain constant.

In each of these six regions the set of broken bonds remains constant:

region	**broken bonds**	**sum of broken bonds**
I	$[100],\ [010],\ [110],\ [423],\ [243]$ $[2\overline{2}3],\ [\overline{2}23],\ [2\overline{2}3],\ [\overline{42}3]$	$\begin{pmatrix} 4 \\ 4 \\ 3 \end{pmatrix}$
II	$[100],\ [010],\ [110],\ [423],\ [243]$ $[2\overline{2}3],\ [\overline{2}23],\ [\overline{24}3],\ [42\overline{3}]$	$\begin{pmatrix} 5\frac{1}{3} \\ 4\frac{2}{3} \\ 2 \end{pmatrix}$
III	$[100],\ [010],\ [110],\ [423],\ [243]$ $[2\overline{2}3],\ [\overline{42}3],\ [24\overline{3}],\ [\overline{2}23]$	$\begin{pmatrix} 4\frac{2}{3} \\ 5\frac{1}{3} \\ 2 \end{pmatrix}$

region	**broken bonds**	**sum of broken bonds**
IV	$[100],\ [010],\ [110],\ [423],\ [243]$	$\begin{pmatrix} 6 \\ 6 \\ 1 \end{pmatrix}$
	$[2\overline{2}3],\ [24\overline{3}],\ [\overline{2}23],\ [42\overline{3}]$	
V	$[100],\ [010],\ [110],\ [423],\ [243]$	$\begin{pmatrix} 6\frac{2}{3} \\ 5\frac{1}{3} \\ 0 \end{pmatrix}$
	$[2\overline{2}3],\ [24\overline{3}],\ [2\overline{2}\overline{3}],\ [42\overline{3}]$	
VI	$[100],\ [010],\ [110],\ [423],\ [243]$	$\begin{pmatrix} 5\frac{1}{3} \\ 6\frac{2}{3}k \\ 0 \end{pmatrix}$
	$[24\overline{3}],\ [\overline{2}23],\ [42\overline{3}],\ [\overline{2}2\overline{3}]$	

The surface energy density e^{hcp} is

$$e^{hcp}(n) = \frac{1}{V|n|} \sum_{u \text{ broken bond}} \langle n, u \rangle , \tag{3.27}$$

where V is the volume of a Voronoi cell in $\mathcal{L}^{hcp}$ and equals $\frac{\sqrt{2}}{2}$ for the lattice parameter one.

Table 3.4.2 and equation (3.27) deliver the surface energy density in question:

$$e^{hcp}(n) = \begin{cases} 2\sqrt{2}n_1 + 2\sqrt{6}n_2 + 4\sqrt{3}n_3, & \text{in region I} \\ 2\sqrt{2}n_1 + \frac{8}{3}\sqrt{6}n_2 + \frac{8}{3}\sqrt{3}n_3, & \text{in region II} \\ 3\sqrt{2}n_1 + \frac{7}{3}\sqrt{6}n_2 + \frac{8}{3}\sqrt{3}n_3, & \text{in region III} \\ 3\sqrt{2}n_1 + 3\sqrt{6}n_2 + \frac{4}{3}\sqrt{3}n_3, & \text{in region IV} \\ 2\sqrt{2}n_1 + \frac{10}{3}\sqrt{6}n_2, & \text{in region V} \\ 4\sqrt{2}n_1 + \frac{8}{3}\sqrt{6}n_2, & \text{in region VI,} \end{cases} \tag{3.28}$$

where the regions are spherical triangles with vertices from Figure 3.5; region IV is the union of two spherical triangles with vertices at $(302), (112), (110)$ and $(112), (110), (032)$. This establishes Proposition 3.2.

Chapter 4

Compactness and Formation of Clusters

Section 4.1 is joint work with G. Friesecke and B. Schmidt and was published in [AFS12]. Section 4.2 for the three dimensional case is new.

In this chapter we show for a prototype model that the key aspects (1) formation of a local lattice structure and (2) the emergence of an overall geometric (Wulff) shape of the atomistic minimiser can be derived as a consequence of surface energy minimisation. We begin by stating our model: We consider N particles $x_1, \dots, x_N$ in $\mathbb{R}^d$, $d = 2, 3$, with total energy

$$E(x_1, \dots, x_N) = \sum_{i \neq j} V(|x_i - x_j|), \tag{4.1}$$

where V is a short–range potential that will be specified below. In this chapter we will prove, that, in the limit $N \to \infty$, a particular overall geometric shape emerges as a weak$*$ limit of re–scaled empirical measures associated to low energy configurations.

While the boundedness assumption on the surface energy is enough in two dimensions, an additional condition on the boundedness of diameters is required to ensure compactness in three space dimensions.
The identification of the geometric shape is then performed in Chapter 5.

One of the key ideas to describe the macroscopic shape is to abandon the popular Lagrangian coordinates for the N–particle configurations, and instead to make use of Eulerian coordinates. A particle configuration $\{x_1, \dots, x_N\}$ is therefore not interpreted as the deformation of some a priori prescribed reference configuration. We rather associate to a configuration $\{x_1, \dots, x_N\}$ its empirical measure $\sum_{i=1}^N \delta_{x_i}$. Note that this representation does neither require an artificial reference configuration, nor does it restrict a particle to only interact with specific particles. This is in contrast to the Lagrangian viewpoint, because the assumption on orientation preservation of deformations constrains the interaction range. The usage of empirical measures is common in the statistical mechanics community, but is less popular for atomistic–to–continuum limits. It was recently used by S. Capet and G. Friesecke in the study of many–particle energies in the context of Coulomb systems.

The strategy is exactly as in the joint paper with G. Friesecke and B. Schmidt [AFS12]:

(1) Associate to any N–particle configuration $\{x_1, \dots, x_N\}$ its empirical measure $\sum_{i=1}^N \delta_{x_i}$.

(2) Re–scale the empirical measure to keep the mass and the expected diameter of the support of order one as $N \to \infty$.

(3) Show that the limit measure is a constant multiple of a characteristic function of a set of finite perimeter. Identify the constant as the density of atoms per unit volume in $\mathcal{L}^{2D}$ or in $\mathcal{L}^{fcc}$ resp.

(4) Derive, from atomistic energy minimisation, a Wulff–Herring type variational principle for the shape, by Gamma–convergence.

(5) Appeal to unique solubility of the Wulff–Herring type variational principle (cf. Taylor [Tay75], Fonseca–Müller [FM91]) to identify the shape.

The rest of this chapter is organised as follows:

Section 4.1 addresses the two–dimensional case. It is a joint work with G. Friesecke and B. Schmidt and was published in [AFS12]. The steps (1)–(3) are performed for a short–range interaction potential with a sufficiently narrow potential well. No assumption on crystalline configurations is needed and even "small" cracks, vacancies and elastic deformations are allowed; in particular, these irregularities do not influence the emergence of a cluster.

Section 4.2 carries out steps (1)–(3) in three dimensions for short–range interaction potentials with a sufficiently narrow potential well. We impose the additional assumption of bounded diameters. Under these assumptions, low energy configurations that belong to some close–packed lattice exhibit a cluster formation. In the language of analysis, we rigorously prove that the weak$*$ limit of the corresponding sequence of re–scaled empirical measures is given by a constant multiple of a characteristic function over a cluster set of prescribed finite perimeter and prescribed volume. The latter result applies in particular to low energy configurations belonging to the face–centred cubic lattice $\mathcal{L}^{fcc}$ or to the hexagonal close–packed lattice $\mathcal{L}^{hcp}$.

4.1 Two dimensions

This Section 4.1 is joint work with G. Friesecke and B. Schmidt and was published in [AFS12].

The first result is not limited to minimisers, but applies to arbitrary states whose energy difference from the ground state is of order $O(N^{1/2})$.

Theorem 4.1. *(Formation of clusters with constant density and finite perimeter) Suppose the energy E is given by (4.1) and the interatomic potential satisfies (H1), (H2), (H3). Let $\{x_1^{(N)}, \dots, x_N^{(N)}\}$ be any sequence of connected (see definition below on page 62) N–particle configurations satisfying an energy bound of form*

$$E(\{x_1^{(N)}, \dots, x_N^{(N)}\}) \leq -6N + CN^{1/2}$$

for some constant C independent of N. Let $\{\mu_N\}$ be the associated sequence of re–scaled empirical measures

$$\mu_N = \frac{1}{N} \sum_{i=1}^{N} \delta_{\frac{x_i^{(N)}}{\sqrt{N}}}. \tag{4.2}$$

Then:

(i) Up to translation (that is to say, up to replacing μ_N by $\mu_N(\cdot + a_N)$ for some $a_N \in \mathbb{R}^2$) and passage to a subsequence, μ_N converges weak in $\mathcal{M}(\mathbb{R}^2)$ to $\mu \in \mathcal{M}(\mathbb{R}^2)$.*

(ii) The limit measure is of the form

$$\mu = \rho \chi_E,$$

*where $\rho = 2/\sqrt{3}$ (*i.e.*, the density of atoms per unit volume of the triangular lattice $\mathcal{L}$) and E is a set of finite perimeter of volume $1/\rho$.*

In fact, any set E of finite perimeter and volume $1/\rho$ can occur in the limit, as we prove in Section 4.1.3.

Note also that on the atomistic level, quite irregular configurations are admitted by our hypotheses. For instance the approximating atomistic configurations may contain elastic deformations, cracks and vacancies, or inclusions of phases with different lattice structure, as long as these only occupy regions of lengthscales smaller than $N^{1/4}$, see Figure 4.1. Theorem 4.1 says that on the macro–scale, there nevertheless result well defined clusters of constant, crystalline density.

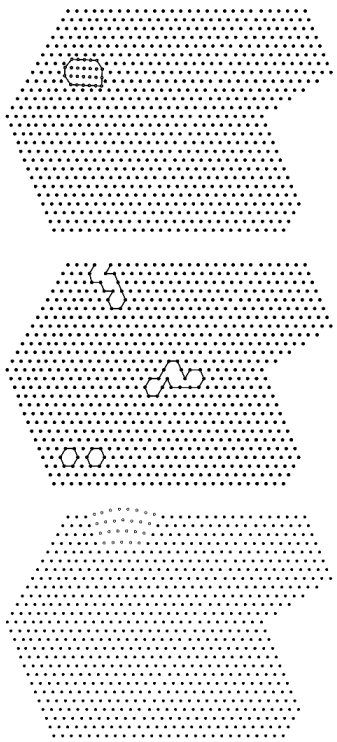

Figure 4.1: Different atomistic configurations satisfying the assumptions of Thm.4.1.

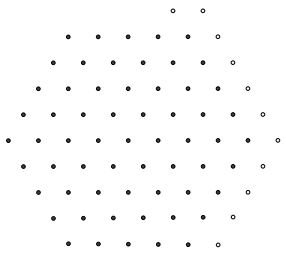

Figure 4.2: A ground state of (4.1), (2.2) for $N = 72$.

4.1.1 Atomistic energy

Our object of study are low–energy states of many–particle potential energy functionals of the form

$$E(x_1, \ldots, x_N) = \sum_{i \neq j} V(|x_i - x_j|) \tag{4.3}$$

on $(\mathbb{R}^2)^N$, where $x_1, \ldots, x_N \in \mathbb{R}^2$ are the particle positions and the potential V is assumed to satisfy the following hypotheses (see Figure 4.3):

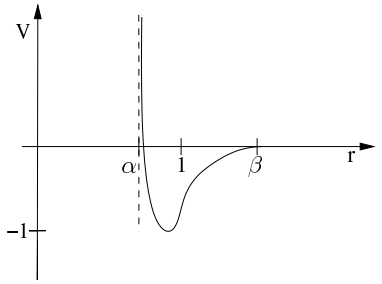

Figure 4.3: Soft Heitmann–Radin potential.

(H1) (minimum at $r = 1$) $V(1) = -1$, $V(r) > -1$ for all $r \neq 1$

(H2) (behavior at short and long range) There exist constants $\alpha \in (0, 1]$, $\beta \in [1, \infty)$ such that $V(r) = +\infty$ for $r < \alpha$, $V(r) = 0$ for $r > \beta$, V continuous on (α, β)

(H3) (narrow potential well) The constants α, β from (H2) satisfy the condition that the ball of radius β contains at most six points whose distance from the center and mutual distance is $\geq \alpha$.

Simple geometric considerations show that (H3) is always satisfied when $\alpha = 1 - \epsilon$, $\beta = 1 + \epsilon$, and $\epsilon > 0$ sufficiently small. The Heitmann–Radin sticky potential (2.2) is contained as a special case ($\alpha = \beta = 1$).

The above hypotheses are not aimed at maximum generality, but at simplicity of proofs. An important feature is that unlike (2.2), they allow elastic deformations.

As a simple consequence of the above hypotheses, one has the following lower bound on the ground state energy:

$$\inf_{x_1,\ldots,x_N \in \mathbb{R}^2} E(x_1, \ldots, x_N) \geq -6N. \tag{4.4}$$

This is because by (H2), (H3), each particle can have a negative interaction energy with at most 6 other particles, and by (H1), the interaction energy with each of them is ≥ -1.

Simple trial configurations show that the true ground state energy differs from the lower bound by at most $O(N^{1/2})$. More precisely we claim that

$$\inf_{x_1,\ldots,x_N \in \mathbb{R}^2} E(x_1, \ldots, x_N) \leq -6N + aN^{1/2} + b \tag{4.5}$$

where we may take $a = 4\sqrt{3}$, $b = 12$. Indeed, consider trial states which are hexagonal subsets of the triangular lattice:

$$\{x_1, \ldots, x_N\} = \Omega \cap \mathcal{L}, \quad \mathcal{L} \text{ as in (4.34)}, \quad h_R \subset \Omega \subset \overline{h_R},$$

where $\overline{h_R}$ is the closed hexagon of radius $R > 0$ with "bottom edge" parallel to e_1,

$$\overline{h_R} = \text{conv}\,\{\pm Re_1,\, \pm Re_2,\, \pm R(e_2 - e_1)\}, \tag{4.6}$$

h_R is its interior, and R and Ω are chosen suitably such that $\#\Omega \cap \mathcal{L} = N$. To infer (4.5), it suffices to estimate the energy of these states from above by the right hand side of (4.5). For completeness we include the (elementary) argument.
First, consider the case when $\Omega = \overline{h_R}$. In this case the number N_s of "surface atoms", *i.e.*the number of atoms in ∂h_R, equals the length of ∂h_R, *i.e.*

$$N_s = 6R. \tag{4.7}$$

The total number of atoms is obtained by summation over the number of atoms in ∂h_r for $r \leq R$,

$$N = 1 + \sum_{r=1}^{R} 6r = 3R^2 + 3R + 1. \tag{4.8}$$

Solving equations (4.7), (4.8) for N_s in terms of N yields $N_s = \sqrt{12N - 3} - 3$. To infer the energy, we only need to count the number of neighbors of each atom, where x is called a neighbor of y if $|x - y| = 1$. Since the 6 "corner" atoms have three missing neighbors, and the remaining $N_s - 6$ surface atoms have two missing neighbors, the energy is

$$E(x_1, \ldots, x_N) = -6N + 6 \cdot 3 + (N_s - 6) \cdot 2 = -6N + 2\sqrt{12N - 3}. \tag{4.9}$$

Now consider the general case $h_R \subset \Omega \subset \overline{h_R}$. Let us add a partial layer of k atoms in ∂h_{R+1} (see Figure 4.2), where k ranges from 1 to $6(R+1) - 1$. Denoting the positions

of the layer atoms by $x_{N+1}, \ldots, x_{N+k}$, the energy of the configuration is

$$\begin{aligned} E(x_1, \ldots, x_N, x_{N+1}, \ldots, x_{N+k}) &= E(x_1, \ldots, x_N) && (4.10) \\ &+ \sum_{\ell=1}^{k} \big(-2 \cdot \#(\text{neighbors of } x_{N+\ell} \text{ in } \overline{h_R}) && (4.11) \\ &\qquad -1 \cdot \#(\text{neighbors of } x_\ell \text{ in } \partial h_{R+1}) \big). && (4.12) \end{aligned}$$

Here the factor 2 appears because interactions between $\overline{h_R}$ and the layer ∂h_{R+1} appear only once in the sum over ℓ, while the layer–layer interactions appear twice. If $k = 1$, it is immediate from (4.9) that $E(x_1, \ldots, x_N, x_{N+1})$ is bounded from above by the right hand side of (4.5), so let us assume $k \geq 2$. We may arrange the layer so that there are at most 5 "corner" atoms with only 3 neighbors, and 2 "end" atoms with only 3 neighbors, while all other atoms in the layer have 4 neighbors (see Figure 4.2).
The 5 corner atoms have 1 neighbor in $\overline{h_R}$ and 2 in ∂h_{R+1}, the end atoms have 2 neighbors in $\overline{h_R}$ and 1 in ∂h_{R+1}, and the remaining layer atoms have 2 neighbors in each set. Consequently by (4.12) and (4.9)

$$\begin{aligned} E(x_1, \ldots, x_N, x_{N+1}, \ldots, x_{N+k}) &\leq E(x_1, \ldots, x_N) + 5(-2 \cdot 1 - 1 \cdot 2) \\ &\quad +2(-2 \cdot 2 - 1 \cdot 1) + (k-7)(-2 \cdot 2 - 1 \cdot 2) \\ &= -6(N+k) + 2\sqrt{12N-3} + 12. \end{aligned}$$

Estimating the square root trivially by $\sqrt{12(N+k)}$ yields the desired upper bound by the right hand side of (4.5). Although this was not needed here, we remark that by the results of [HR80] this trial configuration actually forms a ground state of the potential (2.2).

4.1.2 Compactness and mass conservation

The results in this section are not limited to minimisers, but apply to arbitrary states in which the energy difference from the ground state is of order $O(N^{1/2})$. See Figure 4.1.

Also, we confine ourselves to connected atomic configurations (see the Definition below). In case of disconnected configurations, our analysis can be applied separately to the connected components. Note also that minimisers must always be connected.

Definition. A finite set $S \subset \mathbb{R}^2$ of particle positions is called connected if for any two x, $y \in S$ there exist $x_0, \ldots, x_N \in S$ such that $x_0 = x$, $x_N = y$, and the distance between successive points x_{j-1}, x_j lies within the interaction range of the potential, *i.e.*$|x_j - x_{j-1}| \leq \beta$ for all $j = 1, \ldots, N$.

Also, in the sequel we use the following standard notation. $C_0(\mathbb{R}^2)$ denotes the space of continuous functions on $\mathbb{R}^2$ such that $f(x) \to 0$ as $|x| \to \infty$, $\mathcal{M}(\mathbb{R}^2)$ denotes the space of Radon measures on $\mathbb{R}^2$ of finite mass (recall $\mathcal{M}$ is the dual of C_0), and a sequence of Radon measures μ_N is said to converge weak* to μ, notation: $\mu_N \overset{*}{\rightharpoonup} \mu$, if $\int_{\mathbb{R}^2} f \, \mathrm{d}\mu_N \to \int_{\mathbb{R}^2} f \, \mathrm{d}\mu$ for all $f \in C_0(\mathbb{R}^2)$.

Proposition 4.2. *(Compactness and mass conservation) Assume that the interatomic potential satisfies (H1), (H2), (H3). Let $\{x_1^{(N)}, \ldots, x_N^{(N)}\}$ be any sequence of connected N–particle configurations satisfying the energy bound*

$$E(\{x_1^{(N)}, \ldots, x_N^{(N)}\}) \leq -6N + CN^{1/2}$$

for some constant C independent of N. Let $\{\mu_N\}$ be the associated sequence of Radon measures (4.2)*. Then up to translation (that is to say, up to replacing μ_N by $\mu_N(\cdot + a_N)$*

for some $a_N \in \mathbb{R}^2$) there exists a subsequence converging weak in $\mathcal{M}(\mathbb{R}^2)$ to $\mu \in \mathcal{M}(\mathbb{R}^2)$. Moreover the limit measure satisfies $\mu_N \geq 0$, $\int_{\mathbb{R}^2} d\mu = 1$.*

Proof. Throughout the proof, we write $\mathcal{S} = \{x_1^{(N)}, \ldots, x_N^{(N)}\}$, and denote by C a constant independent of N whose value may change from line to line.

Since the μ_N are nonnegative and have mass 1, they are bounded in $\mathcal{M}(\mathbb{R}^2)$ and hence, by the Banach–Alaoglu theorem, there exists a weak* convergent subsequence. Clearly the limit μ is nonnegative. It remains to show the only really nontrivial assertion above, namely mass conservation $\int_{\mathbb{R}^2} \mathrm{d}\mu = 1$.

The key is to show that

$$\operatorname{diam} \mathcal{S} = \max_{x,y \in \mathcal{S}} |x - y| \leq C N^{1/2}. \tag{4.13}$$

If such a bound holds, then after translation there exists a fixed ball of radius R such that $\operatorname{supp} \mu_N \subset B_R$ for all N. Choose an increasing sequence of functions $\phi_n \in C_0(\mathbb{R}^2)$ such that $0 \leq \phi_n \leq 1$, $\phi_n = 1$ on B_{nR}. By dominated convergence of ϕ_n to 1, the weak* convergence of μ_N to μ, and the fact that $\operatorname{supp} \mu_N \subset B_R$,

$$\int \mathrm{d}\mu = \lim_{n\to\infty} \int \phi_n \, \mathrm{d}\mu = \lim_{n\to\infty} \big(\lim_{N\to\infty} \int \phi_n \, \mathrm{d}\mu_N \big) = \lim_{n\to\infty} 1 = 1,$$

completing the proof of the proposition.

It remains to establish the bound (4.13). We begin by introducing a notion of *neighbors* and a notion of *local energy*. Let $\epsilon \in (0, 1)$, small enough so that condition (H3) is satisfied for $\alpha = 1 - \epsilon$ and $\beta = 1 + \epsilon$.

Definition Let $\mathcal{S} \subset \mathbb{R}^2$ be a finite set of particle positions. We say that $x \in \mathcal{S}$ is a neighbor of $y \in \mathcal{S}$ if $|x - y| \in [1 - \epsilon, 1 + \epsilon]$. The set of neighbors of $x \in \mathcal{S}$ is denoted

by $\mathcal{N}(x)$.

Also, independently of the above notion of neighbors, we define a local energy, as follows:

$$E_{\ell oc}(x) := \sum_{y \in \mathcal{S}\setminus\{x\}} V(|x-y|),$$

so that

$$E(\mathcal{S}) = \sum_{x \in \mathcal{S}} E_{\ell oc}(x).$$

By hypotheses (H1)–(H3) on the potential V and the finiteness of the energy of $\mathcal{S}_N$, it follows that

$$\#\mathcal{N}(x) \leq 6, \;\; E_{\ell oc}(x) \geq -6, \tag{4.14}$$

with both bounds being sharp as is seen by considering points x in the lattice $\mathcal{L}$. A key point now is that when the number of neighbors of x is not equal to 6, the local energy of x is bounded away from its optimum by a finite amount:

$$\#\mathcal{N}(x) < 6 \Longrightarrow E_{\ell oc}(x) \geq -6 + \Delta, \text{ with } \Delta := \min_{r \notin (1-\epsilon, 1+\epsilon)} V(r) - \min_{r} V(r) > 0. \tag{4.15}$$

Next, we construct an appropriate set in the plane associated with the configuration $\mathcal{S}$. For each $x \in \mathcal{S}$, let $\mathcal{V}(x)$ be the Voronoi cell of x,

$$\mathcal{V}(x) = \big\{ y \in \mathbb{R}^2 : |y-x| \leq |y-x'| \text{ for all } x' \in \mathcal{S}\setminus\{x\} \big\}. \tag{4.16}$$

As $\mathcal{V}(x)$ may be unbounded, it is useful to introduce in addition its truncation

$$\mathcal{V}_{trunc}(x) := \mathcal{V}(x) \cap B_1(x), \tag{4.17}$$

where $B_r(x)$ is the ball $\{y \in \mathbb{R}^2 : |y - x| \leq r\}$. We then define

$$\Omega := \bigcup_{x \in \mathcal{S}} \mathcal{V}_{trunc}(x). \tag{4.18}$$

Elementary geometric considerations show that when $\epsilon > 0$ is chosen sufficiently small, then

$$\#\mathcal{N}(x) = 6 \Longrightarrow \partial\Omega \cap \partial\mathcal{V}_{trunc}(x) = \emptyset, \tag{4.19}$$

that is to say the cells associated to points with the maximum number of neighbors do not contribute to the boundary of Ω. Finally, since by construction $\mathcal{V}_{trunc}(x) \subset B_1(x)$ and $\mathcal{V}_{trunc}(x)$ is convex, we have the following bound on the length of its boundary

$$|\partial\mathcal{V}_{trunc}(x)| \leq 2\pi. \tag{4.20}$$

Consequently, denoting

$$\partial\mathcal{S} := \{x \in \mathcal{S} : \#\mathcal{N}(x) < 6\}, \tag{4.21}$$

using the plausible fact proved in Lemma 4.3 below that due to the connectedness of $\mathcal{S}$ the set Ω is connected, and (4.19), (4.20)

$$\operatorname{diam}\mathcal{S} \;\leq\; \operatorname{diam}\Omega \;\leq\; \tfrac{1}{2}|\partial\Omega| \;\leq\; \tfrac{1}{2} \sum_{x \in \mathcal{S} \,|\, \mathcal{V}_{trunc}(x) \cap \partial\Omega \neq \emptyset} |\partial\mathcal{V}_{trunc}(x)| \;\leq\; \pi\, \#\partial\mathcal{S}. \tag{4.22}$$

On the other hand, recalling $N = \#\mathcal{S}$ and using the assumption on $E(\mathcal{S})$ in the lemma and (4.15),

$$-6N + CN^{1/2} \geq E(\mathcal{S}) \geq -6N + \Delta\, \#\partial\mathcal{S}, \tag{4.23}$$

and consequently

$$\#\partial\mathcal{S} \leq \frac{C}{\Delta} N^{1/2}. \tag{4.24}$$

Combining (4.22), (4.24) establishes (4.13). The proof of the proposition is complete, except for the following elementary geometric lemma. □

Lemma 4.3. *If a configuration $\mathcal{S}$ is connected in the sense of the definition in Section 4.1.2 and the energy $E(\mathcal{S})$ is finite, then the set Ω defined in (4.18) is connected.*

Proof. We begin by establishing an elementary inequality relating the constants α and β appearing in the hypotheses on the potential V. By (H3), the ball of radius β around the origin does not contain the regular heptagon around the origin with sidelength α, or equivalently

$$\frac{\alpha}{2} > \beta \sin\frac{\phi}{2}, \quad \phi = \frac{2\pi}{7}.$$

Hence

$$\beta < \frac{\alpha}{2\sin\phi/2} = 1.152382...\,\alpha. \tag{4.25}$$

To prove the lemma, it suffices to show that if $|x-y| < \beta$, the truncated Voronoi cells around x and y have nonzero intersection. To establish this, it is enough to show that the midpoint $m = \frac{x+y}{2}$ belongs to $B_1(x) \cap B_1(y)$ and $\mathcal{V}(x) \cap \mathcal{V}(y)$. The first inclusion is immediate from $|m-x| < \beta/2$, (4.25) and $\alpha \leq 1$. The second inclusion is equivalent to

$$|m-z| > \frac{|x-y|}{2} \; (= |m-x| = |m-y|)$$

for all $z \in \mathcal{S}\backslash\{x,y\}$. Now any such z belongs to $\mathbb{R}^2\backslash(B_\alpha(x) \cup B_\alpha(y)$ (otherwise the energy of the configuration would be infinite), and any closest point p to m in the latter set has distance $|p-m| = \sqrt{\alpha^2 - (|x-y|/2)^2}$, so it suffices to show that

$\sqrt{\alpha^2 - (|x-y|/2)^2} > |x-y|/2$, or equivalently

$$\alpha > \frac{|x-y|}{\sqrt{2}}. \tag{4.26}$$

But thanks to (4.25) we have

$$|x-y| < \beta < 1.152382... \, \alpha < \sqrt{2}\alpha.$$

This establishes (4.26), completing the proof of the lemma. □

4.1.3 Proof of formation of clusters with constant density and finite perimeter

We now prove Theorem 4.1, *i.e.* we show that under the assumptions of Proposition 4.2, the limit measure μ of the re–scaled empirical measures of atomistic configurations is a constant multiple of a characteristic function, the constant being given by the density of atoms per unit volume of the triangular lattice.

Proof of Theorem 4.1. As in the proof of Proposition 4.2 we use the decomposition of $\mathbb{R}^2$ into truncated Voronoi cells $V_{trunc}(x)$ (see (4.16)–(4.17)) associated with the points x of an atomistic configuration $\mathcal{S}$. The main technical idea of the proof is to introduce and investigate the following *volume excess function*

$$\Phi(x) := \Big| \frac{1}{|V_{trunc}(x)|} - \frac{1}{|h'_{1/\sqrt{3}}(x)|} \Big|. \tag{4.27}$$

Here $h'_r(x)$ is the closed hexagon of radius r around x which is obtained from $\overline{h_r}$ (see (4.6)) by a 30^o rotation around the centre. This hexagon is the Voronoi cell of any

interior point x of a particle configuration $\mathcal{S}$ on the triangular lattice (4.34).
Besides the sequence of re–scaled empirical measures (4.2), we will make use of the following auxiliary sequences:

$$\tilde{\mu}_N = \frac{1}{N}\sum_{x\in\mathcal{S}_N}\frac{\chi_{N^{-1/2}V_{trunc}(x)}}{|N^{-1/2}V_{trunc}(x)|}, \tag{4.28}$$

$$\tilde{\tilde{\mu}}_N = \frac{1}{N}\sum_{x\in\mathcal{S}_N}\frac{\chi_{N^{-1/2}V_{trunc}(x)}}{|N^{-1/2}h'_{1/\sqrt{3}}(x)|}. \tag{4.29}$$

Step 1 First we claim that

$$\mu_N - \tilde{\mu}_N \stackrel{*}{\rightharpoonup} 0 \text{ in } \mathcal{M}(\mathbb{R}^2). \tag{4.30}$$

Indeed, since for any $x_0 \in \mathcal{S}_N$, $V_{trunc}(x_0) \subseteq B_1(x_0)$, we have for all test functions $\phi \in C_0(\mathbb{R}^2)$

$$\begin{aligned}
&\Big|\int_{\mathbb{R}^2}\left(\delta_{x_0/\sqrt{N}} - \frac{\chi_{N^{-1/2}V_{trunc}(x_0)}}{|N^{-1/2}V_{trunc}(x_0)|}\right)\phi\Big| \\
&= \Big|\frac{1}{|N^{-1/2}V_{trunc}(x_0)|}\int_{N^{-1/2}V_{trunc}(x_0)}\big(\phi(x_0/\sqrt{N}) - \phi(x)\big)\,\mathrm{d}x\Big| \\
&\leq \sup_{|x-y|\leq N^{-1/2}}|\phi(x)-\phi(y)|
\end{aligned}$$

and consequently

$$\begin{aligned}
\Big|\int\phi\,\mathrm{d}\mu_N - \int\phi\,\mathrm{d}\tilde{\mu}_N\Big| &\leq \frac{1}{N}\sum_{x\in\mathcal{S}_N}\sup_{|x-y|\leq N^{-1/2}}|\phi(x)-\phi(y)| \\
&= \sup_{|x-y|\leq N^{-1/2}}|\phi(x)-\phi(y)| \to 0 \quad (N\to\infty),
\end{aligned}$$

establishing (4.30).

Step 2 Next, we compare the measures $\tilde{\mu}_N$ and $\tilde{\tilde{\mu}}_N$. We will show that

$$\tilde{\tilde{\mu}}_N - \tilde{\mu}_N \to 0 \text{ in } L^1(\mathbb{R}^2) \tag{4.31}$$

(and hence, a fortiori, $\tilde{\tilde{\mu}}_N - \tilde{\mu}_N \overset{*}{\rightharpoonup} 0$ in $\mathcal{M}(\mathbb{R}^2)$). First, we decompose both measures into their "interior" and "boundary" parts, as follows. Here $\partial\mathcal{S}_N$ is as defined in (4.21), and $\operatorname{int}\mathcal{S}_N := \mathcal{S}_N \backslash \partial\mathcal{S}_N$.

$$\tilde{\mu}_N = \tilde{\lambda}_N + \tilde{\nu}_N,\ \tilde{\lambda}_N = \frac{1}{N}\sum_{x\in\operatorname{int}\mathcal{S}_N} \frac{\chi_{N^{-1/2}V_{trunc}(x)}}{|N^{-1/2}V_{trunc}(x)|},\ \tilde{\nu}_N = \frac{1}{N}\sum_{x\in\partial\mathcal{S}_N} \frac{\chi_{N^{-1/2}V_{trunc}(x)}}{|N^{-1/2}V_{trunc}(x)|}$$

and analogously for $\tilde{\tilde{\mu}}_N$. Roughly speaking, we will argue that the difference between $\tilde{\tilde{\nu}}_N$ and $\tilde{\nu}_N$ is small because they are small separately, due to the fact that the number of boundary atoms grows only like $N^{1/2}$, and that the difference between $\tilde{\tilde{\lambda}}_N$ and $\tilde{\lambda}_N$ is small because otherwise this would cost elastic energy.

To make the first argument precise, we use that for any configuration $\mathcal{S} = \{x_1, \dots, x_N\}$ with finite energy, $V_{trunc}(x_i) \supseteq B_{\alpha/2}(x_i)$, due to the fact that $|x_j - x_i| \geq \alpha$ for all $j \neq i$, so that the nearest point in $\mathcal{S}$ to $y \in B_{\alpha/2}(x_i)$ is x_i. Hence

$$0 \leq |\tilde{\tilde{\nu}}_N - \tilde{\nu}_N| \leq \sum_{x\in\partial\mathcal{S}_N} \chi_{N^{-1/2}V_{trunc}(x)} \underbrace{\Big(\frac{1}{|B_{\alpha/2}|} + \frac{1}{|h'_{1/\sqrt{3}}|}\Big)}_{=:K}.$$

Since $\#\partial\mathcal{S}_N \leq (C/\Delta)N^{1/2}$ (see (4.24)) and $V_{trunc}(x) \subseteq B_1(x)$, we infer that

$$\|\tilde{\tilde{\nu}}_N - \tilde{\nu}_N\|_{L^1(\mathbb{R}^2)} \leq \frac{C\,K}{\Delta} N^{1/2} \max_{x\in\mathcal{S}_N} \|\chi_{N^{-1/2}V_{trunc}(x)}\|_{L^1} \leq \frac{C\,K}{\Delta} N^{-1/2}|B_1| \to 0\ (N\to\infty). \tag{4.32}$$

Next we analyse the difference between the interior parts,

$$\tilde{\lambda}_N - \tilde{\tilde{\lambda}}_N = \sum_{x \in \operatorname{int} \mathcal{S}_N} \chi_{N^{-1/2} V_{trunc}(x)} \Big(\frac{1}{|V_{trunc}(x)|} - \frac{1}{|h_{1/\sqrt{3}}(x)|} \Big).$$

For any point $x \in \operatorname{int} \mathcal{S}_N$, $\#\mathcal{N}(x) = 6$, so $\mathcal{N}(x) = \{y_1, \dots, y_6\}$, where we may assume that the y_j are numbered so that $y_j - x = r_j(\cos\phi_j, \sin\phi_j)$, $0 \le \phi_1 < \phi_2 < ... < \phi_6 < 2\pi$. For elementary geometric reasons, namely that the only way to arrange the y_i so that $|y_j - x| = 1$ for all j and $|y_j - y_{j-1}| = 1$ for all j is to place them at the corners of a regular hexagon around x, we have

$$|V_{trunc}(x)| \to |h_{1/\sqrt{3}}(x)| \ \text{ if } \sum_{y \in \mathcal{N}(x)} V(|x-y|) + \sum_{j=1}^{6} V(|y_{j+1} - y_j|) \to -12.$$

Hence by continuity, given $\delta > 0$ there exists $\Delta(\delta) > 0$ such that for all $x \in \operatorname{int} \mathcal{S}_N$ the volume excess (4.27) satisfies the following implication:

$$\begin{aligned} &\Phi(x) \ge \delta \\ &\Longrightarrow \tilde{E}_{\ell oc}(x) := \sum_{y \in \mathcal{N}(x)} V(|x-y|) + \sum_{j=1}^{6} V(|y_{j+1} - y_j|) \ge -12 + \Delta. \end{aligned} \tag{4.33}$$

It will be convenient to extend the function $\tilde{E}_{\ell oc}(x)$ to all of $\mathcal{S}_N$, by setting it equal to -12 when $x \in \partial\mathcal{S}_N$. Combining the energy bound assumed in Theorem 4.1, the fact that each particle pair appears in $\tilde{E}_{\ell oc}(x)$ for at most four $x \in \mathcal{S}_N$ whereas it appears

twice in E, and (4.33) yields

$$\begin{aligned} -6N + C\,N^{1/2} &\geq E(\mathcal{S}_N) \geq \frac{1}{2}\sum_{x\in\mathcal{S}_N} \tilde{E}_{\ell oc}(x) \\ &\geq \frac{1}{2}\big(-12\#\big\{x\in\mathcal{S}_N : x\in\partial\mathcal{S}_N \text{ or } \Phi(x)<\delta\big\} \\ &\quad +(-12+\Delta)\#\big\{x\in\operatorname{int}\mathcal{S}_N : \Phi(x)\geq\delta\big\}\big) \\ &\geq -6N + \frac{\Delta}{2}\#\big\{x\in\operatorname{int}\mathcal{S}_N : \Phi(x)\geq\delta\big\}. \end{aligned}$$

Consequently

$$\#\big\{x\in\operatorname{int}\mathcal{S}_N : \Phi(x)\geq\delta\big\} \leq \frac{2\,C}{\Delta}N^{1/2}$$

and so

$$\begin{aligned} \|\tilde{\tilde{\lambda}}_N - \tilde{\lambda}_N\|_{L^1(\mathbb{R}^2)} &= \int_{\mathbb{R}^2}\Big|\sum_{x\in\operatorname{int}\mathcal{S}_N}\chi_{N^{-1/2}V_{trunc}(x)}\big(\frac{1}{|V_{trunc}(x)|}-\frac{1}{|h_{1/\sqrt{3}}(x)|}\big)\Big| \\ &\leq \sum_{x\in\operatorname{int}\mathcal{S}_N}\Phi(x)\|\chi_{N^{-1/2}V_{trunc}(x)}\|_{L^1} \\ &\leq N^{-1}|B_1|\sum_{x\in\operatorname{int}\mathcal{S}_N}\Phi(x) \\ &\leq N^{-1}|B_1|\big(\delta\,N + \underbrace{\max_{x\in\operatorname{int}\mathcal{S}_N}\Phi(x)}_{\leq K}\ \underbrace{\#\big\{x\in\operatorname{int}\mathcal{S}_N : \Phi(x)\geq\delta\big\}}_{\leq\frac{2C}{\Delta}N^{1/2}}\big). \end{aligned}$$

Letting $N\to\infty$ gives

$$\limsup_{N\to\infty}\|\tilde{\tilde{\lambda}}_N - \tilde{\lambda}_N\|_{L^1(\mathbb{R}^2)} \leq |B_1|\delta.$$

Since $\delta>0$ was arbitrary, the left hand side equals zero, that is to say $\tilde{\tilde{\lambda}}_N - \tilde{\lambda}_N \to 0$ in $L^1(\mathbb{R}^2)$. Together with (4.32), this establishes (4.31).

Step 3 Having established that the limits of μ_N, $\tilde{\mu}_N$, $\tilde{\tilde{\mu}}_N$ all coincide, it suffices to study the limiting behavior of the sequence $\tilde{\tilde{\mu}}_N$, which – as we shall see – is compact

in a much "stronger" space. After a change on a set of measure zero,

$$\tilde{\tilde{\mu}}_N = \frac{1}{|h'_{1/\sqrt{3}}|}\chi_{N^{-1/2}\Omega_N}, \quad \Omega_N = \bigcup_{x\in\mathcal{S}_N} V_{trunc}(x).$$

Clearly the $\tilde{\tilde{\mu}}_N$ only take values in $\{0,\rho\}$, belong to the space $BV(\mathbb{R}^2)$, are bounded in $L^1(\mathbb{R}^2)$, and – by (4.13) – after translation are supported in some fixed ball of radius R. We claim that they are also bounded in $BV(\mathbb{R}^2)$. This is because $|\partial\Omega_N|$ is bounded by a constant times $N^{1/2}$, by (4.22) and (4.24). Consequently by the Banach–Alaoglu theorem and the compact embedding $BV(B_R) \hookrightarrow L^1(B_R)$, a subsequence converges weak* in BV and strongly in L^1 to some limit $\tilde{\tilde{\mu}} \in BV$. By the strong L^1 convergence, $\tilde{\tilde{\mu}}$ only takes values in $\{0,\rho\}$, and by Steps 1 and 2, $\tilde{\tilde{\mu}} = \mu$. The proof of Theorem 4.1 is complete. □

4.2 Three dimensions

The emergence of a well–defined cluster is now performed in three dimensions. Contrary to the two–dimensional case, the boundedness of the diameter is not trivially implied by the connectedness of configurations and by bounded surface energy. We therefore assume additionally that the configurations have bounded diameter.

Throughout this section our energy is given by (4.1), *i.e.*,

$$E(x_1, \ldots, x_N) = \sum_{i \neq j} V(|x_i - x_j|),$$

and applies to short–range potentials V fulfilling (H1)–(H3) on page 58. Note that (H3) is dimension dependent: the number of particles with which one particle may interact is bounded above by the dimension–dependent kissing number. For the sake of completeness, we record the modified conditions in three dimensions:

(H1) (minimum at $r = 1$) $V(1) = -1$, $V(r) > -1$ for all $r \neq 1$

(H2) (behavior at short and long range) There exist constants $\alpha \in (0, 1]$, $\beta \in [1, \infty)$ such that $V(r) = +\infty$ for $r < \alpha$, $V(r) = 0$ for $r > \beta$, V continuous on (α, β).

(H3') (narrow potential well) The constants α, β from (H2) satisfy the condition that the ball of radius β contains at most twelve points whose distance from the center and mutual distance is $\geq \alpha$.

Our Theorem on cluster formation allows configurations to belong to quite general lattices, namely close–packed lattices, as long as their energies deviate from the bulk energy $-12N$ only by a surface energy contribution of order $O(N^{2/3})$.
We quickly introduce the notion of a three–dimensional close–packed lattice:

Recall that the triangular lattice is defined as

$$\mathcal{L}^{2D} := e_1\mathbb{Z} \oplus e_2\mathbb{Z}, \qquad e_1 = \begin{pmatrix} 1 \\ 0 \end{pmatrix}, \quad e_2 = \tfrac{1}{2}\begin{pmatrix} 1 \\ \sqrt{3} \end{pmatrix}. \tag{4.34}$$

First, any sequence $s = (s_j)_{j\in\mathbb{Z}} \subset \mathbb{R}^2$ satisfying $s_j \in \{A, B, C\}$ and $s_{j+1} \neq s_j$ for all $j \in \mathbb{Z}$ is called *stacking sequence*. Here, A, B, C denote shift vectors (see Figure 4.4) and are, for our purposes, given by the origin and the barycentres of the triangles with vertices $0, -e_2, e_1 - e_2$ and $0, e_2, e_2 - e_1$:

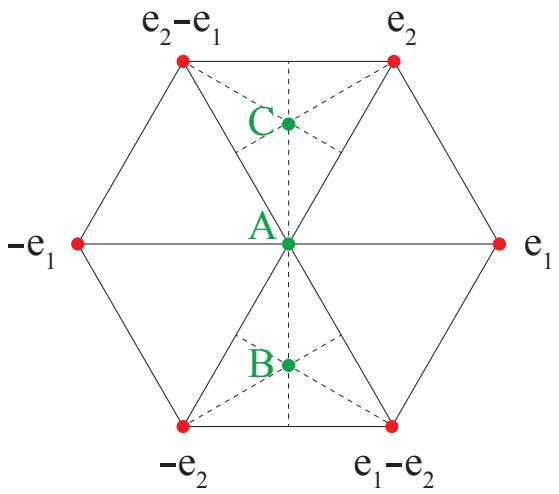

Figure 4.4: The vectors e_1, e_2 span the two–dimensional triangular lattice $\mathcal{L}^{2D}$. The three shift vectors are plotted in green. Note that A is a shift and also the origin. The other two shift vectors are precisely the barycentres of the two triangles with vertices $0, -e_2, e_1 - e_2$ and with vertices $0, e_2, e_2 - e_1$.

The precise coordinates of the shift vectors are:

$$
\begin{aligned}
A &:= \begin{pmatrix} 0 \\ 0 \end{pmatrix}, \\
B &:= \frac{1}{3}(0 + (-e_2) + (e_1 - e_2)) = \begin{pmatrix} 0 \\ -\frac{\sqrt{3}}{3} \end{pmatrix}, \\
C &:= \frac{1}{3}(0 + e_2 + (e_2 - e_1)) = \begin{pmatrix} 0 \\ \frac{\sqrt{3}}{3} \end{pmatrix}.
\end{aligned}
$$

Second, we associate to any stacking sequence $s = (s_j)_{j\in\mathbb{Z}}$ the three–dimensional close–packed lattice $\mathcal{L}(s)$. This is obtained by first stacking triangular lattices on each other at the mutual interplanar distance $d = \frac{\sqrt{6}}{3}$. Finally, shifting the j–th triangular lattice by s_j completes the construction of the close–packed lattice; in formula,

$$
\mathcal{L}(s) := \bigcup_{j\in\mathbb{Z}} \left(s_j + \mathcal{L}^{2D} \right) \times \{jd\}, \qquad d = \tfrac{\sqrt{6}}{3}. \tag{4.35}
$$

The close–packed lattice $\mathcal{L}(s)$ turns out to be the face–centred cubic and the hexagonal close–packed lattice resp. if we choose $s^{fcc} = (\ldots ABCABCABC\ldots)$ or $s^{hcp} = (\ldots ABABAB\ldots)$ resp., *i.e.*,

$$
(s^{fcc})_j := \begin{cases} A, & j \in 3\mathbb{Z} \\ B, & j \in 3\mathbb{Z}+1 \\ C, & j \in 3\mathbb{Z}+2, \end{cases} \qquad (s^{hcp})_j := \begin{cases} A, & j \in 2\mathbb{Z} \\ B, & j \in 2\mathbb{Z}+1. \end{cases}
$$

The next figure (Figure 4.5) shows an example of how to staple the lattices $\mathcal{L}^{fcc}$, $\mathcal{L}^{hcp}$.

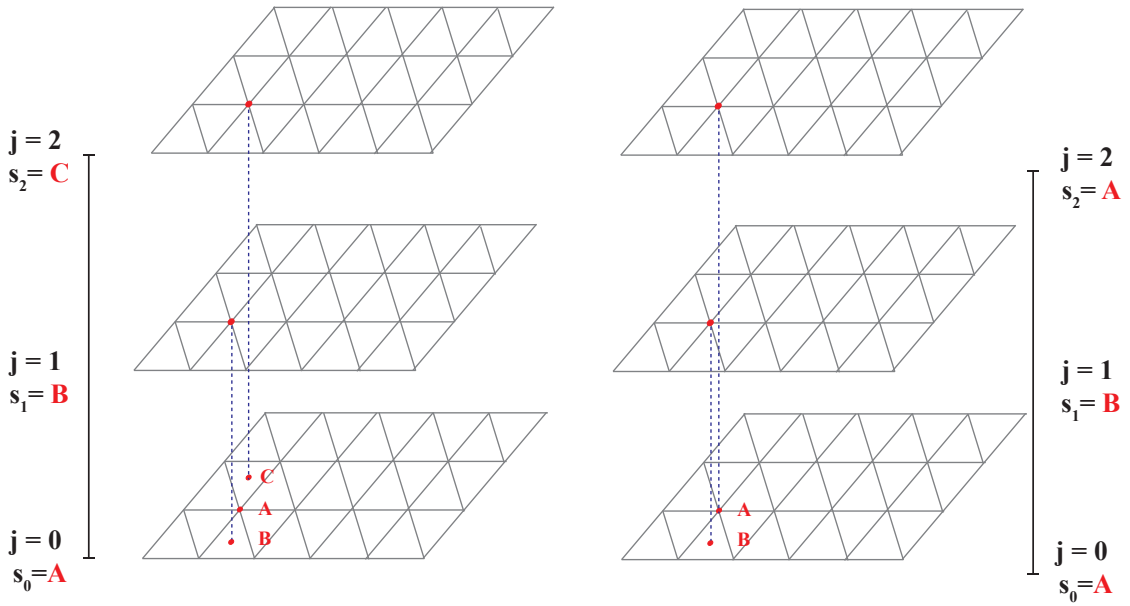

Figure 4.5: The first three layers of the lattices $\mathcal{L}^{fcc}$ and $\mathcal{L}^{hcp}$ are stapled.
Left: The "lowest" layer is not shifted and placed at the origin $(0,0,0)^T$. The next layer is first shifted in $\mathbb{R}^2$ by B and then translated by $(0,0,\frac{\sqrt{6}}{3})^T$. Finally, the "upper" layer is shifted by C and translated by $(0,0,2\cdot\frac{\sqrt{6}}{3})^T$. By continuing periodically in this way, we obtain the staple sequence s^{fcc} and we end up with $\mathcal{L}^{fcc}$.
Right: Again the "lowest" layer remains at the origin. The next layer is first shifted by B and then translated by $(0,0,\frac{\sqrt{6}}{3})^T$. Note that the stapling period begins again at the third layer, *i.e.*, the third layer is an A–layer which is translated by $(0,0,2\cdot\frac{\sqrt{6}}{3})^T$. By following in this fashion, we obtain the hexagonal close–packed arrangement $\mathcal{L}^{hcp}$.

We are now capable of stating our main Theorem on cluster formation in three dimensions.

Theorem 4.4. *(Compactness and formation of cluster)*
Suppose that the energy is given by (4.1), where V is any short–range potential satisfying (H1),(H2) and (H3'). For a stacking sequence s and its associated close–packed lattice $\mathcal{L}(s)$, introduced in (4.35), let $\{x_1^{(N)}, \ldots, x_N^{(N)}\} \subset \mathcal{L}(s)$ be any sequence of connected N–particle configurations that is bounded, i.e.*,*

$$\max_{i,j} |x_i^{(N)} - x_j^{(N)}| \leq CN^{1/3} \tag{4.36}$$

and that satisfies an energy bound, i.e.*,*

$$E(x_1^{(N)}, \ldots, x_N^{(N)}) \leq -12N + CN^{2/3}, \tag{4.37}$$

for some constant C independent of N. Let μ_N be the associated sequence of re–scaled empirical measures

$$\mu_N = \frac{1}{N} \sum_{i=1}^{N} \delta_{N^{-1/3} x_i^{(N)}}.$$

Then

1. *Up to translation (that is to say, up to replacing μ_N by $\mu_N(\cdot + a_N)$ for some constant $a_N \in \mathbb{R}^3$) and passage to a subsequence, μ_N weak$*$ converges in $\mathcal{M}(\mathbb{R}^3)$ to $\mu \in \mathcal{M}(\mathbb{R}^3)$. Moreover, μ has mass one,* i.e.*, $\int_{\mathbb{R}^3} \mathrm{d}\mu = 1$*

2. *The limit measure is of the form*

$$\mu = \rho \chi_E,$$

*where $\rho = \sqrt{2}$ (*i.e.*, the density of atoms per unit volume of the close–packed lattice $\mathcal{L}(s)$) and E is a set of finite perimeter of volume ρ^{-1}.*

Remark. Our soft potential restricted on subsets of closed packed lattices coincides with the Heitmann–Radin sticky disc potential; hence, the considered energy for a lattice state configuration amounts to "bond–counting".
Moreover, the proof relies on the fact that the Voronoi cells in $\mathcal{L}(s)$ tile the space.

Proof of compactness. The re–scaled empirical measures are nonnegative, have mass one and are bounded in $\mathcal{M}(\mathbb{R}^3)$. From the Banach–Alouglu theorem we infer that there must exist a subsequence which weak$*$ converges to some measure $\mu \in \mathcal{M}(\mathbb{R}^3)$.
The mass conservation now follows immediately from the diameter bound (4.36). Indeed, the measures μ_N are—after translation—supported on a ball of radius $R > 0$. Now choose an increasing sequence $\phi_n \in C_0(\mathbb{R}^3)$ such that $0 \leq \phi_n \leq 1$, $\phi_n = 1$ on B_{nR} and apply the dominated convergence of ϕ_n to 1, the weak$*$ convergence of μ_N to μ, and the fact that the measures μ_N are supported in B_R, to deduce

$$\int_{\mathbb{R}^3} \mathrm{d}\mu = \lim_{n\to\infty} \int_{\mathbb{R}^3} \phi_n \,\mathrm{d}\mu = \lim_{n\to\infty} \left(\lim_{N\to\infty} \int_{\mathbb{R}^3} \phi_n \,\mathrm{d}\mu_N \right) = \lim_{n\to\infty} 1 = 1.$$

Proof of formation of cluster. Throughout the proof we denote by $\mathcal{S}_N$ an N–particle configuration $\{x_1^{(N)}, \ldots, x_N^{(N)}\} \subset \mathcal{L}(s)$ for a stacking sequence s.
Recall that the surface of $\mathcal{S}_N$ is defined by

$$\partial\mathcal{S}_N := \Big\{ x \in \mathcal{S}_N \ : \ \sharp\{y \in \mathcal{S}_N \ : \ |x-y| = 1\} < 12 \Big\}.$$

and that the interior of $\mathcal{S}_N$ is defined as $\mathrm{int}\mathcal{S}_N := \mathcal{S}_N \backslash \partial\mathcal{S}_N$. The energy bound allows us to estimate the number of surface particles in $\mathcal{S}_N$,

$$-12N + CN^{2/3} \geq E(\mathcal{S}_N) \geq -12N + \sharp\partial\mathcal{S}_N,$$

so that

$$\sharp\partial\mathcal{S}_N \leq CN^{2/3}. \tag{4.38}$$

We follow the gist in two dimensions and regularise the empirical measures suitably. For this sake, we denote by $\mathcal{V}(x)$ the Voronoi cell at x w.r.t. the ambient lattice $\mathcal{L}(s)$. Note that $\mathcal{V}(x)$ has the same volume for all $x \in \mathcal{S}_N$ and is—up to translation—a rhombic or a trapezo–rhombic dodecahedron. The choice of dodecahedron depends on the stacking sequence. Any particle $x \in \mathcal{S}_N$ belongs to a specific "layer" in $\mathcal{L}(s)$, *i.e.*, there exists a $j \in \mathbb{Z}$ such that

$$x \in (s_j + \mathcal{L}^{2D}) \times \left\{ j\tfrac{\sqrt{6}}{3} \right\},$$

and the Voronoi cell at x w.r.t. $\mathcal{L}(s)$ is—up to translation—a

$$\begin{cases} \text{rhombic dodecahedron} & \text{if } s_{j-1} \neq s_{j+1} \\ \text{trapezo–rhombic dodechaedron} & \text{if } s_{j-1} = s_{j+1}. \end{cases}$$

We introduce a regularisation of μ_N via

$$\mu'_N := \frac{1}{N} \sum_{x \in \mathcal{S}_N} \frac{\chi_{N^{-1/3}\mathcal{V}(x)}}{|N^{-1/3}\mathcal{V}(x)|}. \tag{4.39}$$

and claim that

Step 1.

$$\mu_N - \mu'_N \overset{*}{\rightharpoonup} 0 \qquad \text{in } \mathcal{M}(\mathbb{R}^3). \tag{4.40}$$

To verify the weak$*$ convergence, we test the measures $\mu_N - \mu'_N$ against an arbitrary test function $\phi \in C_0(\mathbb{R}^3)$. Let $x_0 \in \mathcal{S}_N$. A straightforward calculation first shows

$$\left| \int_{\mathbb{R}^3} \left(\delta_{N^{-1/3}x_0}(x) - \frac{\chi_{N^{-1/3}\mathcal{V}(x_0)}(x)}{|N^{-1/3}\mathcal{V}(x_0)|} \right) \phi(x)\,\mathrm{d}x \right|$$

$$= \left| \frac{1}{|N^{-1/3}\mathcal{V}(x_0)|} \int_{N^{-1/3}\mathcal{V}(x_0)} \left[\phi(N^{-1/3}x_0) - \phi(x) \right]\,\mathrm{d}x \right|$$
$$\leq \sup_{|x-y|\leq N^{-1/3}} |\phi(x) - \phi(y)|,$$

where we have made use of $\mathcal{V}(x_0) \subseteq B_{\sqrt{2}/2}(x_0)$ in the last step, and second we deduce

$$\left| \int_{\mathbb{R}^3} \phi(x)\mathrm{d}\mu_N - \int_{\mathbb{R}^3} \phi(x)\mathrm{d}\mu'_N \right| \leq \frac{1}{N} \sum_{x_0 \in \mathcal{S}_N} \sup_{|x-y|\leq N^{-1/3}} |\phi(x) - \phi(y)|$$
$$= \sup_{|x-y|\leq N^{-1/3}} |\phi(x) - \phi(y)|.$$

Finally, the latter converges to zero as $N \to \infty$, because $\phi \in C_0(\mathbb{R}^3)$, and step 1 is established.

Step 2. The preceding step guarantees that the weak$*$ limits of μ_N and μ'_N coincide. After a change on a set of measure zero,

$$\mu'_N = \frac{1}{|\mathcal{V}|} \chi_{N^{-1/3}\Omega_N}, \qquad \Omega_N := \bigcup_{x \in \mathcal{S}_N} \mathcal{V}(x).$$

Here, $|\mathcal{V}|$ denotes the volume of any Voronoi cell in $\mathcal{L}(s)$ and equals $2^{-1/2}$.
We claim that the sequence (μ'_N) is bounded in $BV(\mathbb{R}^3)$. This is because μ'_N belongs to $BV(\mathbb{R}^3)$, only attains the values 0 and $|\mathcal{V}|^{-1}$, is bounded in $L^1(\mathbb{R}^3)$, and is—after

translation—supported on some ball of radius R, due to the diameter estimate (4.36). In fact, μ'_N is not only bounded in $L^1(\mathbb{R}^3)$, but also in $BV(\mathbb{R}^3)$. This is because the number of boundary particles $\sharp\partial\mathcal{S}_N$ is bounded by $CN^{2/3}$ (confer estimate (4.38)), only Voronoi cells at boundary particles contribute to the boundary of Ω_N and because the area of $\mathcal{V}$ is of order one:

$$|\partial\Omega_N| \leq \sharp\partial\mathcal{S}_N \cdot \mathcal{H}^2(\mathcal{V}) \leq CN^{2/3}$$

for some constant C independent of N. Re–scaling yields that the boundary of $N^{-1/3}\Omega_N$ is uniformly bounded.

Finally, the Banach–Alaoglu theorem yields a weak$*$ convergent subsequence in BV and by the compact embedding $BV(B_R) \hookrightarrow L^1(B_R)$ we get yet another subsequence which strongly converges to μ' in $L^1(B_R)$. From the strong convergence and from the mass conservation we infer strong convergence in $L^1(\mathbb{R}^3)$ and that μ' only attains the values 0 and $|\mathcal{V}|^{-1}$.

Finally, step 1 yields that μ' must equal μ. □

Chapter 5

Wulff Shapes through Atomistics

The results in this chapter for the two dimensional case (Section 5.1) is joint work with G. Friesecke and B. Schmidt and was published in [AFS12].
i Section 5.2 on the three dimensional case is new.

This chapter is solely devoted to the identification of the overall macroscopic cluster shape E in two and three dimensions. We implement the missing two items (4) and (5) of the strategy on page 54. Our methods are restricted to exact minimisers of energies that have crystalline ground states.
By crystallised ground states we mean the following.

Definition. *(Crystallised ground states) We say that an energy* $E : (\mathbb{R}^d)^N \to \mathbb{R}$, $d = 2, 3$, *has* crystallised ground states *if its infimum is attained and any minimiser—after translation and rotation—is a subset of the triangular lattice* $\mathcal{L}^{2D}$ *in the case* $d = 2$ *and in the case* $d = 3$ *is a subset of the face–centred cubic lattice* $\mathcal{L}^{fcc}$.

The specific choices of the triangular lattice and face–centred cubic lattice in the definition of crystallised ground states owe to our expectation that minimisers of E among

all N particle configurations for a potential V satisfying our hypotheses (H1)–(H3) (or (H1),(H2),(H3') resp.) are indeed—up to translation and rotation—subsets of $\mathcal{L}^{2D}$ and $\mathcal{L}^{fcc}$ resp.

Rigorous proofs have only been found in two dimensions for the Heitmann–Radin 'sticky disc' potential (see [Har74], [HR80])

$$V(r) = \begin{cases} +\infty, & 0 \leq r < 1 \\ -1, & r = 1 \\ 0, & r > 1 \end{cases} \tag{5.1}$$

and for the 'soft disc' potential

$$V(r) = \begin{cases} +\infty, & 0 \leq r < 1 \\ 24r - 25, & 1 \leq r < \frac{25}{24} \\ 0, & \frac{25}{24} \leq r < \infty. \end{cases} \tag{5.2}$$

Minimisers of energies with other interaction potentials V could also be crystalline, but may well—dependent of V—self–arrange into other lattices, such as the square lattice or the hexagonal lattice. For instance, [EL09] suggested the inclusion of an empirical three–body Stillinger–Weber potential in the energy favouring specific bond angles (different from those appearing in the triangular lattice) to admit ground states in the hexagonal lattice. However, rigorous analysis of such minimisers and analysis for other potentials has not yet been carried out.

For analogous results for the closely related sphere–packing problem in two dimensions see [CS99, Tót40], and for insights into more general potentials see [The06, EL09].

However, in three dimensions there are no characterisations of ground states even in the case of Heitmann–Radin potential. In fact, we do not believe that in three dimensions all minimisers are—up to translation and rotation—subset of a unique lattice, but rather subset of a close–packed lattice.

Variational Formulation. Item (4) consists in writing down a Wulff–Herring variational type problem and in passing to the Gamma–limit. Our programme is as follows.

1. Express the re–scaled surface energies of an N–particle configuration $\{x_1^{(N)}, \dots, x_N^{(N)}\} \subset \mathbb{R}^d$, $d = 2, 3$,

$$N^{-\frac{d-1}{d}} \left(E(\{x_1^{(N)}, \dots, x_N^{(N)}\}) + NE_b \right), \tag{5.3}$$

   where E_b is the bulk energy per particle and equals 6 in two dimensions, 12 in three dimensions resp., as functionals acting on the space of probability measures $\mathcal{P}(\mathbb{R}^d)$.

2. Show that, under appropriate hypotheses, the sequence of surface energy functionals Gamma–converge to a Curie–Gibbs–Wulff–type functional I_∞.

The first step can be realised by expressing the energy $E(\{x_1^{(N)}, \dots, x_N^{(N)}\})$ as a functional $I_N : \mathcal{P}(\mathbb{R}^d) \to \mathbb{R} \cup \{\infty\}$, so that the surface energy in (5.3) becomes

$$N^{-\frac{d-1}{d}} (I_N(\mu_N) + NE_b).$$

Subsequently, we analyse the limiting behaviour of the sequence and show that it Gamma–converges to the effective surface functional I_∞,

$$I_\infty(\mu) = \begin{cases} \int_{\partial^* E} e(n)\,\mathrm{d}\mathcal{H}^{d-1}, & \mu = \rho\chi_E \text{ for some set } E \text{ of} \\ & \text{finite perimeter and volume } \frac{1}{\rho}, \\ +\infty, & \text{otherwise.} \end{cases} \tag{5.4}$$

Here, ρ equals $2/\sqrt{3}$ in two dimensions and $\sqrt{2}$ in three dimensions resp. and the function e is the surface energy density function for the triangular lattice and for the face–centred cubic lattice resp., derived in Propositions 3.1 and 3.2. To keep notation simple, we will make the convention that the vector n in integrals of form $\int_{\partial E} e(n)\,\mathrm{d}\mathcal{H}^d$ will always denote the outward unit normal to the respective domain of integration.

B. Identification of cluster. From Chapter 4 we already know that sequences of re–scaled empirical measures associated to exact minimisers weak$*$ converge to $\mu = \rho\chi_E$, E set of finite perimeter and volume $\frac{1}{\rho}$.

The major tool to identify the cluster E is to use the uniqueness theorem for Herring type energies due to Taylor (in the language of geometric measure theory), in the version by Fonseca and Müller (who work in the present setting of boundary integrals for sets of finite perimeter):

Theorem 5.1. *([Tay75, FM91]) A functional of form*

$$I(E) = \int_{\partial^* E} e(n)\,\mathrm{d}\mathcal{H}^{d-1},$$

with $e : S^{d-1} \to [0,\infty)$ continuous and bounded away from zero, is minimised over sets $E \subset \mathbb{R}^d$ of finite perimeter and volume 1 if and only if E agrees, up to translation

and up to a set of measure zero, with λW_e, where W_e is the Wulff set

$$W_e := \left\{ x \in \mathbb{R}^d : x \cdot \nu \leq e(\nu) \text{ for all } \nu \in S^{d-1} \right\} \tag{5.5}$$

and $\lambda > 0$ is the unique normalisation constant such that λW_e has volume 1.

Finally, the compactness results in Proposition 4.2 and Theorem 4.4 enable us to apply the Theorem on minimisers of Gamma–converging functionals (p. 132), so that the cluster set E turns out to be a constant multiple of the Wulff set, that is to say that $E = cW_e$, $c = \frac{1}{\rho|W_e|}$.

The above cited Theorem could also be used to discuss variational problems which contain an additional bulk functional. Such problems arise for instance when the competitive behaviour between the bulk term and an anisotropic surface energy comes into play, see e.g. [FFLM11] for an application to material voids.

5.1 Two dimensions: triangular lattice

This section is joint work with Gero Friesecke and Bernd Schmidt and has been published in [AFS12]. Throughout this section, $\mathcal{L}$ is the triangular lattice.

In case of low–energy states, we now study the shape of the limitingi cluster E obtained in the previous section.

Our current methods are restricted to exact minimisers and to energies with crystallised ground states. Here the problem simplifies because by (H1), (H2) and (H3) we may without loss of generality assume that the interaction potential is given by the Heitmann–Radin potential (2.2) (see Figure 5.1). For such configurations, we can derive a limiting variational principle, as follows. It is useful (as in [CF09]) to re–

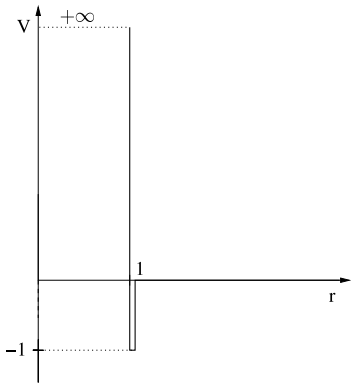

Figure 5.1: The Heitmann–Radin 'sticky disc' potential.

formulate the minimisation problem for the atomistic energy E in terms of empirical measures instead of particle configurations. Define the following energy functionals on the set $\mathcal{P}$ of probability measures on $\mathbb{R}^2$ (*i.e.*, nonnegative Radon measures on $\mathbb{R}^2$ of mass 1):

$$I_N(\mu) := \begin{cases} \int_{\mathbb{R}^4 \setminus diag} NV(N^{1/2}|x-y|)\,\mathrm{d}\mu \otimes \mathrm{d}\mu, & \mu = \frac{1}{N}\sum_{i=1}^{N} \delta_{x_i/\sqrt{N}} \\ & \text{for some distinct } x_i \in \mathcal{L} \\ +\infty, & \text{otherwise.} \end{cases} \tag{5.6}$$

This definition says that $I_N(\mu_N) = E(x_1, \ldots, x_N)$ when μ_N is the re–scaled empirical measure (4.2) of the configuration $\{x_1, \ldots, x_N\}$. In particular, the re–scaled empirical measure minimises I_N if and only if the underlying configuration minimises E.
We show in Sections 5.1.1, 5.1.2:

Theorem 5.2. *The sequence of functionals $N^{-1/2}(I_N + 6N)$ Gamma–converges, with respect to weak∗ convergence of probability measures, to the limit functional I_∞ given by $I_\infty : \mathcal{P} \to \mathbb{R} \cup \{\infty\}$,*

$$I_\infty(\mu) := \begin{cases} \int_{\partial^* E} e(\nu)\, \mathrm{d}\mathcal{H}^1, & \mu = \frac{2}{\sqrt{3}}\chi_E \text{ for some set } E \text{ of} \\ & \text{finite perimeter and mass } \frac{\sqrt{3}}{2}, \\ +\infty, & \text{otherwise,} \end{cases} \tag{5.7}$$

where e is the function

$$e(\nu) = 2\left(\nu_2 - \frac{\nu_1}{\sqrt{3}}\right) \text{ for } \nu = \begin{pmatrix} -\sin\varphi \\ \cos\varphi \end{pmatrix},\ \varphi \in [0, \tfrac{2\pi}{6}], \tag{5.8}$$

extended $\frac{2\pi}{6}$–periodically.

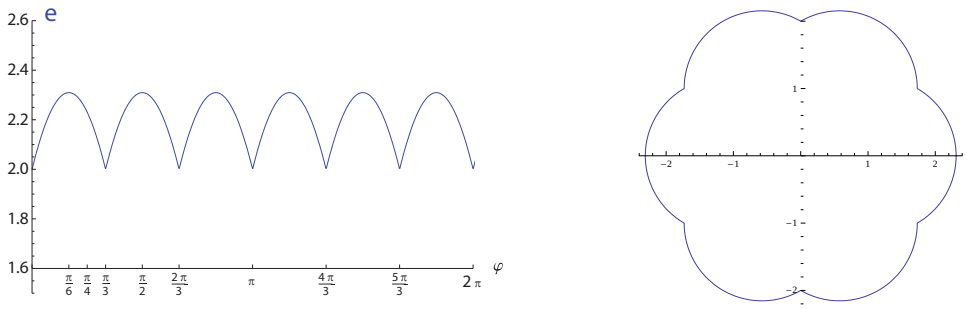

Figure 5.2: Plot of the limiting surface energy density e in dependence of φ and polar plot of e as a function of the normal ν.

The physical idea which is made quantitative here that crystalline anisotropy gives rise to nontrivial surface energies goes back to Wulff (1901) and Herring (1951) in the physics literature. Rigorous interfacial energy results have a large and sophisticated statistical mechanics literature, particularly in the context of the Ising model (see e.g.

the book by Dobrushin, Kotecky, and Shlosman [DKS92]). For a previous treatment of an interfacial energy problem via Gamma–convergence see [ABC06].
For exact minimisers the ensuing cluster has a unique shape:

Theorem 5.3. *Suppose the energy E is given by (4.1) and the interatomic potential satisfies (H1), (H2), (H3). Assume in addition that E has crystallised ground states (as is rigorously known e.g. when V is given by (2.2)). Let $\{x_1^{(N)}, \dots, x_N^{(N)}\}$ be any minimising N–particle configuration of E, and let μ_N be the associated re–scaled empirical measure (4.2). As $N \to \infty$, up to translation and rotation (that is to say, up to replacing μ_N by $\mu_N(R_N \cdot + a_N)$ for some rotation $R_N \in SO(2)$ and some translation vector $a_N \in \mathbb{R}^2$) μ_N converges weak* to the limit measure*

$$\mu = \frac{2}{\sqrt{3}} \chi_{\overline{h}} \tag{5.9}$$

where $\overline{h}$ is the regular hexagon $\operatorname{conv}\{\pm\frac{1}{\sqrt{3}}e_1, \pm\frac{1}{\sqrt{3}}e_2, \pm\frac{1}{\sqrt{3}}(e_2 - e_1)\}$.

The proof is postponed to Section 5.1.3. Finally we remark that macroscopic uniqueness of the limit shape in Theorem 5.3 contrasts with an unexpectedly large amount of non–uniqueness of the discrete minimisers. In the preprint [Sch13], it was proven for the two dimensional case that the optimal bound on the difference between two ground state configurations μ_N and μ'_N,

$$\min\{\|\mu'_N - \mu_N(R \cdot + a)\| : R \in O(2), a \in \mathbb{R}^2\}$$

(in suitable norms) scales like $N^{-1/4}$. Here optimal means that there exists a sequence $N_j \to \infty$ of particle numbers for which there is a matching lower bound. Note that simple rearrangements of surface atoms only lead to differences of order $N^{-\frac{1}{2}}$ in the

associated empirical measures. Hence the $N^{-1/4}$ law shows unexpectedly strong fluctuations of finite ground state configurations about the limiting Wulff shape.

5.1.1 Lower bound: lower semicontinuity

Let $\mathcal{S}_N = \{x_1^{(N)}, \dots, x_N^{(N)}\} \subset \mathcal{L}$ be any sequence of N–particle configurations whose associated sequence of Radon measures μ_N (see (4.2)) weak$*$–converges to a probability measure $\mu \in \mathcal{P}$. We need to show that $\liminf N^{-1/2}(I_N(\mu_N)+6N) \geq I_\infty(\mu)$. Associate to $\mathcal{S}_N$ the following auxiliary set

$$H_N := \bigcup_{x \in \mathcal{S}_N} \overline{N^{-1/2} h'_{1/\sqrt{3}}(x)},$$

where $h'_r(x)$ denotes the open hexagon around x of radius r introduced in the previous section. Note that for $x \in \mathcal{L}$, the closure of $h'_{1/\sqrt{3}}(x)$ is the Voronoi cell of x with respect to the complete lattice $\mathcal{L}$.

The boundary ∂H_N is a disjoint union of simple closed polygons $V_1, \dots, V_M$. Because the boundary ∂H_N oscillates on the atomic scale, we define yet another auxiliary set H'_N (see Figure 5.3) which removes these oscillations and will hence allow us to obtain a sharp lower bound on $I_N(\mu_N)$ via standard weak lower semicontinuity results on surface functionals. If $V_j \subset \partial H_N$ is a simple closed polygon, then $V_j = \bigcup_{i=1}^m [v_{i+1}, v_i]$ with segments $[v_{i+1}, v_i]$ of length $1/\sqrt{3N}$ for

$$v_1, \dots, v_m \in \left(\frac{1}{3\sqrt{N}}(e_1+e_2) + \frac{1}{\sqrt{N}}\mathcal{L}\right) \cup \left(\frac{1}{3\sqrt{N}}(2e_2-e_1) + \frac{1}{\sqrt{N}}\mathcal{L}\right), \quad v_{m+1} := v_1.$$

As the corner points v_i alternate between the lattices $\frac{1}{3\sqrt{N}}(e_1+e_2)+\frac{1}{\sqrt{N}}\mathcal{L}$ and $\frac{1}{3\sqrt{N}}(2e_2-e_1)+\frac{1}{\sqrt{N}}\mathcal{L}$ comprising the dual lattice of $\mathcal{L}$, m is an even number, and the set $V'_j =$

$\bigcup_{i=1}^{m/2}[v_{2i-1}, v_{2i+1}]$ is a simple closed polygon. We now define the set $H'_N \subset \mathbb{R}^2$ as the unique closed set with $\mathcal{S}_N \subset H'_N$ such that $\partial H'_N = \bigcup_{J=1}^{M} V'_j$. It can be easily seen that

$$|H'_N \triangle H_N| \leq \frac{\#\partial \mathcal{S}_N}{8N\sqrt{3}}. \tag{5.10}$$

Here, for two sets A and B, $A\triangle B$ denotes the symmetric difference $(A\backslash B) \cup (B\backslash A)$.

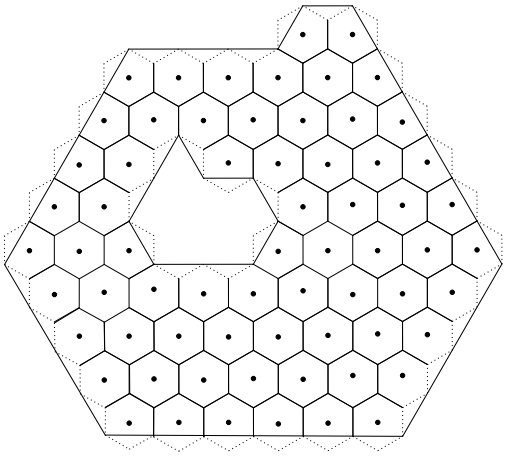

Figure 5.3: Constructing H'_N from H_N.

Note that $[v, w] \cap [x, y] \neq \emptyset$ defines a one–to–one correspondence between boundary segments $[v, w]$ of H_N and nearest neighbor bonds $[x, y]$ of $\frac{1}{\sqrt{N}}\mathcal{L}$, *i.e.* $x, y \in \frac{1}{\sqrt{N}}\mathcal{L}$ with $|x - y| = \frac{1}{\sqrt{N}}$, such that $x \in \frac{1}{\sqrt{N}}\mathcal{S}_N$ and $y \notin \frac{1}{\sqrt{N}}\mathcal{S}_N$. But then there is a one–to–two correspondence between boundary segments $[v, w]$ of H'_N and nearest neighbour bonds $[x, y]$ such that $x \in \mathcal{S}_N$ and $y \notin \mathcal{S}_N$. Since boundary segments of H'_N are of length $\frac{1}{\sqrt{N}}$, this shows that

$$I_N(\mu_N) + 6N = 2\sqrt{N}\mathcal{H}^1(\partial H'_N). \tag{5.11}$$

Precisely as in Step 1 in the proof of Theorem 4.1 we see that

$$\mu'_N := \frac{1}{N} \sum_{x \in \mathcal{S}_N} \frac{\chi_{N^{-1/2} h'_{1/\sqrt{3}}}(x)}{|N^{-1/2} h'_{1/\sqrt{3}}(x)|} \tag{5.12}$$

weak$*$ converges to μ. Now—similarly as in Step 3 in the proof of Theorem 4.1—we obtain that after a change on a set of measure zero

$$\mu'_N = \rho \chi_{H_N}.$$

Moreover, if $\frac{1}{\sqrt{N}}(I_N(\mu_N) + 6N)$ is bounded it follows from (5.11) that the restrictions $\mu_N|_{B_R}$ are bounded in $BV(B_R)$ for each $R > 0$, and hence converge to $\mu|_{B_R}$ in $L^1(B_R)$, due to the compact embedding $BV(B_R) \hookrightarrow L^1(B_R)$. Since $\|\mu\|_{L^1(\mathbb{R}^2)} = \|\mu_N\|_{L^1(\mathbb{R}^2)} = 1$ for all N, we obtain that even $\mu_N \to \mu$ in $L^1(\mathbb{R}^2)$ and $\mu = \rho \chi_E$ for a set E of finite perimeter and area $\frac{1}{\rho}$.

Furthermore, if (a subsequence of) $\frac{1}{\sqrt{N}}(I_N(\mu_N) + 6N)$ is bounded, then by (5.10) and (4.24) $\rho \chi_{H'_N} \to \mu = \rho \chi_E$ in $L^1(\mathbb{R}^2)$, whereas by (5.11), (5.8) and the fact that each boundary segment of H'_N is parallel to e_1 , e_2 or $e_1 - e_2$

$$\frac{1}{\sqrt{N}}(I_N(\mu_N) + 6N) = 2\mathcal{H}^1(\partial H'_N) = \int_{\partial(H'_N)} e(\nu) \, \mathrm{d}\mathcal{H}^1.$$

Now since e, extended to a 1–homogeneous function on $\mathbb{R}^2$, is convex and satisfies a growth condition of the type $e(\nu) \geq c|\nu|$ for some $c > 0$, a lower semicontinuity result for SBV functions (cf. Theorem 5.22 in Ambrosio–Fusco–Pallara [AFP00]) establishes the lower bound

$$\liminf_{N \to \infty} \frac{1}{\sqrt{N}}(I_N(\mu_N) + 6N) \geq \int_{\partial^* E} e(\nu) \, \mathrm{d}\mathcal{H}^1.$$

5.1.2 Upper bound: attainment of lower bound

The idea to find a recovery sequence is to approximate gradually a set of finite perimeter E by sets of simpler geometric shape. To be more precise, a set of finite perimeter will be approximated by C^∞ sets, C^∞ sets by sets with polygonal boundaries and polygonal sets by polygonal sets having all their corners in $\frac{1}{n}\mathcal{L}$ for some $n \in \mathbb{N}$. The recovery sequence for E will then be extracted through a diagonalisation process. Finally, a suitable continuity property of surface integrals,

$$\lim_{N\to\infty} \int_{\partial^* P_N} e(\nu)\, \mathrm{d}\mathcal{H}^1 = \int_{\partial^* P} e(\nu)\, \mathrm{d}\mathcal{H}^1,$$

where (P_N) is the approximation sequence and P denotes the approximated set in the respective step, will complete the proof.

Step 1 First, let $P \subset \mathbb{R}^2$ be a bounded set with polygonal boundary such that every corner of ∂P lies in $\frac{1}{n}\mathcal{L}$ for some $n \in \mathbb{N}$. Assume that the volume of P is $\frac{\sqrt{3}}{2} + \alpha_n$. Consider the sequence of particle configurations $\tilde{\mathcal{S}}_{n,N} = \mathcal{L} \cap \sqrt{N}P$ consisting of $M = M_{n,N}$ atoms. Elementary geometric considerations show that

$$|M_{n,N} - N| \leq c(\alpha_n N + \sqrt{N}). \tag{5.13}$$

for a constant c independent of n and N. Let $\mu_{n,N}$ denote the associated rescaled empirical measures. Clearly, $\mu_{n,N} \overset{*}{\rightharpoonup} \rho\chi_P$ as $N \to \infty$. In addition, a straightforward calculation of the associated energy by evaluating the surface energy contribution

$$\frac{1}{\sqrt{N}} \sum_{x\in\partial\tilde{\mathcal{S}}_{n,N}} \#\left\{x' \in \mathcal{L} \setminus \tilde{\mathcal{S}}_{n,N} : |x - x'| = 1\right\},$$

along line segments of ∂P gives

$$\left|\frac{1}{\sqrt{N}}(I_M(\mu_{n,N})+6M)-\int_{\partial P} e(\nu)\,\mathrm{d}\mathcal{H}^1\right| \le c\left(\alpha_n+\frac{1}{\sqrt{N}}\right) \tag{5.14}$$

for a constant c independent of n and N. Indeed, an elementary argument shows that if S is a boundary segment of P of length L with normal ν, then the number of pairs $(x,y)\in\tilde{\mathcal{S}}_{n,N}\times(\mathcal{L}\setminus\tilde{\mathcal{S}}_{n,N})$ with $|x-y|=1$ such that the segment $[x,y]$ intersects $\sqrt{N}S$ is equal to

$$\lfloor\sqrt{N}\rfloor e(\nu)L+O\left(L\right)=\sqrt{N}\left(e(\nu)L+O\left(\frac{L}{\sqrt{N}}\right)\right).$$

Step 2 Now let $P\subset\mathbb{R}^2$ be any set of volume $\frac{\sqrt{3}}{2}$ with polygonal boundary. By perturbing the corners of ∂P slightly, it is easy to see that there is a sequence of polygonal sets P_n whose boundary vertices lie in $\frac{1}{n}\mathcal{L}$ satisfying

$$|P_n\triangle P|\to 0 \text{ as } n\to\infty \tag{5.15}$$

and

$$\int_{\partial^* P_n} e(\nu)\,\mathrm{d}\mathcal{H}^1\to\int_{\partial^* P} e(\nu)\,\mathrm{d}\mathcal{H}^1 \text{ as } n\to\infty. \tag{5.16}$$

Now choosing $n=n(N)\to\infty$ appropriately, we obtain a sequence of configurations

$$\tilde{\mathcal{S}}_N:=\tilde{\mathcal{S}}_{n(N),N}$$

from the configurations constructed in Step 1 such that the associated rescaled empirical measures $\tilde{\mu}_N$ satisfy $\tilde{\mu}_N\overset{*}{\rightharpoonup}\rho\chi_P$ and

$$\frac{1}{\sqrt{N}}(I_M(\tilde{\mu}_N)+6M)\to\int_{\partial P} e(\nu)\,\mathrm{d}\mathcal{H}^1$$

by (5.15), (5.14) and (5.16).

Now if $\#\tilde{\mathcal{S}}_N \neq N$, then the configuration $\tilde{\mathcal{S}}_N$ needs to be modified either by adding or removing some set of points with negligible surface term. By (5.13) $\frac{1}{N}|M-N| \to 0$ as $N \to \infty$. If $\tilde{\mathcal{S}}_N$ contains less than N particles, then we can add the missing number of points on lattice sites within some parallelogram whose sidelengths are of order $\sqrt{N-M}$ and such that the points in the parallelogram are a distance greater than 1 away from $\tilde{\mathcal{S}}_N$. Then none of the new points interacts with $\tilde{\mathcal{S}}_N$. In case $M > N$, just remove $M-N$ points of $\tilde{\mathcal{S}}_N$ lying in a common parallelogram whose sidelengths are of order $\sqrt{M-N}$. (This is always possible if N is large enough.)

Denoting the corresponding rescaled empirical measure by μ_N and recalling that $\frac{1}{N}|M-N| \to 0$ it is not hard to see that $\mu_N \overset{*}{\rightharpoonup} \rho\chi_P$ as $N \to \infty$. Since furthermore

$$\left| \frac{1}{\sqrt{N}}(I_M(\tilde{\mu}_N) + 6M) - \frac{1}{\sqrt{N}}(I_N(\mu_N) + 6N) \right| \leq c\sqrt{\frac{1}{N}(M-N)}$$

for some constant $c > 0$, we also obtain

$$\frac{1}{\sqrt{N}}(I_N(\mu_N) + 6N) \to \int_{\partial P} e(\nu)\, \mathrm{d}\mathcal{H}^1$$

by (5.13) and (5.14).

Step 3 A recovery sequence for a general set E of finite perimeter is now obtained by a diagonalisation argument due to the following density and continuity results.

Suppose first E is a bounded set of finite perimeter with C^∞–boundary and volume $\frac{\sqrt{3}}{2}$. By piecewise linear approximations of ∂E and scaling with factors close to 1 we easily construct approximations P_n which have the same volume, a polygonal boundary and

satisfy

$$\chi_{P_n} \overset{*}{\rightharpoonup} \chi_E \quad \text{and} \quad \int_{\partial^* P_n} e(\nu)\,\mathrm{d}\mathcal{H}^1 \to \int_{\partial^* E} e(\nu)\,\mathrm{d}\mathcal{H}^1.$$

Now let E be a bounded set of finite perimeter with volume $\frac{\sqrt{3}}{2}$. As shown e.g. in [Bra98, Proposition 4.7 and Remark 4.8], there are bounded sets E_n of finite perimeter with C^∞–boundary and— after rescaling with a factor close to 1—volume $\frac{\sqrt{3}}{2}$ such that, as $n \to \infty$,

$$\chi_{E_n} \overset{*}{\rightharpoonup} \chi_E \text{ and } \int_{\partial^* E_n} e(\nu)\,\mathrm{d}\mathcal{H}^1 \to \int_{\partial^* E} e(\nu)\,\mathrm{d}\mathcal{H}^1.$$

Finally note that a truncation argument yields that an analogous result holds for approximating sets of finite perimeter with bounded sets of finite perimeter. This concludes the proof. □

5.1.3 Identification of Wulff set

To complete the proof of Therem 5.3, it remains to infer convergence of minimisers. A technical detail we need to pay attention to is that, unlike in many other Gamma–convergence results, here sequences with bounded energy are not in general compact in the topology in which the Gamma–convergence occurs. This is because, due to the translation invariance of the functionals $N^{-1/2}(I_N + 6N)$, sequences can lose mass as $N \to \infty$.

Proof of Theorem 5.3 Let μ_N be a sequence of re–scaled empirical measures (4.2) corresponding to exact minimisers of E. By the connectedness of minimising configurations and Proposition 4.2, after suitable translations $\mu_N \mapsto \mu_N(\cdot + a_N)$ the limit measure μ has full mass. Hence sequences of exact minimisers are compact in the topology in

which the Gamma–convergence occurs (namely weak* convergence of probability measures). By standard arguments in Gamma–convergence, μ is a minimiser of the limit functional I_∞.

We now appeal to the uniqueness theorem for Herring type energies due to Taylor, Fonseca and Müller (Theorem 5.1).

In the present case of the energy (5.8), an elementary calculation shows that the Wulff set is given by the intersection of the six half–spaces $x \cdot \nu \leq e(\nu)$ for the minimising normals $\nu_{2\pi j/6}$, $j = 1, \ldots, 6$, *i.e.*a regular hexagon with bottom face parallel to the e_1–axis (see Figure 5.4). This completes the proof of Theorem 5.3.

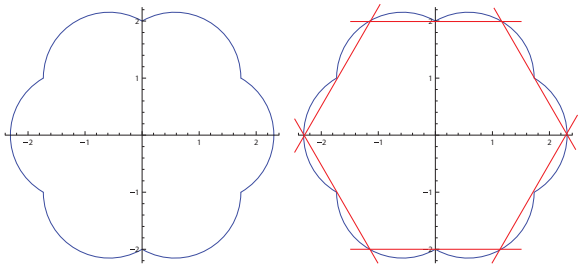

Figure 5.4: Left: Polar plot of the energy density function e. Right: The Wulff set is constructed as the intersection of the six red hyperplanes.

5.2 Three dimensions: face–centred cubic lattice

This section on the three dimensional case is new.

Similarly to the two dimensional case, we will prove that the sequence of surface energy functionals $N^{-2/3}(I_N + 12N)$ Gamma–converges to an effective limiting functional I_∞. Recall that a major reason why we establish Gamma–convergence is to employ the following property: Minimisers of the functionals $N^{-2/3}(I_N + 12N)$ converge to

minimisers of I_∞. This property is fulfilled thanks to Theorem 4.4.

Our energy E is assumed to be of pair–potential type (4.1) and we assume that the ground states are up to translation and rotation subsets of the face–centred cubic lattice $\mathcal{L}^{fcc} = e_1\mathbb{Z} \oplus e_2\mathbb{Z} \oplus e_3\mathbb{Z}$, where

$$e_1 = \frac{1}{\sqrt{2}} \begin{pmatrix} 0 \\ 1 \\ 1 \end{pmatrix}, \; e_2 = \frac{1}{\sqrt{2}} \begin{pmatrix} 1 \\ 0 \\ 1 \end{pmatrix}, \; e_3 = \frac{1}{\sqrt{2}} \begin{pmatrix} 1 \\ 1 \\ 0 \end{pmatrix}.$$

The energy E will now be interpreted as a functional on $\mathcal{P}(\mathbb{R}^3)$ via

$$I_N(\mu) := \begin{cases} \int_{\mathbb{R}^6 \setminus \mathrm{diag}} NV(N^{1/3}|x-y|)\mathrm{d}\mu \otimes \mathrm{d}\mu, & \mu = \frac{1}{N}\sum_{i=1}^N \delta_{N^{-1/3}x_i} \\ & \text{for some distinct } \; x_i \in \mathcal{L}^{fcc} \\ +\infty, & \text{otherwise.} \end{cases}$$

By dividing the energy excess between $E(\{x_1^{(N)}, \ldots, x_N^{(N)}\})$ and $-12N$ by the leading order of the surface energy $N^{2/3}$, we obtain the re–scaled surface energy of $\mathcal{S}_N$, namely

$$N^{-2/3}\Big(E(\{x_1^{(N)}, \ldots, x_N^{(N)}\}) + 12N\Big) = N^{-2/3}\Big(I_N(\mu_N) + 12N\Big).$$

For the latter functional we claim the following variational limit.

Theorem 5.4. *The sequence of functionals $N^{-2/3}(I_N + 12N)$ Gamma–converges, with respect to weak∗ convergence of probability measures, to the limit functional I_∞ given by $I_\infty : \mathcal{P}(\mathbb{R}^3) \to \mathbb{R} \cup \{\infty\}$,*

$$I_\infty(\mu) := \begin{cases} \int_{\partial^* E} e(n)\, \mathrm{d}\mathcal{H}^2, & \mu = \sqrt{2}\chi_E \text{ for some set E of} \\ & \text{finite perimeter and mass } \frac{\sqrt{2}}{2} \\ +\infty, & \text{otherwise.} \end{cases} \tag{5.17}$$

The function e is derived in Proposition 3.2. It equals the periodic extension (according to the point group of $\mathcal{L}^{fcc}$) of the function $n \mapsto 2n_2 + 4n_3$, where n is a rational unit normal that can be represented by Miller indices $h \geq k \geq \ell \geq 0$.

For crystalline configurations we can identify the cluster set for energies with crystalline ground states.

Theorem 5.5. *Suppose the energy E is given by (4.1) and the interatomic potential satisfies (H1), (H2) and (H3') on page 73. Assume in addition that E has crystallised ground states,* i.e., *every ground state is—after translation and rotation—a subset of the face–centred cubic lattice $\mathcal{L}^{fcc}$. Let $\{x_1^{(N)}, \ldots, x_N^{(N)}\}$ be any minimising N–particle configuration of E of bounded diameters,*

$$\max_{i,j} |x_i^{(N)} - x_j^{(N)}| \leq CN^{1/3},$$

and of bounded energies,

$$E(x_1^{(N)}, \ldots, x_N^{(N)}) \leq -12N + CN^{2/3},$$

where C is some generic constant independent of N. Let μ_N be the associated re–scaled

empirical measure

$$\mu_N := \frac{1}{N}\sum_{i=1}^{N} \delta_{N^{-1/3}x_i^{(N)}}.$$

As $N \to \infty$, up to translation and rotation (that is to say, up to replacing μ_N by $\mu_N(R_N \cdot + a_N)$ for some rotation $R_N \in SO(3)$ and some translation vector $a_N \in \mathbb{R}^3$) μ_N converges weak$*$ to the limit measure

$$\mu = \sqrt{2}\chi_E. \tag{5.18}$$

Here the set E is the c–multiple of the regular truncated octahedron whose vertices are given by all permutations of $(0, 2, 4)^T$, $(0, -2, 4)^T$, $(0, 2, -4)^T$, $(0, -2, -4)^T$, with the constant c being $\frac{\sqrt{2}}{512}$.

The proof of Theorem 5.4 is performed in Sections 5.2.1 and 5.2.2. Section 5.2.3 is devoted to the proof of Theorem 5.5.

5.2.1 Lower bound: lower semicontinuity

We must verify that the lower bound holds, *i.e.*,

$$\liminf_{N\to\infty} N^{-2/3}(I_N(\mu_N) + 12N) \geq I_\infty(\mu). \tag{5.19}$$

for all sequences μ_N that weak$*$ converge to μ.
Let $\mathcal{S}_N := \{x_1^{(N)}, \ldots, x_N^{(N)}\} \subset \mathcal{L}^{fcc}$ be any sequence of N–particle configurations whose associated sequence of Radon measures

$$\mu_N := \frac{1}{N}\sum_{x\in\mathcal{S}_N} \delta_{N^{-1/3}x}$$

weak$*$ converges to some probability measure $\mu = \sqrt{2}\chi_E \in \mathcal{P}(\mathbb{R}^3)$, E set of finite perimeter with mass $\sqrt{2}/2$. Our proof is divided into two steps:

Step 1. Find a sequence of sets P_N such that

$$N^{-2/3}(I_N(\mu_N) + 12N) \geq \int_{\partial P_N} e(n)\,\mathrm{d}\mathcal{H}^2. \tag{5.20}$$

and such that $\rho\chi_{P_N} \to \mu$ in L^1.

Step 2. Apply a lower semicontinuity result for SBV functions, w.r.t. L^1 convergence, by Ambrosio–Fusco–Pallara [AFP00] to deduce that

$$\liminf_{N\to\infty} \int_{\partial P_N} e(n)\,\mathrm{d}\mathcal{H}^2 \geq \int_{\partial^* E} e(n)\,\mathrm{d}\mathcal{H}^2.$$

Proof of first step.

Construction of polygonal sets. A key difficulty arises in the construction of P_N. It is difficult to modify the two dimensional construction to three dimensions, because it is absolutely not clear which of the boundary vertices are the most appropriate to be removed.

We will therefore present another construction which we call the *shrinking argument*. Our construction remains valid in two dimensions and, in fact, the author believes that an (adapted) argument may be useful to establish lower semicontinuity results for ground states which crystallise in other lattices than $\mathcal{L}^{fcc}$.

To begin with and to see where the difficulty arises, we define a natural prototype of polygonal set associated to $\mathcal{S}_N$.

Place at each $x \in \mathcal{S}_N$ its Voronoi cell w.r.t. to $\mathcal{L}^{fcc}$, that is to say, place at each x the rhombic dodecahedron whose radius of inscribed sphere equals $\frac{1}{2}$ and whose unit face

normals are given by $\pm e_1, \pm e_2, \pm e_3, \pm(e_2 - e_1), \pm(e_3 - e_2), \pm(e_3 - e_1)$ (see Figure 5.5). Let us denote this rhombic dodecahedron around x by $\mathcal{V}(x)$ and let us define first the polygonal set

$$P_N^{(1)} := \bigcup_{x \in \mathcal{S}_N} N^{-1/3} \mathcal{V}(x). \tag{5.21}$$

We claim that the desired bound in (5.20) does not hold for this choice of $P_N^{(1)}$. This is because $\partial P_N^{(1)}$ is the union of parallelograms of area $N^{-2/3}\frac{\sqrt{2}}{4}$ and because normals to parallelograms on $\partial P_N^{(1)}$ show in the direction of a 2–fold rotation axis; hence, $e(n) = 3\sqrt{2}$, whenever n is a unit normal to a parallelogram on $\partial P_N^{(1)}$. Moreover, there is a one–to–one correspondence between the parallelograms of $\partial P_N^{(1)}$ and the broken bonds of $\mathcal{S}_N$, which finally yields

$$\begin{aligned} \int_{\partial P_N^{(1)}} e(n)\, \mathrm{d}\mathcal{H}^2 &= \sum_{\text{parallelograms}} \text{area(parallelogram)} \cdot e(n) \\ &= N^{-2/3} \frac{\sqrt{2}}{4} \cdot 3\sqrt{2} \cdot (\sharp\text{parallelograms on } \partial P_N^{(1)}) \\ &= \frac{3}{2} \cdot N^{-2/3} \cdot (\sharp\text{broken bonds in } \mathcal{S}_N) \\ &= \frac{3}{2} \cdot N^{-2/3} \cdot (I_N(\mu_N) + 12N), \end{aligned} \tag{5.22}$$

and from which we finally infer that $P_N^{(1)}$ is inappropriate. Our interpretation why $P_N^{(1)}$ fails to work is as follows: The surface energy density attains its maximum value at the normals to $\partial P_N^{(1)}$; hence, the parallelograms have energetically unfavourable normals.

A way out would be to keep the facets small which have unfavourable energies and to glue them by facets with energetically favourable normals, *i.e.*, normals for which the energy has at least a local minimum. By inspection, the surface energy density

possesses critical points in the direction of the 2–, 3– and 4–fold axis:

$$\text{2–fold axis: } e(n) = 3\sqrt{2} \approx 4.2426 \tag{5.23}$$

$$\text{3–fold axis: } e(n) = 2\sqrt{3} \approx 3.4641 \tag{5.24}$$

$$\text{4–fold axis: } e(n) = 4. \tag{5.25}$$

Local minima are therefore achieved at normals in the directions of 3–fold and 4–fold rotation axes. It is obvious that

$$\sharp\{y \in \mathcal{S}_N \ : \ |x-y| = 1\} = 12 \implies \partial P_N^{(1)} \cap \partial(N^{-1/3}\mathcal{V}(x)) = \emptyset,$$

that is to say that only cells $N^{-1/3}\mathcal{V}(x)$ contribute to the boundary of $P_N^{(1)}$ if and only if x is a surface particle; hence, it suffices to modify appropriately the cells around each surface particle to influence the number and size of energetically unfavourable facets. To make the facets with unfavourable normals small, we shrink the boundary cells $\mathcal{V}(x)$ by a factor $\varepsilon > 0$, *i.e.*, we replace $\mathcal{V}(x)$ by

$$\mathcal{V}_\varepsilon(x) := \begin{cases} \mathcal{V}(x), & x \in \text{int}\mathcal{S}_N \\ \varepsilon\mathcal{V}(x), & x \in \partial\mathcal{S}_N. \end{cases}$$

The union of $\mathcal{V}_\varepsilon(x)$ covers $\mathcal{S}_N$ and has polygonal boundary, but is still insufficient for our purposes, for (1) it is disconnected and (2) cells around interior points in $\mathcal{S}_N$ contribute to the boundary of the polygonal set (see Figure 5.5 for a typical Voronoi cell and a typical shrank Voronoi cell). We therefore glue the cells $\mathcal{V}_\varepsilon$ with energetically favourable sets. First, observe that the cells of any two $x, y \in \partial\mathcal{S}_N$, $|x-y| = 1$, have a common quadrilateral facet (parallelogram) of side length $\sqrt{6}/4$; hence, the shrank

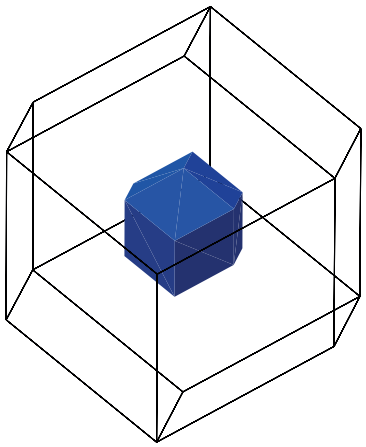

Figure 5.5: The Voronoi cell around x w.r.t. the $\mathcal{L}^{fcc}$ is a rhombic dodecahedron with edge lengths $\frac{\sqrt{6}}{4}$. The blue cell is a shrank Voronoi cell with $\varepsilon = \frac{1}{3}$.

cells at x and y have a parallel quadrilateral facet of side length $\varepsilon\sqrt{6}/4$. Every facet on $\mathcal{V}(x)$ is a parallelogram and is spanned by two vectors u and v

(i) of length $\sqrt{6}/4$ and

(ii) of angle $\alpha := \measuredangle(u, v) = \arccos(1/3)$.

In fact, one could find the spanning vectors by calculating the cross products of two vectors in $\mathcal{L}^{fcc}$ which have unit lengths and which have mutual distance one and by re–scaling their resulting lengths to $\frac{\sqrt{6}}{4}$. This yields for our lattice base vectors e_1, e_2, e_3 the spanning vectors (in Cartesian coordinates)

$$\frac{\sqrt{2}}{4}\begin{pmatrix}1\\1\\1\end{pmatrix}, \frac{\sqrt{2}}{4}\begin{pmatrix}-1\\1\\1\end{pmatrix}, \frac{\sqrt{2}}{4}\begin{pmatrix}1\\1\\-1\end{pmatrix}, \frac{\sqrt{2}}{4}\begin{pmatrix}-1\\1\\-1\end{pmatrix}.$$

Our strategy is as follows: On a given Voronoi cell, with its shrank cell inscribed, we glue all facets F with their shrank facet εF whenever F is the intersection of two Voronoi cells $\mathcal{V}(y) \cap \mathcal{V}(z)$, $y, z \in \mathcal{S}_N$.

Remark 5.6. For symmetry reasons and for the sake of simplicity, we will henceforth only explain how we connect εF with F within one Voronoi cell. The corresponding shrank facet in the other Voronoi cell will be glued with F in the same vein.

The gluing set will be constructed as the image of a function g: We define two curves x_ε and x on the shrank facet and on the respective non–shrank facet. The function g then connects x_ε with x,

$$g : [0,1] \times [0,1] \to \mathbb{R}^3, \qquad g(s,t) := (1-s)x_\varepsilon(t) + sx(t).$$

To begin with and to define the two curves, we assume that a vertex of a facet is given by b and that the remaining vertices are

$$a := b + u,\ c := b + v,\ d := b + u + v.$$

Then the vertices a, c have degree three, whereas the remaining vertices b, d are of degree four (see Figure 5.6 a)).
The respective vertices in the shrank facet are denoted by $a_\varepsilon, b_\varepsilon, c_\varepsilon, d_\varepsilon$.
The curve x_ε is defined as a piecewise linear function which connects b_ε with ξ_ε and ξ_ε

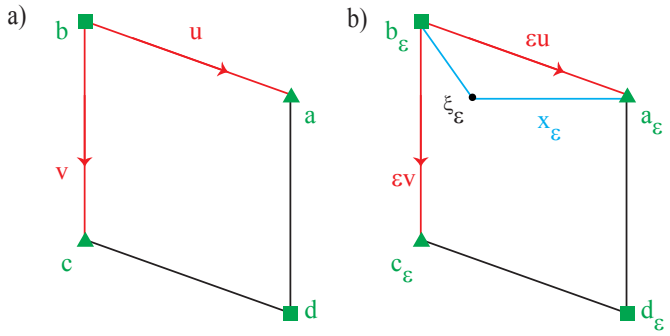

Figure 5.6: a) shows the parallelogram spanned by u, v. b) shows the shrank facet and the piecewise linear curve x_ε (blue line).

with a_ε by a straight line (see Figure 5.6 b)), *i.e.*,

$$x_\varepsilon : [0,1] \to \mathbb{R}^3, \;\; x_\varepsilon(t) := \begin{cases} \frac{1}{1-\varepsilon}\big[(1-\varepsilon-t)a_\varepsilon + t\xi_\varepsilon\big], & t \in [0, 1-\varepsilon], \\ \frac{1}{\varepsilon}\big[(1-t)\xi_\varepsilon + (t-(1-\varepsilon))b_\varepsilon\big], & t \in [1-\varepsilon, 1]. \end{cases} \tag{5.26}$$

For this sake, we define (see Figure 5.7)

$$\xi_\varepsilon := b_\varepsilon + h_\varepsilon \frac{v}{|v|} + \ell_\varepsilon \frac{u_\perp}{|u_\perp|},$$

where

$$h_\varepsilon := \varepsilon h, \;\; h := \frac{\langle u, v\rangle}{|v|}, \;\; \ell_\varepsilon := h_\varepsilon \tan\frac{\alpha}{2}.$$

Here, $u_\perp$ denotes the orthogonal part of u w.r.t. v and equals

$$u_\perp = u - h\frac{v}{|v|}.$$

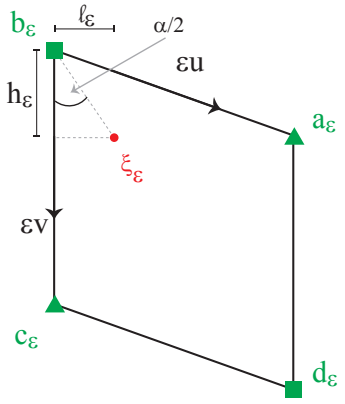

Figure 5.7: Construction of the point ξ_ε. The length h_ε is the length of the vector εu projected onto εv.

We now define the corresponding curve x on the non–shrank facet with vertices a, b, c, d. Let $\Pi(b_\varepsilon)$ and $\Pi(a_\varepsilon)$ denote the orthogonal projections of b_ε and a_ε resp. onto the line segments $\overline{bc}$ and $\overline{ad}$ resp. Then the curve x is, similarly to (5.26), the piecewise linear function that connects $\Pi(a_\varepsilon)$ with ξ and that connects ξ with $\Pi(b_\varepsilon)$,

$$x : [0,1] \to \mathbb{R}^3, \qquad x(t) := \begin{cases} \frac{1}{1-\varepsilon}\big[(1-\varepsilon-t)\Pi(a_\varepsilon) + t\xi\big], & t \in [0, 1-\varepsilon], \\ \frac{1}{\varepsilon}\big[(1-t)\xi + (t-(1-\varepsilon))\Pi(b_\varepsilon)\big], & t \in [1-\varepsilon, 1]. \end{cases} \tag{5.27}$$

Here, ξ is the point

$$\xi := \Pi(b_\varepsilon) + h_\varepsilon \frac{v}{|v|} + \varepsilon \frac{u_\perp}{|u_\perp|}.$$

As introduced above, the gluing set is the image $g([0,1]^2)$ of the function g (see Figure 5.8 for a sketch of M),

$$g : [0,1] \times [0,1] \to \mathbb{R}^3, \;\; g(s,t) := (1-s)x_\varepsilon(t) + sx(t).$$

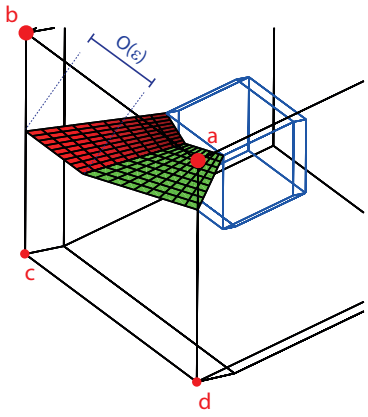

Figure 5.8: A Voronoi cell $\mathcal{V}$ and a corresponding shrank Voronoi cell $\mathcal{V}_\varepsilon$ with $\varepsilon = \frac{1}{3}$ are plotted. The gluing M can be decomposed into M_1 and M_2. The green set is M_1, whereas the red set is M_2. Note that the major mass sits at the trapezoid M_1 and that M_2 has only area of order $O(\varepsilon)$. This construction is suitable for our purposes, for the function e attains a minimum on M_1.

The reason why M suits our purposes is the following: This set can be decomposed into the union of two pieces, namely $M_1 := g([0,1]\times[0,1-\varepsilon])$ and $M_2 := g([0,1]\times[1-\varepsilon,1])$. The crucial point now is that the major mass sits at M_1 and that the energy density e attains its minimum on M_1!

The first set $M_1 := g([0,1]\times[0,1-\varepsilon])$ is a trapezoid whose normal shows in the direction of a 3–fold axis, whose parallel sides have lengths $\frac{\sqrt{3}}{3}(\varepsilon - \ell_\varepsilon)$, $\frac{\sqrt{3}}{3}(1-\varepsilon)$ and height $\frac{1}{2}(1-\varepsilon)$; hence,

$$\begin{aligned}\operatorname{area}(g([0,1]\times[0,1-\varepsilon])) &= \frac{1}{2}(1-\varepsilon)\cdot\frac{\frac{\sqrt{3}}{3}(\varepsilon-\ell_\varepsilon)+\frac{\sqrt{3}}{3}(1-\varepsilon)}{2}\\ &= \frac{\sqrt{3}}{12}(1+O(\varepsilon)).\end{aligned}$$

On the other hand, M_2 has energetically unfavourable normal, but has area of negligible order $O(\varepsilon)$. Next, we claim that

$$\int_M e(n)\,\mathrm{d}\mathcal{H}^2 = \frac{1}{2} + C\varepsilon \tag{5.28}$$

for some non–negative C. Indeed, from $e(n) = O(1)$ for all $n \in S^2$ and from the fact that $e(n) = 2\sqrt{3}$ on M_1 (, because normals to M_1 are equivalent to threefold axes), we infer

$$\begin{aligned}\int_M e(n)\,\mathrm{d}\mathcal{H}^2 &= \int_{M_1} e(n)\,\mathrm{d}\mathcal{H}^2 + \int_{M_2} e(n)\,\mathrm{d}\mathcal{H}^2 &(5.29)\\ &= \frac{\sqrt{3}}{12}\cdot(1+O(\varepsilon))\cdot 2\sqrt{3} + O(\varepsilon) &(5.30)\\ &= \frac{1}{2} + C\varepsilon &(5.31)\end{aligned}$$

for some constant C. This constant is non–negative: The projected area of M onto a plane whose normal shows into the direction of a 3–fold axis is exactly $\sqrt{3}/12$. Because the projected area $M^\perp$ must not exceed $\mathcal{H}^2(M)$ and because e attains a global minimum on $M^\perp$, the value $\int_{M^\perp} e(n)\,\mathrm{d}\mathcal{H}^2 = \frac{1}{2}$ is a lower bound for $\int_M e(n)\,\mathrm{d}\mathcal{H}^2$. The latter implies the constant C to be non–negative.

Next, we must state exactly in which cases we glue the set M from the above construction. Loosely speaking, the set M connects a shrank edge on the surface of $\bigcup \mathcal{V}_\varepsilon(x)$ with its corresponding non–shrank edge, whenever this edge belongs to two adjacent Voronoi cells.

However, this naive approach violates our desired estimate (5.20) and we have to pay more attention. We must not consider each "edge on the boundary" on its own, but rather to regard simultaneously all edges per facet. To keep definitions short, we in-

troduce the notation

$$\tilde{\Omega}_N := \bigcup_{x \in \mathcal{S}_N} \mathcal{V}(x).$$

and we introduce a set of facets through

$$\mathcal{F} := \left\{ F : \ F = \mathcal{V}(x) \cap \mathcal{V}(y) \text{ for some } x, y \in \partial \mathcal{S}_N \text{ with } |x - y| = 1 \right\}. \tag{5.32}$$

We associate to each facet $F \in \mathcal{F}$ all edges that contribute to the boundary of $\tilde{\Omega}_N$, and we define for $F \in \mathcal{F}$ (see Figure 5.9),

$$edge(F) := \left\{ \text{edge of } F \ : \ \text{edge is a subset of } \ \partial \tilde{\Omega}_N \right\}.$$

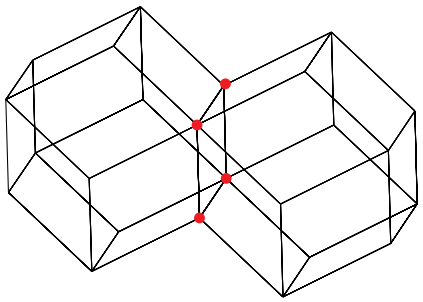

Figure 5.9: This is an example for $\mathcal{S}_N = \{x, y\}$ such that $|x - y| = 1$. Their Voronoi cells are rhombic dodecahedrons and are next to each other. The set $\mathcal{F}$ consists of exactly one parallelogram, namely the one with the red vertices. Moreover, all edges of this facet belong to $edge(F)$.

Depending on the cardinality of $edge(F)$, namely depending on whether it contains one, two, three or four edges, we give rules of gluing the set M. If $edge(F)$ is empty, we do not glue anything at F.

► $|edge(F)| = 4$ or $|edge(F)| = 3$:

In either case, there is at least one pair of parallel edges in $edge(F)$. Glue M to one pair of parallel of edges, that is to say glue the sets $g_1([0,1]^2)$ and $g_2([0,1]^2)$, where

$$g_j : [0,1] \times [0,1] \to \mathbb{R}^3, \;\; g_j(s,t) = (1-s)x_\varepsilon^j(t) + sx^j(t), \;\; j = 1,2,$$

for appropriate functions x_ε^j and x^j. Further, connect these two sets by

$$\begin{aligned} C :&= \mathrm{conv}(\{g_1(0,1), g_1(1,1), g_2(0,0), g_2(1,0)\}) \\ &\cup \mathrm{conv}(\{g_1(0,0), g_1(1,0), g_2(0,1), g_2(1,1)\}). \end{aligned}$$

See Figure 5.10 for the configurations of $edge(F)$. Also note that the mass of C is of order $O(\varepsilon)$.

► $|edge(F)| = 2$:

The two edges in $edge(2) = 2$ are either parallel, that is to say they are disjoint, or they have one point in common, that is to say they occur "successively" (see Figure 5.11 for the three possible edge configurations). In case a), where two parallel edges in $edge(F)$ exist, proceed exactly as above. In the remaining two configurations b) and c), we modify slightly one of the gluing sets M. Without loss of generality we modify the gluing set corresponding to x^1 and x_ε^1.

Recall, that the gluing set M at the jth edge is obtained from the convex combination of the curves x_ε^j and x^j, whose traces are on the shrank and non–shrank facet F. Let us denote by x_ε^j, x^j, $j = 1,2$, the corresponding curves for the two edges in $edge(F)$. We "truncate" the curve x^1 (see Figure 5.12):

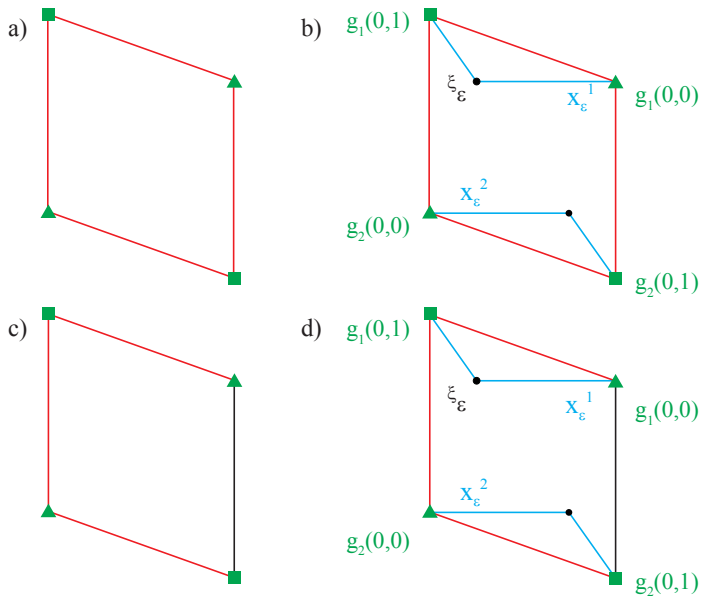

Figure 5.10: $|edge(F)| = 4$ and $= 3$. Figures a),b) and c), d) show the shrank facet εF and the edge configurations, whenever $|edge(F)| = 4$ and $= 3$ resp. The red edges are elements of $edge(F)$, whereas the black edges do not belong to $edge(F)$. The green squares and triangles indicate vertices of degree four and three. In both cases $|edge(F)| = 4$ and $= 3$ we glue the set M at each of the blue lines in Figures b) and d). Moreover, the vertices of the connecting set C which lie on the shrank facet εF are also plotted in Figures b) and d).

Let $\tau \in [0, 1-\varepsilon]$ be such that

$$x^1(\tau) = x^2(\tau)$$

and denote this position by ζ. Note that, for reasons of symmetry, there indeed exists a τ such that x and y coincide simultaneously.

In case the common vertex has order four: We substitute x^1 and x^1_ε—again

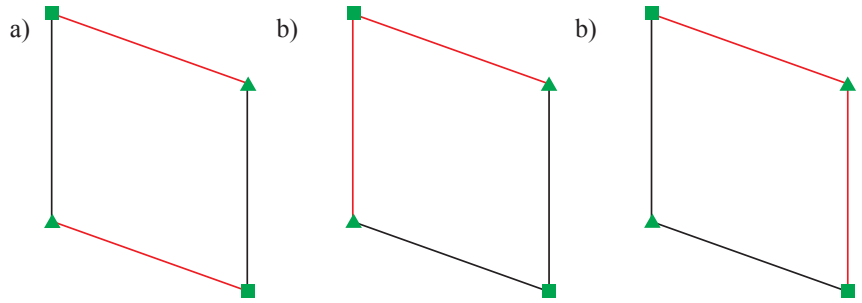

Figure 5.11: $|edge(F)| = 2$. Configurations of the edges in $edge(F)$. In a) the edges are parallel, in b) and c) the edges in $edge(F)$ occur successively, but their common vertex is of degree four in b) and of degree three in c).

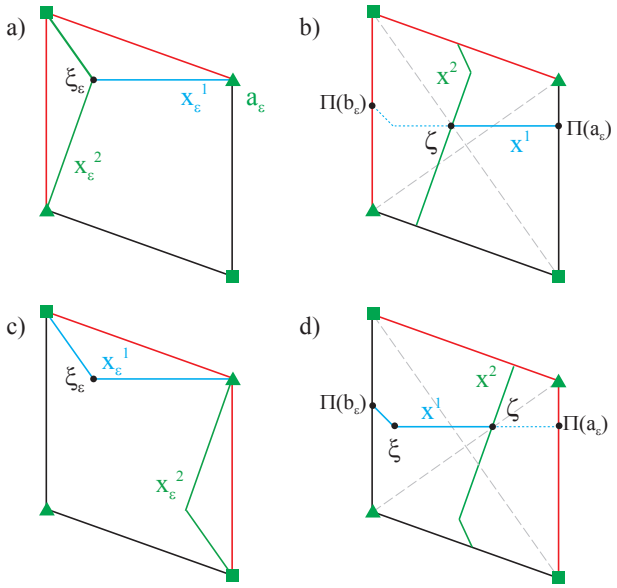

Figure 5.12: $|edge(F)| = 2$. Figures a) and b) show the case when the common vertex of the edges in $edge(F)$ has degree four, whereas figures c) and d) illustrate the case when the common vertex has degree three.
In a) and c) we see the curves x_ϵ^j, $j = 1, 2$, on the shrank facet εF. In b) and d) we see the curves x^j on the non–shrank facet F. The substitution for x^1 (solid blue line) could be interpreted as a "truncation" of the former x^1 (solid and dashed blue lines together).

labeled by x^1 and x^1_ε—by the curves

$$x^1 : [0,1] \to \mathbb{R}^3, \;\; x^1(t) = (1-t)\Pi(a_\varepsilon) + t\zeta,$$
$$x^1_\varepsilon : [0,1] \to \mathbb{R}^3, \;\; x_\varepsilon(t) = (1-t)a_\varepsilon + t\xi_\varepsilon.$$

In case the common vertex has order three: Here, we only substitute the curve x^1, again labeled by x^1, by

$$x^1 : [0,1] \to \mathbb{R}^3, \;\; x^1(t) = \begin{cases} \frac{1}{1-\varepsilon}\big[(1-\varepsilon-t)\zeta + t\xi\big], & t \in [0, 1-\varepsilon], \\ \frac{1}{\varepsilon}\big[(1-t)\xi + (t-(1-\varepsilon))\Pi(b_\varepsilon)\big], & t \in [1-\varepsilon, 1]. \end{cases}$$

The gluing sets are then defined as images of the functions g_1 and g_2,

$$g_j : [0,1] \times [0,1] \to \mathbb{R}^3, \;\; g_j(s,t) = (1-s)x^j_\varepsilon(t) + sx^j(t), \;\; j = 1, 2,$$

- $|edge(F)| = 1$: This is the most straightforward case, because we only need to glue the set M at the edge of $edge(F)$ (see Figure 5.13)

To avoid ambiguity in the freedom of choosing edges in the cases $|edge(F)| = 4$ and $= 2$, we appeal to Remark 5.6. Recall that F is by definition a facet of two neighbouring Voronoi cells. Once we have chosen one or two edges resp. from $edge(F)$, at which we glue (possibly truncated) sets M, we may not select other edges from $edge(F)$ for the neighbouring Voronoi cell.

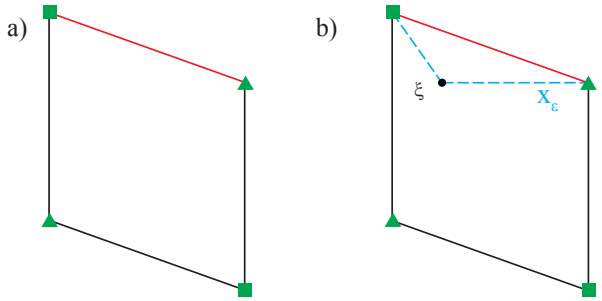

Figure 5.13: $|edge(F)| = 1$. The set $edge(F)$ consists of the red edge, whereas the black edges do not belong to $edge(F)$. Figure b) shows the shrank facet εF, and it illustrates that the set M is attached at the red edge.

We now glue, according to the rules from above,

$$\bigcup_{x \in \mathcal{S}_N} \mathcal{V}_\varepsilon(x),$$

with sets M and C, and we call this set $P_N^{(2)}$. Recall that facets on the boundary of

$$\bigcup_{x \in \mathcal{S}_N} \mathcal{V}(x)$$

have a one–to–one correspondence with the set of broken bonds of $\mathcal{S}_N$. Further, there is a one–to–one correspondence between the facets F on $P_N^{(1)}$ and the "facets" F' on $P_N^{(2)}$.[1] A "facet" F' on $P_N^{(2)}$ is the union of εF with either

- zero,
- one or
- two

[1]Strictly speaking, $P_N^{(2)}$ is not polyhedral, so that the notion of "facet" is not well–defined.

set(s) glued at it. To be more precise, in the cases of one and two gluing sets there are also one (and two resp.) additional triangles on F' of area $O(\varepsilon^2)$ (see for instance the triangle that is bounded by the dotted blue and the solid red curves in Figure 5.13 b)). Depending on the number of zero, one or two gluing sets, we say that F is a facet of type zero, one or two. The amount of facets of type zero, one or two on $P_N^{(2)}$ will be denoted by b_0, b_1 and b_2. Summarised,

$$\sharp\text{broken bonds} = b_0 + b_1 + b_2. \tag{5.33}$$

We claim that

$$\int_{\partial P_N^{(2)}} e(n)\,\mathrm{d}\mathcal{H}^2 \leq \sharp\text{broken bonds}. \tag{5.34}$$

Indeed, any facet F' of type zero contributes to the left hand side of (5.34)

$$\int_{F'} e(n)\,\mathrm{d}\mathcal{H}^2 = \int_{\varepsilon F} e(n)\,\mathrm{d}\mathcal{H}^2 \overset{5.22}{=} \frac{3}{2}\varepsilon^2, \tag{5.35}$$

Any facet F' of type one is the union of εF with one gluing set (either M or C) and with a triangle of area $O(\varepsilon^2)$. Because $\mathcal{H}^2(M) = O(1)$, but $\mathcal{H}^2(C) = O(\varepsilon)$, F' contributes to (5.34)

$$\int_{F'} e(n)\,\mathrm{d}\mathcal{H}^2 \leq \int_{\varepsilon F} e(n)\,\mathrm{d}\mathcal{H}^2 + \int_M e(n)\,\mathrm{d}\mathcal{H}^2 + O(\varepsilon^2) \overset{(5.35,5.28)}{\leq} \frac{3}{2}\varepsilon^2 + \frac{1}{2} + O(\varepsilon). \tag{5.36}$$

Finally, any facet F' of type two is the union of εF with two gluing sets (M or C) and possibly at most two triangles of area $O(\varepsilon^2)$. Again C has area of order $O(\varepsilon)$, integration of F' against the function e gives rise to

$$\int_{F'} e(n)\,\mathrm{d}\mathcal{H}^2 \leq \int_{\varepsilon F} e(n)\,\mathrm{d}\mathcal{H}^2 + 2\int_M e(n)\,\mathrm{d}\mathcal{H}^2 + O(\varepsilon^2) \overset{5.35,5.28}{\leq} \frac{3}{2}\varepsilon^2 + 1 + O(\varepsilon). \tag{5.37}$$

From equation (5.35), estimates (5.36)–(5.37) and from the fact that $b_0 > 0$ we deduce for sufficiently small ε:

$$\begin{aligned}\int_{\partial P_N^{(2)}} e(n)\,\mathrm{d}\mathcal{H}^2 &= \sum_{F' \text{ type } 0} \int_{F'} e(n)\,\mathrm{d}\mathcal{H}^2 + \sum_{F' \text{ type } 1} \int_{F'} e(n)\,\mathrm{d}\mathcal{H}^2 + \sum_{F' \text{ type } 1} \int_{F'} e(n)\,\mathrm{d}\mathcal{H}^2 \\ &\overset{(5.35),(5.36),(5.37)}{\leq} \frac{3}{2}\varepsilon^2(b_0+b_1+b_2) + \frac{1}{2}b_1 + b_2 + O(\varepsilon) \leq b_0 + b_1 + b_2 \\ &\overset{(5.33)}{=} \sharp\,\text{broken bonds.}\end{aligned}$$

establishing our claim (5.34).

To end up, we re–scale $P_N^{(2)}$ and define $P_N := \varepsilon P_N^{(2)}$. This set indeed satisfies the key estimate (5.20) in the first step of our lower bound proof, as can be easily seen from

$$N^{-2/3}(I_N(\mu_N) + 12N) = N^{-2/3} \cdot \sharp\,\text{broken bonds} \overset{(5.34)}{\geq} \int_{\partial P_N} e(n)\,\mathrm{d}\mathcal{H}^2.$$

We proceed to show that $\rho\chi_{P_N}$ converges to μ in L^1.

***L*^{1} convergence.** In order to proceed to the second step in the proof of the lower bound, it remains to verify that, as $N \to \infty$,

$$\rho\chi_{P_N} \to \mu \qquad \text{in } L^1. \tag{5.38}$$

Recall that μ is the weak$*$–limit of the sequence of re–scaled empirical measures μ_N. Following the ideas in [AFS12], the required convergence of $\rho\chi_{P_N}$ will be shown by investigating the measures

$$\mu'_N := \frac{1}{N} \sum_{x \in \mathcal{S}_N} \frac{\chi_{N^{-1/3}\mathcal{V}(x)}}{|N^{-1/3}\mathcal{V}(x)|}$$

and

$$\mu_N'' := \rho\chi_{P_N}.$$

We will prove this by showing gradually that

i. μ_N and μ_N' have the same weak$*$ limit in $\mathcal{M}(\mathbb{R}^3)$, *i.e.*,

$$\mu_N - \mu_N' \overset{*}{\rightharpoonup} 0 \qquad \text{in } \mathcal{M}(\mathbb{R}^3),$$

ii. μ_N' converges in a stronger space, namely in L^1, to μ, *i.e.*,

$$\mu_N' - \mu \to 0 \qquad \text{in } L^1(\mathbb{R}^3),$$

iii. μ_N' and μ_N'' share the same L^1 limit, *i.e.*,

$$\mu_N' - \mu_N'' \to 0 \qquad \text{in } L^1(\mathbb{R}^3).$$

Ad i.

For $x_0 \in \mathcal{S}_N$ the cell $\mathcal{V}(x_0)$ is contained in the ball of radius $\frac{\sqrt{2}}{2}$ centred at x_0. Let $\phi \in C_0(\mathbb{R}^3)$ be any test function. From the estimate

$$\begin{aligned}
&\left| \int_{\mathbb{R}^3} \left(\delta_{N^{-1/3}x_0}(y) - \frac{\chi_{N^{-1/3}\mathcal{V}(x_0)}(y)}{|N^{-1/3}\mathcal{V}(x_0)|} \right) \phi(y)\, \mathrm{d}y \right| \\
&\qquad = \frac{1}{|N^{-1/3}\mathcal{V}(x_0)|} \cdot \left| \int_{N^{-1/3}\mathcal{V}(x_0)} \left[\phi(N^{-1/3}x_0) - \phi(y) \right] \mathrm{d}y \right| \\
&\qquad \leq \sup_{|x-y| \leq N^{-1/3}} |\phi(x) - \phi(y)|
\end{aligned}$$

we infer

$$\left|\int_{\mathbb{R}^3}\phi\,\mathrm{d}\mu_N-\int_{\mathbb{R}^3}\phi\,\mathrm{d}\mu'_N\right|\leq\frac{1}{N}\sum_{x_0\in\mathcal{S}_N}\sup_{|x-y|\leq N^{-1/3}}|\phi(x)-\phi(y)| \tag{5.39}$$

$$=\sup_{|x-y|\leq N^{-1/3}}|\phi(x)-\phi(y)|. \tag{5.40}$$

Because ϕ is a test function, the last term vanishes as N gets large establishing the claim.

Ad ii.

After a change on a set of measure zero, the measures μ'_N can be written as

$$\mu'_N=\frac{1}{|\mathcal{V}(0)|}\chi_{\Omega_N},\qquad \Omega_N:=\bigcup_{x\in\mathcal{S}_N}N^{-1/3}\mathcal{V}(x). \tag{5.41}$$

Note that there is one–to–one correspondence between a facet on Ω_N and a broken bond $[x,y]$ in $N^{-1/3}\mathcal{S}_N$, *i.e.*, there exist $x\in N^{-1/3}\mathcal{S}_N, y\in N^{-1/3}(\mathcal{L}^{fcc}\backslash\mathcal{S}_N)$ such that $|x-y|=N^{-1/3}$; hence, the number of facets on $\partial\Omega_N$ equals the number of broken bonds in $\mathcal{S}_N$ and the latter amounts to $I_N(\mu_N)+12N$. Taking further into consideration that any facet on Ω_N has area $N^{-2/3}\dfrac{\sqrt{2}}{4}$ one obtains that

$$\begin{aligned}\mathcal{H}^2(|\partial\Omega_N|)&=(\sharp\,\text{facets on}\,\partial\Omega_N)\cdot\text{area}\,(\text{facet on}\,\partial\Omega_N)\\&=(I_N(\mu_N)+12N)\cdot N^{-2/3}\cdot\frac{\sqrt{2}}{4}.\end{aligned}$$

and in particular

$$N^{-2/3}(I_N(\mu_N)+12N)=2\sqrt{2}\mathcal{H}^2(|\partial\Omega_N|). \tag{5.42}$$

Given (up to a subsequence of) $N^{-2/3}(I_N(\mu_N)+12N)$ is bounded, we deduce by (5.42) that the restrictions $\mu'_N|_{B_R}$ are bounded in $BV(B_R)$ for any $R>0$ and converge to $\mu|_{B_R} \in L^1(B_R)$ by the compact embedding $BV(B_R) \hookrightarrow L^1(B_R)$. Finally, the mass preservation $\|\mu\|_{L^1(B_R)} = \|\mu'_N\|_{L^1(B_R)}$ for all N ensures the strong convergence $\mu'_N \to \mu$ in $L^1(\mathbb{R}^3)$ and further that $\mu = \rho\chi_E$ for some set E of finite perimeter and mass ρ^{-1}.

Ad iii.

The measures μ''_N and μ'_N coincide on cells centred at interior points $N^{1/3}x \in \mathrm{int}\mathcal{S}_N$ and only differ on "surface" cells by a mass of order N^{-1}. If (up to a subsequence of) $N^{-2/3}(I_N(\mu_N)+12N)$ is bounded, then by (4.38) the number of "surface particles" is bounded by $CN^{2/3}$. The symmetric difference between the supports of μ'_N and μ''_N can then be estimated as follows

$$\begin{aligned} |\Omega_N \triangle P_N| &\leq \sharp(\text{boundary particles}) \cdot \text{mass of a "surface" cell} \\ &\leq CN^{2/3} \cdot N^{-1} = CN^{-1/3}, \end{aligned} \tag{5.43}$$

and consequently, as $N \to \infty$,

$$\|\mu''_N - \mu'_N\|_{L^1(\mathbb{R}^3)} \to 0. \tag{5.44}$$

Further, if (a subsequence of) $N^{-2/3}(I_N(\mu_N)+12N)$ is bounded, then μ''_N strongly converges to μ in L^1. Indeed, by the triangle inequality, by the L^1 strong convergence of μ'_N to μ shown in ii. and finally by (5.44),

$$\|\mu''_N - \mu\|_{L^1(\mathbb{R}^3)} \leq \|\mu''_N - \mu'_N\|_{L^1(\mathbb{R}^3)} + \|\mu'_N - \mu\|_{L^1(\mathbb{R}^3)} \to 0, \tag{5.45}$$

as N tends to infinity.

Proof of second step.

Lower semicontinuity argument We first state a lower semicontinuity result in [AFP00] in a quite general form.

Theorem. *([AFP00], Theorem 5.22) Let $K \subset \mathbb{R}^m$ be compact and $\phi : K \times K \times \mathbb{R}^n \to [0, \infty]$ be a jointly convex function satisfying*

$$\phi(i, j, p) \geq c|p| \qquad \forall i, j \in K, i \neq j, p \in \mathbb{R}^n$$

*for some constant $c > 0$. Let (u_h) be a sequence of special functions of bounded variation on Ω which converges in $L^1(\Omega)$ to u such that $(|\nabla u_h|)$ is equiintegrable (*i.e.*, relatively compact w.r.t. weak topology of L^1) and, for any $h \in \mathbb{N}$, $u_h(x) \in K$ for λ^n–a.e. $x \in \Omega$. Then u is a special function of bounded of variation, $u(x) \in K$ for λ^n–a.e. $x \in \Omega$ and*

$$\int_{J_u} \phi(u^+, u^-, n) \, \mathrm{d}\mathcal{H}^{n-1} \leq \liminf_{h \to \infty} \int_{J_{u_h}} \phi(u_h^+, u_h^-, n) \, \mathrm{d}\mathcal{H}^{n-1}.$$

The surface energy density e can be extended to a 1–homogenous function on $\mathbb{R}^3$, is convex and satisfies a growth condition of the type $e(n) \geq c \cdot |n|$ for some $c > 0$; hence, by the above cited Theorem the functional

$$u \mapsto \int_{J_u} e(n) \, \mathrm{d}\mathcal{H}^2 \tag{5.46}$$

is lower semicontinuous along bounded sequences $(u_h) \subset SBV$ for which $(|\nabla u_h|)$ is equiintegrable.

To this end, let $u_N := \rho \chi_{P_N}$, where P_N is the set constructed in the first step. Let $K := \{0, \rho\}$. Assuming $N^{-2/3}(I_N(\mu_N'') + 12N)$ is bounded, we claim that the functional

above is lower semicontinuous along (u_N). Indeed,

1. u_N strongly converges in $L^1(\mathbb{R}^3)$ by (5.45),

2. (u_N) is bounded in $BV(\mathbb{R}^3)$,

3. $|\nabla u_N|$ is equiintegrable.

Thanks to the estimate (5.20) in Step 1, the lower semicontinuity of (5.46) and the convergence $\rho\chi_{P_N} \to \rho\chi_E$ in L^1 we conclude

$$\liminf_{N\to\infty} N^{-2/3}(I_N(\mu_N) + 12N) \geq \liminf_{N\to\infty} \int_{\partial P_N} e(n)\,\mathrm{d}\mathcal{H}^2 \geq \int_{\partial^* E} e(n)\,\mathrm{d}\mathcal{H}^2, \tag{5.47}$$

establishing the lower bound. □

5.2.2 Upper bound: attainment of lower bound

Let $\mu \in \mathcal{P}(\mathbb{R}^3)$ be arbitrary for which I_∞ is finite. We need to find a (recovery) sequence, *i.e.*, measures μ_N that weak$*$ converge to μ fulfilling

$$I_\infty(\mu) = \lim_{N\to\infty} N^{-2/3}(I_N(\mu_N) + 12N).$$

The recovery sequence for μ will be found by approximating gradually a set of finite perimeter E by sets of simpler geometric shape: A set of finite perimeter will be first approximated by a regular C^∞ set, then by C^∞ sets with polygonal boundaries and at the end by polygonal sets with vertices in $\frac{1}{n}\mathcal{L}^{fcc}$. A diagonalisation process finally delivers an appropriate recovery sequence.

Step 1 (Approximation by polygonal sets with vertices in $\frac{1}{n}\mathcal{L}^{fcc}$)

Let $P \subset \mathbb{R}^3$ be a bounded set with polygonal boundary such that every vertex of P lies

in $\frac{1}{n}\mathcal{L}^{fcc}$. Assume that the volume of P equals $m + \alpha_n$. We consider the set of particle configurations $\tilde{\mathcal{S}}_{n,N} := \mathcal{L}^{fcc} \cap N^{1/3}P$.

It is clear, that the empirical measures $\mu_{n,N}$ weak$*$ converge to $\frac{1}{m}\chi_P$, *i.e.*,

$$\mu_{n,N} \overset{*}{\rightharpoonup} \frac{1}{m}\chi_P \text{ in } \mathcal{M}(\mathbb{R}^3). \tag{5.48}$$

The cardinality of $\tilde{\mathcal{S}}_{n,N}$ will now be denoted by $M_{n,N}$, or M for short.
A straightforward estimation shows that

$$|M_{n,N} - N| \leq c(|\alpha_n|N + N^{2/3}) \tag{5.49}$$

for some constant c independent of n and N. Since P is polygonal, its boundary ∂P can be written as a finite union of plane facets ∂P_i, $i = 1, ..., p$, with normals n_i. It suffices to evaluate I_M and I_∞ on an arbitrary hypersurface of ∂P, say ∂P_i, with normal n.

The density e from Chapter 3 times the area of ∂P_i is *not* the number of bonds which intersect the hyperplane $N^{2/3}\partial P_i$, because the neighbouring surfaces $N^{2/3}\partial P_j$ could violate the brokenness of bonds near the edges. Therefore the number of pairs $(x, y) \in \tilde{\mathcal{S}}_{n,N} \times (\mathcal{L}^{fcc} \backslash \tilde{\mathcal{S}}_{n,N})$ with $|x - y| = 1$ such that the line segment $\overline{xy}$ intersects $N^{2/3} \cdot \partial P_i$ equals

$$\lfloor N^{2/3} \rfloor A \cdot e(n) + O(A) = N^{2/3}\left(e(n)A + O\left(\frac{A}{N^{2/3}}\right)\right). \tag{5.50}$$

Here, A is the area of the facet ∂P_i in question. From the summation along all normals n_i and from equation (5.50) we infer

$$\begin{aligned}
&\left| N^{-2/3}(I_M(\mu_{n,N}) + 12M) - \int_{\partial P} e(n)\,\mathrm{d}\mathcal{H}^2 \right| \\
&\overset{(5.50)}{\leq} \sum_{i=1}^{p} \left| N^{-2/3}\left(M^{2/3} e(n_i) A_i + O(A_i)\right) - e(n_i)A_i \right| \\
&= \sum_{i=1}^{p} \left| N^{-2/3} M^{2/3} e(n_i) A_i + O\left(\frac{A_i}{N^{2/3}}\right) - e(n_i)A_i \right| \\
&\leq \sum_{i=1}^{p} \left| N^{-2/3}(N + |N-M|)^{2/3} e(n_i) A_i + O\left(\frac{A_i}{N^{2/3}}\right) - e(n_i)A_i \right| \qquad (5.51) \\
&= \sum_{i=1}^{p} \left| \left(1 + \frac{|N-M|}{N}\right)^{2/3} e(n_i)A_i - e(n_i)A_i + O\left(\frac{A_i}{N^{2/3}}\right) \right| \\
&\overset{(5.49)}{\leq} \sum_{i=1}^{p} \left| \left(1 + c|\alpha_n| + c\frac{1}{N^{1/3}}\right)^{2/3} e(n_i)A_i - e(n_i)A_i + O\left(\frac{A_i}{N^{2/3}}\right) \right| \\
&\overset{(5.49)}{\leq} c\left(|\alpha_n| + \frac{1}{N^{1/3}} + \frac{1}{N^{2/3}}\right) \leq c\left(|\alpha_n| + \frac{1}{N^{1/3}}\right)
\end{aligned}$$

for N large. Here c is a generic constant (independent of n and N) that may change its value from line to line. In the penultimate step we used that $x^{2/3} \leq x$ for $x \geq 1$ and the fact that $e(n_i)A_i$ is bounded from above.

Step 2.

The preceding step can now be used to find a recovery sequence for a bounded set $P \subset \mathbb{R}^3$ with polygonal boundary and volume m: By perturbing the corners of ∂P slightly, we can obtain a sequence of polygonal sets P_n whose vertices lie in $\frac{1}{n}\mathcal{L}^{fcc}$ such that, as n gets large,

$$|P_n \triangle P| \to 0 \qquad (5.52)$$

$$\int_{\partial^\star P_n} e(n)\,\mathrm{d}\mathcal{H}^2 \to \int_{\partial^\star P} e(n)\,\mathrm{d}\mathcal{H}^2. \tag{5.53}$$

After choosing $n(N)$ appropriately in Step 1 we readily get a recovery sequence $\tilde{\mathcal{S}}_N := \mathcal{S}_{n(N),N}$ with associated re–scaled empirical measure $\tilde{\mu}_N$. One can, by using similar arguments as in Step 1 and by using (5.52), show that $\tilde{\mu}_N \overset{*}{\rightharpoonup} \frac{1}{m}\chi_E$ and that

$$N^{-2/3}(I_M(\tilde{\mu}_N) + 12M) \to I_\infty(\mu) \text{ for } N \to \infty. \tag{5.54}$$

To understand this, one first applies the triangle inequality, then uses the bound in (5.51):

$$\begin{aligned}
&\left|N^{-2/3}\left(I_M(\tilde{\mu}_N) + 12M\right) - I_\infty(\mu)\right| \\
&= \left|N^{-2/3}\left(I_M(\tilde{\mu}_N) + 12M\right) - \int_{\partial^\star P} e(n)\,\mathrm{d}\mathcal{H}^2\right| \\
&\leq \left|N^{-2/3}\left(I_M(\tilde{\mu}_N) + 12M\right) - \int_{\partial^\star P_n} e(n)\,\mathrm{d}\mathcal{H}^2 + \int_{\partial^\star P_n} e(n)\,\mathrm{d}\mathcal{H}^2 - \int_{\partial^\star P} e(n)\,\mathrm{d}\mathcal{H}^2\right| \\
&\leq c\left(|\alpha_{n(N)}| + \frac{1}{N^{1/3}}\right) + \left|\int_{\partial^\star P_n} e(n)\,\mathrm{d}\mathcal{H}^2 - \int_{\partial^\star P} e(n)\,\mathrm{d}\mathcal{H}^2\right|.
\end{aligned} \tag{5.55}$$

By virtue of (5.52) we deduce that $\alpha_n \to 0$, hence implying the first summand going to zero as N gets large, and by (5.53) the second summand becomes arbitrarily small for sufficiently large N, which together establish the desired convergence in (5.54).

It might happen that $\sharp\tilde{\mathcal{S}}_N \neq N$: In case $\tilde{\mathcal{S}}_N$ contains less than N particles, we can add the missing particles with positions in $\mathcal{L}^{fcc}$ such that

- they lie in some parallelepiped with side length of order $(N-M)^{1/3}$ and
- none of the additional particles has distance ≤ 1 from $\tilde{\mathcal{S}}_N$.

In the remaining case, $\sharp\tilde{S}_N > N$, we remove $M-N$ points of $\tilde{\mathcal{S}}_N$ which lie in a common parallelepiped with side length of order $(M-N)^{1/3}$. (The latter is always feasible if N is large.)

Step 3

A recovery sequence for a general set E of finite perimeter with volume m can be found through density and diagonalisation arguments:

A set E of finite perimeter can be approximated in measure by sets E_n of finite perimeter with smooth boundaries such that the perimeters also converge to the perimeter of E; hence, a fortiori

$$\chi_{E_n} \overset{*}{\rightharpoonup} \chi_E.$$

This is for example shown in [AFP00] (Theorem 3.42) or in [Bra98] (Proposition 4.7). Remark 4.8 in [Bra98] delivers the required continuity of the surface integral for the sets E_n (possibly after a rescaling of E_n to ensure they all have volume m):

$$\int_{\partial^\star E_n} e(n)\,\mathrm{d}\mathcal{H}^2 \to \int_{\partial^\star E} e(n)\,\mathrm{d}\mathcal{H}^2.$$

As ∂E_n is smooth, it can be approximated with piecewise linear functions to construct approximating sets P_m^n which have (after a possible rescale) the same volume as E_n and which have a polygonal boundary and satisfy

$$\chi_{P_m^n} \overset{*}{\rightharpoonup} \chi_{E_n} \qquad \text{and} \qquad \int_{\partial^\star P_m^n} e(n)\,\mathrm{d}\mathcal{H}^2 \to \int_{\partial^\star E_n} e(n)\,\mathrm{d}\mathcal{H}^2$$

as $m \to \infty$. This concludes the proof of Theorem 5.4. □

5.2.3 Identification of Wulff shape

We proceed to establish Theorem 5.5. Let μ_N be a sequence of re–scaled empirical measures (4.2) corresponding to exact minimisers $\{x_1^{(N)}, \ldots, x_N^{(N)}\}$ of E with uniformly bounded diameters,

$$\max_{i,j} |x_i^{(N)} - x_j^{(N)}| \leq CN^{1/3},$$

and bounded energies,

$$E(x_1^{(N)}, \ldots, x_N^{(N)}) \leq -12N + CN^{2/3}$$

for some constant C independent of N. After a possible translation of μ_N, that is to say after replacing μ_N by $\mu_N(\cdot + a_N)$ for some vector $a_N \in \mathbb{R}^3$, the limit measure has full mass by Theorem 4.4. Therefore, sequences of exact minimisers are compact in the weak* convergence of probability measures. By the Theorem in Appendix A, μ is a minimiser of the limit functional I_∞.

Again Theorem 5.1 by Fonseca and Müller concludes our proof:

An elementary calculation shows that the Wulff set W is given by a truncated octahedron whose vertices are given by all permutations of $(0, 2, 4)^T$, $(0, -2, 4)^T$, $(0, 2, -4)^T$ and $(0, -2, -4)^T$. The volume of W is 256, because the edges in the truncated octahedron are of length $2\sqrt{2}$.

A normalisation to one, completes our proof: The cluster set is given by cW, $c = \frac{\sqrt{2}}{512}$; in particular, $\mu = \sqrt{2}\chi_{cW}$ by Theorem 5.1 $\square$.

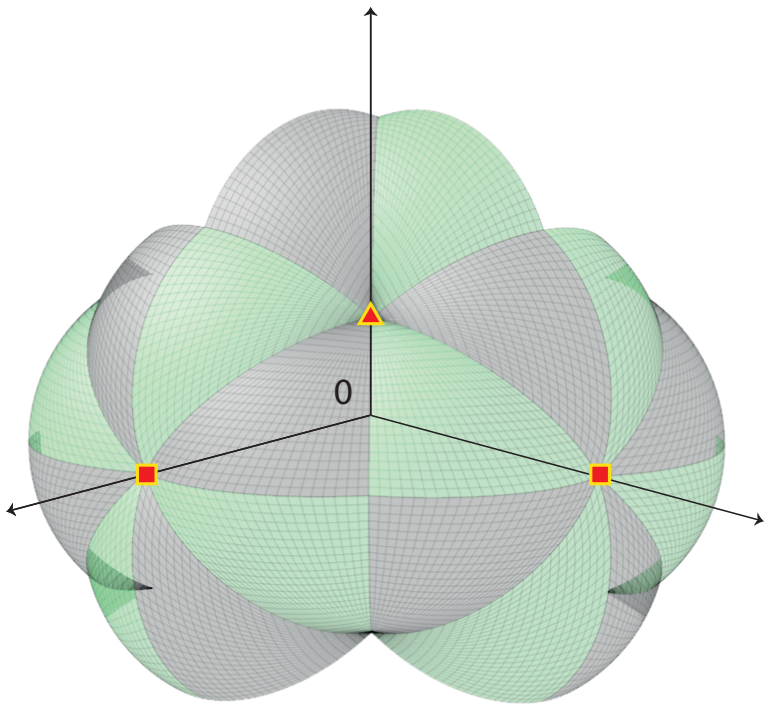

Figure 5.14: This is a part of the spherical plot of the surface energy density e in the face–centred cubic lattice. A spherical plot of $e : S^2 \to \mathbb{R}$ plots the set $\{e(n)n \ : \ n \in S^2\}$. The squares and the triangle on the spherical plot indicate that two specific 4–fold rotation axis and a specific 3–fold rotation axis intersect the spherical plot. The respective distances between the intersection points and the origin is exactly $e(n)$, namely 4 in the case of the squares and $2\sqrt{3}$ in the case of the triangle.

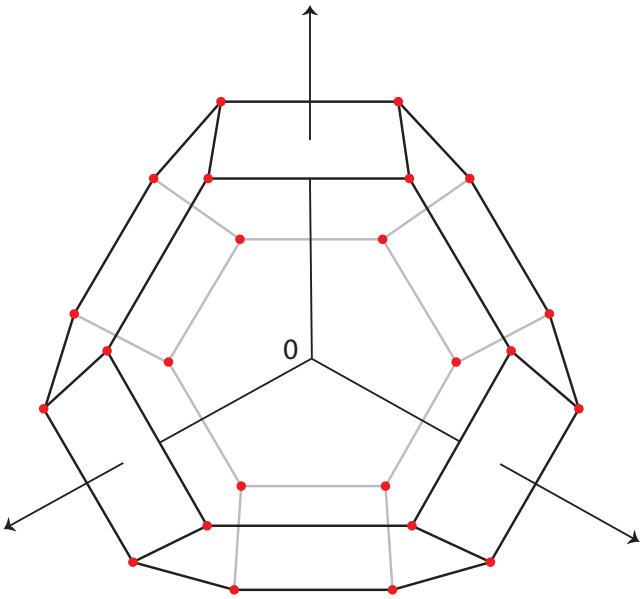

Figure 5.15: The Wulff shape for the face–centred cubic lattice $\mathcal{L}^{fcc}$ is a regular truncated octahedron of volume 256. The normals to the facets show in the direction, where e attains a (local) minimum, namely in the direction of the 3–fold and 4–fold rotation axes. In fact, these (local) minima give rise to the emergence of the hexagons and squares. The indicated coordinate system is orthogonal and intersects the facets at positive values.

Appendix A

Gamma–convergence

In 1975 Ennio De Giorgi introduced the variational notion of Gamma–convergence in [Gio75] and [GF75] (according to [AMF$^+$06]). An English translation of his seminal paper can be found in [AMF$^+$06].
An introductory text on Gamma–convergence covering selected applications can be found in [Bra02]. A more advanced treatment in non–metrisable topological spaces is [Mas93].

Definition. (Γ–convergence) Let (X, d) be a metric space. A sequence of functionals $I_N : X \to [-\infty, \infty]$ is said to *Gamma–converge* in X to the functional $I_\infty : X \to [-\infty, \infty]$ if for all $x \in X$

(a) (lower bound, lower semicontinuity)
I_N is lower semicontinuous along all sequences (x_N) which converge to x, i.e.,

$$I_\infty(x) \leq \liminf_{N\to\infty} I_N(x_N),$$

(b) (upper bound, attainment of lower bound)
there exists a sequence (x_N) which converges to x such that

$$I_\infty(x) = \lim_{N\to\infty} I_N(x_N).$$

Sequences for the upper bound are often called *recovery sequences*. Given an additional coercivity condition the major merits of Gamma–convergence appear; namely

(1) it guarantees the existence of minimisers of the limiting functional and

(2) a minimiser of the limiting functional I_∞ can be found by following a sequence of minimisers (x_N) of (I_N).

Theorem. (Convergence of minimisers) Let (X, d) be a metric space, (I_N) be a sequence of functionals X which Gamma–converges to I_∞. If the sequence (I_N) is equi–mildly coercive, *i.e.*, there exists a non–empty compact set $K \subset X$ such that $\inf_X I_N = \inf_K I_N$ for all $N \in \mathbb{N}$, then

(a) I_∞ possesses a minimiser,

(b) $\min_X I_\infty = \lim_{N\to\infty} \inf_X I_N$.

Appendix B

Functions of bounded variation

We present the very basic definition of and theorems about BV functions. For more details, we refer to [Bra98], [AFP00]. Throughout this appendix let Ω be an open subset of $\mathbb{R}^N$.

Definition and Theorem. (BV functions) Let $u \in L^1(\Omega)$. We say that u is a *function of bounded variation in* Ω if the distributional derivative of u is a finite Radon measure in Ω, *i.e.*, if there exists finite Radon measures Du_i, $i = 1, \ldots, N$, such that for any test function $\phi \in C_c^\infty(\Omega)$

$$\int_\Omega u \frac{\partial \phi}{\partial x_i} \, \mathrm{d}x = -\int_\Omega \phi \, \mathrm{d}D_i u.$$

The space of functions of bounded variations, or simply BV functions, is denoted by $BV(\Omega)$. It can be equipped with a norm

$$\|u\|_{BV} := \int_\Omega |u| \, \mathrm{d}x + |Du|(\Omega),$$

where $|Du|(\Omega)$ is the total variation of u in Ω,

$$|Du|(\Omega) := \sup\left\{\int_\Omega u \operatorname{div}\phi_i \ : \ \phi \in C_c^1(\Omega;\mathbb{R}^N),\ \|\phi\|_\infty \le 1\right\}.$$

Functions of bounded variation can exhibit jumps: For any $u \in BV(\Omega)$ we define the *approximate upper* and *lower limits of* u as

$$u^+(x) := \inf\left\{t \in \mathbb{R} \ : \ \{u > t\} \text{ has density } 0 \text{ in } x\right\}$$

and

$$u^-(x) := \sup\left\{t \in \mathbb{R} \ : \ \{u < t\} \text{ has density } 0 \text{ in } x\right\}.$$

By $\{u < t\}$ has density γ, $0 \le \gamma \le 1$, in x we mean that, as $\varepsilon \to 0$, the ratio

$$\frac{\mathcal{L}^N(\{y \in \Omega \cap B_\varepsilon(x)\})}{\mathcal{L}^N(B_\varepsilon(0))}$$

approaches γ. The jump set $S(u)$ of u is defined as

$$S(u) = \left\{x \in \Omega \ : \ u^-(x) < u^+(x)\right\}.$$

Definition. (Sets of finite perimeter) We say that a Lebesgue measurable set $E \subset \mathbb{R}^N$ is a *set of finite perimeter in* Ω if $\chi_E \in BV(\Omega)$. We call the quantity $|D\chi_E|(\Omega)$ the *perimeter of* E *in* Ω.

The perimeter of any set of finite perimeter E in Ω can be alternatively expressed via the $(N-1)$–dimensional Hausdorff measure through

$$|D\chi_E|(\Omega) = \mathcal{H}^{N-1}(\partial^* E).$$

Here, $\partial^* E$ is the *reduced boundary of E in Ω, i.e.*, $\partial^* E \cap \Omega = S_{\chi_E} \cap \Omega$.

Definition. (Weak$*$ convergence in BV) Let $(u_n) \subset BV(\Omega)$ and $u \in BV(\Omega)$. We say that u_n weakly$*$ converges to u in $BV(\Omega)$ if

(a) u_n converges to u in $L^1(\Omega)$ and

(b) Du_n weak$*$ converges to Du.

The distributional derivative of any BV function u can be decomposed into an absolutely continuous $\nabla u \mathcal{L}^N$, a jump $(u^+ - u^-)\mathcal{H}^{N-1}\lfloor S(u)$ and a Cantor part $D^c u$:

$$Du = \nabla u \mathcal{L}^N + (u^+ - u^-) \otimes \nu_u \, \mathcal{H}^{N-1}\lfloor S(u) + D^c u.$$

Definition. (SBV functions) A function $u \in BV(\Omega)$ is called a *special function of bounded variation in Ω* if the distributional derivative of u has no Cantor part, *i.e.*, if $D^c = 0$.

List of publications

The following article has been published prior to submission of this thesis:

- Y. Au Yeung, G. Friesecke, and B. Schmidt. Minimizing atomic configurations of short range pair potentials in two dimensions: crystallization in the Wulff shape. Calc. Var. PDE, 44:81–100, 2012.

Bibliography

[ABC06] R. Alicandro, A. Braides, and M. Cicalese. Phase and anti-phase boundaries in binary discrete systms: a variational viewpoint. *Netw. Heterog. Media*, 1(1):85–107, 2006.

[AFP00] L. Ambrosio, N. Fusco, and D. Pallara. *Functions of Bounded Variation and Free Discontinuity Problems*. Oxford University Press, 2000.

[AFS12] Y. Au Yeung, G. Friesecke, and B. Schmidt. Minimizing atomic configurations of short range pair potentials in two dimensions: crystallization in the Wulff shape. *Calc. Var. PDE*, 44:81–100, 2012.

[AMF+06] L. Ambrosio, G. Dal Maso, M. Forti, M. Miranda, and S. Spagnolo, editors. *Selected Papers of Ennio De Giorgi*. Springer, 2006.

[AT90] L. Ambrosio and V. M. Tortorelli. Approximation of Functionals Depending on Jumps by Elliptic Functionals via Γ-Convergence. *Commun. Pure Appl. Math.*, 43:999–1036, 1990.

[BCF51] W. K. Burton, N. Cabrera, and F. C. Frank. The Growth of Crystals and the Equilibrium Structure of their Surfaces. *Phil. Trans. Roy. Soc. London Ser. A*, 243:299–358, 1951.

[BM09] A. Ben-Menahem. *Historical Encyclopedia of Natural and Mathematical Sciences*, volume 4. Springer, 2009.

[Bra98] A. Braides. *Approximation of Free-Discontinuity Problems*. Number 1694 in Lecture Notes in Mathematics. Springer, 1998.

[Bra02] A. Braides. Γ-*convergence for Beginners*. Oxford University Press, 2002.

[Caf06] R. E. Caflish. Multiscale modeling in epitaxial growth. *Proc. Intl. Congress Math.*, III:1419–1432, 2006.

[CF09] S. Capet and G. Friesecke. Minimum energy configurations of classical charges: Large N asymptotics. *Appl. Math. Research Express*, doi:10.1093/amrx/abp002 (2009).

[CLT97] M. Carriero, A. Leaci, and F. Tomarelli. Strong Minimizers of Blake&Zisserman Functional. *Ann. Scuola Norm. Sup. Pisa Cl. Sci.*, 25(4):257–285, 1997.

[CMO+99] R. E. Caflish, M. F. Merriman, B. Osher, S. Ratsch, C. Vvedensky, and D. D. Zinck. Island dynamics and the level set method for epitaxial growth. *Appl. Math. Lett.*, 12(13):13–22, 1999.

[CS99] J. H. Conway and N. J. A. Sloane. *Sphere Packings, Lattices and Groups*. Springer, third edition edition, Berlin · Heidelberg · New York 1999.

[Cur85] M. P. Curie. Sur la formation des cristaux et sur les constantes capillaires de leurs diverse faces. *Bull. de la Société Minéralogique de France*, 6:145–150, 1885.

[DKS92] R. Dobrushin, R. Kotecký, and S. Shlosman. *Wulff Construction: A Global Shape from Local Interaction*, volume 104 of *Translations of Mathematical Monographs*. AMS, 1992.

[EH65] G. Ehrlich and F. G. Hudda. Atomic View of Surface Self–Diffusion: Tungsten on Tungsten. *J. Chem. Phys.*, 44(3):1039–1049, 1965.

[EL09] W. E and D. Li. On the Crystallization of 2D Hexagonal Lattices. *Comm. Math. Phys.*, 286(3):1099–1140, 2009.

[FFLM11] I. Fonseca, N. Fusco, G. Leoni, and V. Millot. Material voids in elastic solids with anisotropic surface energies. *J. Math. Pures Appl.*, 96(6):591–639, 2011.

[FL07] I. Fonseca and G. Leonni. *Modern Methods in the Calculus of Variations: L^p Spaces*. Springer, 2007.

[FM91] I. Fonseca and S. Müller. A uniqueness proof for the Wulff theorem. *Proc. Roy. Soc. Edinburgh Sect. A*, 119:125–136, 1991.

[FMS07] I. Fonseca, M. Morini, and V. Slastikov. Surfactants in Foam Stability: A Phase-Field Model. *Arch. Rational Mech. Anal.*, 183(3):411–456, 2007.

[Gal99] G. Gallavotti. *Statistical Mechanics: A short treatise*. Springer, 1999.

[GCL89] E. De Giorgi, M. Carriero, and A. Leaci. Existence theorem for a minimum problem with free discontinuity set. *Arch. Rational Mech. Anal.*, 108(4):195–218, 1989.

[GF75] E. De Giorgi and T. Franzoni. Su un tipo di convergenza variazionale. *Atti Accad. Naz. Lincei Rend. Cl. Sci. Mat. Fis. Natur*, 58:842–850, 1975.

[Gib78] J. W. Gibbs. On the Equilibrium of Heterogenous Substances. *Trans. Conn. Acad.*, 3:108–248 and 343–524, 1878.

[Gio75] E. De Giorgi. Sulla convergenza di alcune successioni d'integrali del tipo dell'area. *Rend. Mat.*, 8(6):277–294, 1975.

[GK10] H. Garcke and C. Kraus. An anisotropic, inhomogeneous, elastically modified Gibbs-Thomson law as singular limit of a diffuse interface model. *Proc. Appl. Math. Mech.*, 10:519–520, 2010.

[GR79] C. S. Gardner and C. Radin. The Infinite–Volume Ground State of the Lennard–Jones Potential. *J. Stat. Phys.*, 20(6):719–724, 1979.

[Har74] H. Harborth. Lösung zu Problem 664a. *Elem. Math.*, 29:14–15, 1974.

[Her51] C. Herring. Some Theorems on the Free Energies of Crystal Surfaces. *Phys. Rev.*, 82(1):87–93, 1951.

[Hoo65] R. Hooke. *Micrographia: or some Physiological Descriptions of minute bodies made by magnifying glasses with Observations and Inquiries thereupon.* J. Marty and J. Allestry (Printers to the Royal Society), 1665.

[HR80] R. C. Heitmann and C. Radin. The ground state for sticky disks. *J. Stat. Phys.*, 22:281–287, 1980.

[IS98] K. Ishii and H. M. Soner. Regularity and convergence of crystalline motion. *SIAM J. Math. Anal.*, 30(1):19–37, 1998.

[JW99] H.-C. Jeong and E. D. Williams. Steps on surfaces: experiment and theory. *Surf. Sci. Rep.*, 34:171–294, 1999.

[LB96] X.-Y. Liu and P. Bennema. Theoretical consideration of the growth morphology of crystals. *Phys. Rev. B*, 53(5):2314–2325, 1996.

[Lea97] R. H. Leary. Global optima of Lennard–Jones clusters. *J. Glob. Optim.*, 11(1), 1997.

[Lea00] R. H. Leary. Global Optimization on Funneling Landscapes. *J. Glob. Optim.*, 18:367–383, 2000.

[Lee56] J. Leech. The Problem of Thirteen Spheres. *Math. Gaz.*, 40:22–23, 1956.

[LM10] S. Luckhaus and L. Mugnai. On a mesoscopic many-body Hamiltonian describing elastic shears and dislocations. *Contin. Mech. Thermodyn.*, 22(4):251–290, 2010.

[Mac62] A. L. Mackay. A dense non–crystallographic packing of equal spheres. *Acta Crystallogr.*, 15:916–918, 1962.

[Mae01] H. Maehara. Isoperimetric theorem spherical polygons and the problem of 13 spheres. *Ryuku Math. J.*, 14:41–57, 2001.

[Mas93] G. Dal Maso. *An Introduction to* Γ*-convergence*. Birkhauser, 1993.

[MK06] D. Margetis and R. V. Kohn. Continuum Relaxation of Interacting Steps on Crystal Surfaces in 2+1 Dimensions. *Multiscale Model. Simul.*, 5(3):729–758, 2006.

[MMN62] J. K. Mackenzie, A. J. W. Moore, and J. F. Nicholas. Bonds broken at atomically flat crystal surfaces - I, face-centred and body-centred cubic crystals. *J. Phys. Chem. Solids*, 23:185–196, 1962.

[MN62] J. K. Mackenzie and J. F. Nicholas. Bonds broken at atomically flat crystal surfaces - II, crystals containing many atoms in a primitive unit cell. *J. Phys. Chem. Solids*, 23:197–205, 1962.

[Nor87] J. A. Northby. Structure and binding of Lennard–Jones clusters: $13 \leq N \leq 147$. *J. Chem. Phys.*, 87(10):6166–6177, 1987.

[Pei36] R. Peierls. On Ising's Model of Ferromagnetism. *Math. Proc. Cambridge*, 32(03):477–481, 1936.

[Pre09] E. Presutti. *Scaling Limits in Statistical Mechanics and Microstructures in Continuum Mechanics*. Springer, 2009.

[PV98] A. Pimpinelli and J. Villain. *Physics of Crystal Growth*. Cambridge University Press, 1998.

[Rad81] C. Radin. The ground state for soft disks. *J. Stat. Phys.*, 26:365–373, 1981.

[SCC04] X. Shao, L. Cheng, and W. Cai. A Dynamic Lattice Searching Method for Fast Optimization of lennard–jones Clusters. *J. Comp. Chem.*, 25(14):1693–1698, 2004.

[Sch66] R. L. Schwoebel. Step Motion on Crystal Surfaces. *J. Appl. Phys.*, 37(10):3682–3686, 1966.

[Sch13] B. Schmidt. Ground states of the 2D sticky disc model: fine properties and $N^{3/4}$ law for the deviation from the asymptotic Wulff shape. *arXiv:1302.6513*, (preprint in 2013).

[Spo93] H. Spohn. Surface dynamics below the roughening transition. *J. Phys.*, 3(1):69–81, 1993.

[Sti99] F. H. Stillinger. Exponential multiplicity of inherent structures. *Phys. Rev. E*, 59(1):48–59, 1999.

[SvdW53] K. Schütte and B. L. van der Waerden. Das Problem der dreizehn Kugeln. *Math. Ann.*, 125:325–334, 1953.

[Tay75] J. E. Taylor. Unique structure of solutions to a class of nonelliptic variational problems. *In: Differential geometry (Proc. Sympos. Pure. Math., Vol. XXVII), Part 1, AMS, Providence, R.I.*, pages 419–427, 1975.

[Tay91] J. E. Taylor. On the global structure of crystalline surfaces. *Discrete Comput. Geom.*, 6(1):225–262, 1991.

[TFar] F. Theil and G. Friesecke. *Geometry optimization, Binding of molecules.* In: Encyclopedia of Applied and Computational Mathematics. Springer, to appear.

[The06] F. Theil. A Proof of Crystallization in Two Dimensions. *Comm. Math. Phys.*, 262(1):209–236, 2006.

[Tót40] F. Tóth. Über einen geometrischen Satz. *Math. Z.*, pages 79–83, 1940.

[WH12] X. Wu and C. He. Stable structures of $Al_{510-800}$ clusters and lowest energy sequence of truncated octahedral Al clusters up to 10,000 atoms. *Chem. Phys.*, 405:100–106, 2012.

[Wul02] G. Wulff. Zur Frage der Geschwindigkeit des Wachsthums und der Auflösung der Krystallflächen. *Z. Kristallogr.*, 34:449–530, 1902.